Department of Physics
Indian Institute of Technology Guwahati
Ph.D. Thesis

Percolation Under Crossed Bias Fields: Criticality and Scaling

By: **Santanu Sinha**

Supervisor: Dr. S. B. Santra
May, 2007.

Percolation Under Crossed Bias Fields: Criticality and Scaling

A thesis submitted by

Santanu Sinha

to

Indian Institute of Technology Guwahati
in partial fulfillment of the requirements
for the award of the degree of
Doctor of Philosophy in Physics

Department of Physics
Indian Institute of Technology Guwahati
Guwahati - 781039, Assam, India

Statement

The work contained in the thesis entitled "*Percolation Under Crossed Bias Fields: Criticality and Scaling*" has been carried out by me under the supervision of Dr. S. B. Santra, Associate Professor, Department of Physics, Indian Institute of Technology Guwahati. This work has not been submitted elsewhere for the award of any degree.

(Santanu Sinha)
Department of Physics
Indian Institute of Technology Guwahati
Guwahati - 781039

May 22, 2007

Certificate

It is certified that the work contained in the thesis entitled "*Percolation Under Crossed Bias Fields: Criticality and Scaling*" by Mr. Santanu Sinha, a Ph.D. student of the Department of Physics, Indian Institute of Technology Guwahati for the award of Doctor of Philosophy has been carried out under my supervision. This work has not been submitted elsewhere for the award of any degree.

(Dr. S. B. Santra)
Department of Physics
Indian Institute of Technology Guwahati
Guwahati - 781039

May 22, 2007

To my parents...

Acknowledgements

I express my sincere gratitude and indebtedness to my supervisor Dr. Sitangshu Bikash Santra for his invaluable guidance, persistent supervision, creative ideas and constant encouragement throughout my research work. I am also very much thankful to him for introducing me to many advanced subjects in physics like critical phenomena, percolation, self organized criticality, etc., helping me to learn them and apply to physical problems. I will never forget his company and suggestions throughout my life. I will remain ever grateful to him for his great assistance to make this thesis possible.

I would like to thank my doctoral committee members, Dr. C. Y. Kadolkar, Dr. P. K. Giri and Dr. S. Adhikari for valuable discussions and help whenever I needed. My special thanks goes to Professor A. Srinivasan for his critical comments and suggestions in various areas of this work. I am also very thankful to the course coordinators for teaching me the advance topics of physics during my Ph.D. course work.

I feel a deep sense of gratitude to late Dr. Sasanka Ghosh, former Head, Department of Physics and my initial supervisor, for bringing me in the field of research and to grow my interest towards theoretical physics. His memories are always an inspiration to me towards way of research.

I wish to thank Department of Physics, Indian Institute of Technology, to provide me necessary computational facilities. I wish to thank Indian Institute of Technology Guwahati for providing a great library facility and the computer center with outstanding network connectivity and various computational resources. I am also thankful to all the departmental staff for their technical assistance. My special thanks goes to my seniors Dr. Debojit Sarma, Dr. Manoranjan Kar, Dr. Kamlesh Alti, Dr. Munima Saharia, Dr. Ardhendu Sekhar Patra, Dr. Pramoda Nayak and all of my colleagues and juniors for their nice co-operation. I also grateful to Mr. Ashis Sarkar, Principal, Dinhata College, for allowing me to continue my research even after joining the college as a lecturer.

I have been fortunate to come across many good and helpful friends, without whom life would be bleak. My special thanks go to Biplab Sarkar, Krishna Kanti Dey, Arnab Chatterjee, Rupjyoti Gogoi, Runu Sona, Jasmine Sinha, Santanu Maity, Vimal Kishore, for their timely help, support and encouragement.

This thesis is dedicated to my parents, my father Mr. Harekrishna Sinha and my mother Ms. Anjali Sinha whose unconditional love and support, encouragement to fulfill my dreams as well as honest and pointed advice, during the most difficult stages of my graduate life have been instrumental to me for the completion of my degree. I am also greatly indebted to my sisters Swati Sinha and Smriti Sinha and my brother Abhisek Sinha for listening to my complaints and frustrations and for believing in me always.

And finally, I would like to thank Council of Scientific and Industrial Research, India, for providing scholarship and financial support to carry out the present thesis work.

- *Santanu.*

Abstract

A new site percolation model namely the directed spiral percolation (DSP) model is constructed imposing directional and rotational constraints simultaneously on the ordinary percolation model. The DSP model can be used to study the critical properties of disordered systems under crossed external bias fields. The bias fields could be of electric and magnetic in nature when the motion of charged particles are considered. In order to study the geometrical phase transition in the DSP model at the percolation threshold, a single cluster growth Monte Carlo (MC) algorithm has been developed. The DSP clusters are found anisotropic, rarefied with chiral dangling ends. It is the first percolation model in which the appearance of a Hall type field is observed. The model exhibits a new and an interesting critical behaviour at the percolation threshold. A full scaling theory has been developed and found consistent with the numerical results obtained. A new set of critical exponents are found to characterize the critical properties of the model. Consequently, the model belongs to a new universality class. Quite unexpectedly, the model shows a breakdown of universality in the values of the critical exponents between the square and the triangular lattices in two dimensions. The model has been studied by different methods and techniques such as finite size scaling, determination of hull, effect of field direction and intensity, multifractality and the dynamical critical behaviour to explore different critical aspects of the model. An anisotropic finite size scaling (FSS) theory has been developed to verify the effect of finite system size on the MC results. The FSS results are found in good agreement with that of the MC results. Though there is a breakdown of universality in the cluster properties, the critical behaviour of hull exhibits universal character in $2D$. A new conjecture has been proposed for the hull fractal dimension in terms of the connectivity exponents suitable for the anisotropic percolation hulls. A phase diagram has been obtained in the parameter space of field intensities. The DSP model corresponds to different percolation models like ordinary percolation, directed percolation and spiral percolation depending on the field intensities. DSP is then a generalized percolation

model under external bias fields. Introducing the occupation state formalism, the DSP spanning clusters are analyzed and found to be multifractal. The multifractal spectra confirm the universality class of the model. The dynamical critical exponents characterized by the topological bias of the DSP clusters are determined. The values of the dynamical critical exponents are in accordance with that of the static scaling exponents and reconfirm the universality class of the DSP model. DSP model thus represents a new, important and unusual critical behaviour at the percolation threshold applicable to disordered systems in the presence of crossed external bias fields.

Contents

Chapter 1

Introduction

Complexity and criticality are like conjugate phenomena in physical sciences. Complexity is a synonymous with randomness or disorder. Most natural objects have a complex irregular shape or structure. Examples are clouds, mountains, trees, the pattern created in lightning, the coastline of a country, etc. There are many physical systems which are inherently disordered. A dilute magnet consisting of a random distribution of non-magnetic and magnetic atoms or ions is a disordered system. Conductor-insulator composite materials, composite superconductor-metal materials, discontinuous metal films, glasses and many others are just a glimpse of a long list of disordered systems. There exist many natural physical and chemical processes which are also random. The flow of a liquid through a porous medium, metal atom dispersion in an insulator, spread of a disease in a population, forest fire, etc. all are random in nature. On the other hand, criticality is a well defined concept in statistical physics. Criticality refers to the behaviour of extended systems at a phase transition where observables are scale free, that is, no characteristic length scale exists for these observables. Lattice statistical models were developed and used to understand the macroscopic critical behaviour of these disordered systems and random physical processes. A lattice statistical model has on one hand disorder or randomness as a major ingredient and on the other hand, the lattice structure makes the physical problem easier to study. In most of the cases, it was observed that the lattice structure turns out to be irrelevant as far as the macroscopic observations are concerned.

In the beginning of 1940s, Flory [1] and Stockmayer [2] studied polymerization of a large number of monomers in solution. In this process, macromolecular clusters are formed by forming bonds randomly between the monomers. During the process of polymerization, they observed that depending upon the concentration of monomers,

the solution becomes a gel which is a network of macromolecules spanning the whole system. This is what is called percolation. Percolation thus incorporates randomness as a major ingredient and tuning of certain parameter like concentration in the system. In 1957, Broadbent and Hammersley[3] first introduced percolation theory mathematically to deal with random systems using the geometrical and probabilistic concepts. Soon after the introduction of the percolation theory various physical applications were considered by Domb[4], Sato *et al*[5], Elliott *et al*[6], Isichenko[7] and many others. Krikpatrick[8–10], Stauffer[11], Essam[12], Deutscher *et al*[13], Guyon *et al*[14] and many others then developed the theory of percolation in the context of phase transition and critical phenomena. The percolation problem on a lattice will now be introduced and the main results and their importance in disordered systems in the context of critical phenomena will be summarized.

1.1 Percolation model

In percolation processes a continuous path which spans the entire system is created by the random addition of a number of objects. The percolation model is defined here on a square lattice of linear size L in 2 dimensions ($2D$). The percolation model and its elaborate theory developed by several authors during last few decades are available in the literature[15–17]. There are two versions of the model, namely site and bond. The site percolation model is described in the following. A lattice is composed of a periodic array of sites. Initially the lattice is empty, *i.e.* none of the sites are occupied. Sites are then randomly occupied with a probability p or remains unoccupied with a probability $q = 1-p$. A site is randomly occupied means that its occupation is independent of whether its nearest neighbors are occupied or empty. Occupied sites form clusters. A cluster of occupied sites is a collection of a number of occupied sites connected by nearest neighbor bonds. The smallest cluster can then be a single site if none of the nearest neighbor sites are occupied. For small values of p, only small clusters of occupied sites are generated. Since only small isolated clusters exist, there is no connection from one edge of the lattice to the opposite edge. The average size of the clusters increases with increasing value of p. On the other hand, for $p = 1$ all the sites are occupied and there is only one large cluster of size L^2. As p increases from a small value, there exists a particular value of p between 0 and 1 at which a cluster of occupied sites spanning from left to right or top to bottom appears for the first time in the system. The percolation threshold p_c is equal to this particular value of p, below which there is no spanning

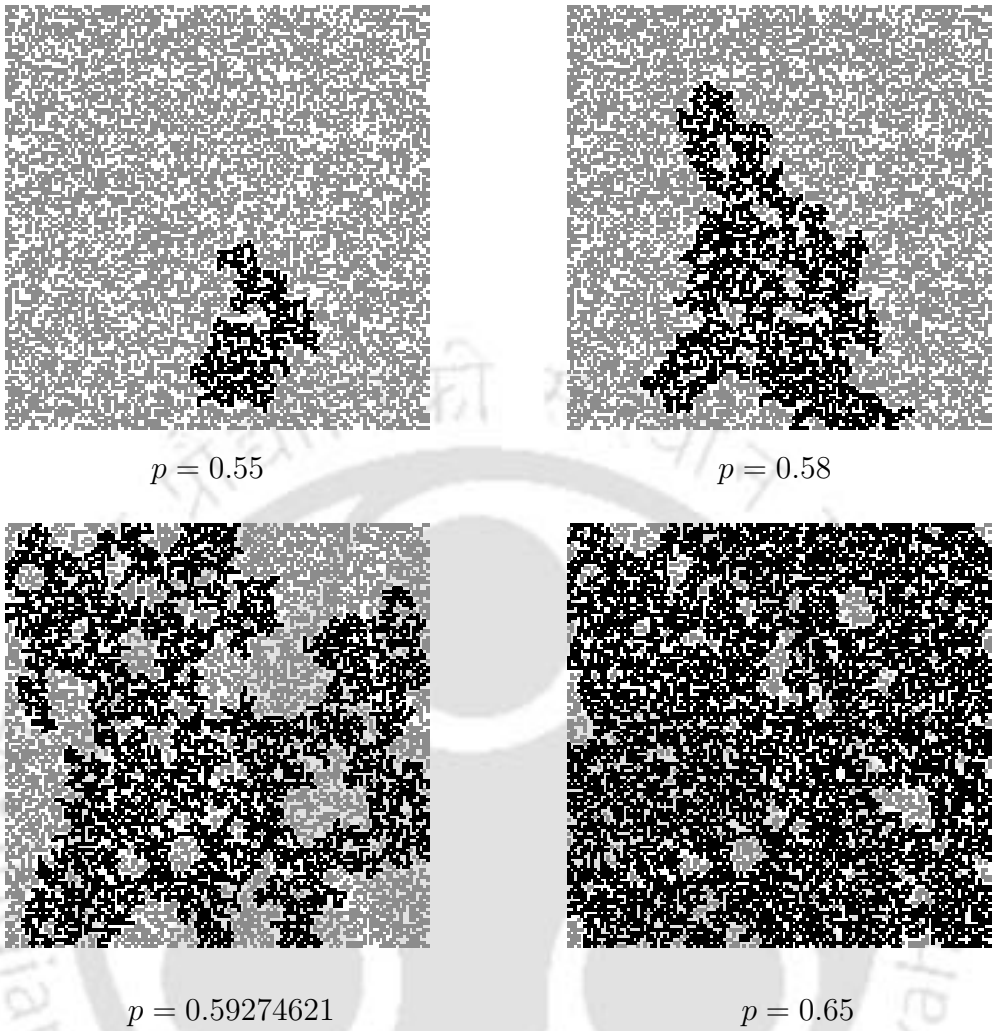

Figure 1.1: Percolation clusters generated at different site occupation probabilities. The largest clusters are shown by dark black dots.

cluster and above which there is always a spanning cluster present in the system. This is called percolation transition. The spanning cluster percolates through the lattice just as water percolates through wet sand along the network of wet pores. For an infinitely large lattice, p_c has a sharp and unique value determined by the lattice structure and the dimension d of the lattice. For a finite lattice, the value of p_c has a small spread. In Figure 1.1, four realizations on a square lattice of size $2^7 \times 2^7$ are shown for $p = 0.55$, 0.58, 0.59274621 and 0.65. The largest cluster is shown by darker gray scale. A spanning cluster appears in the system for the first time at $p = 0.59274621$. This is the percolation threshold p_c on the square lattice for site percolation. It should be mentioned here that it has been shown rigorously by Grimmett [18] that there is no percolating infinite cluster at $p = p_c$ for $d = 2$. The

large but finite clusters that emerge at $p = p_c$ are called 'incipient infinite clusters'. Throughout this thesis, the incipient infinite clusters at $p = p_c$ will be referred as percolating spanning clusters.

The percolation model has extensive applications in different branches of science. The application of percolation model in disordered systems are well documented in the literature[19–24]. A few relevant applications are in oil recovery in porous media[25,26], epidemic modeling[27], networks[28,29], fracture[30], metal insulator transition[31], ionic transport in glasses[32], earthquakes in rocks[21] among others. In recent times, percolation model is also applied to business firm growth[33], fragmentation of solids[34], polyatomic species[35], electrical conductivity of colloidal dispersions[36], conductivity of DNA[37], living neural networks[38], propagation of information on scale free networks[39], seismic process[40], gelation[41], hydration water in bio-systems[42], solar dynamo[43] and many others. The applications of percolation range from confinement - non-confinement transition of quarks in nuclear matter to metal insulator transition in conductor-insulator composite materials to containment - epidemic transition of a disease in a society to stochastic star formation in spiral galaxies. In all these systems, the common ingredient is randomness or disorder and a transition from connectivity to non-connectivity or propagation to non-propagation, etc., occurs in the system at a sharply defined parameter value. This indicates a phase transition in the geometry of the system at the percolation threshold p_c very similar to thermodynamic phase transition of physical systems at a critical temperature T_c[44–46]. It is then important to understand the geometrical properties of the percolating spanning cluster at $p = p_c$ as well as the statistical properties of finite clusters below p_c and investigate whether this geometrical phase transition in percolation is equivalent to thermal phase transition or critical phenomena.

1.2 Percolation as critical phenomena

A phase transition in a thermodynamic system signifies a qualitative change in the properties of the system at a temperature T_c known as the critical temperature. As temperature $T \to T_c$, the system exhibits phenomena which are described as 'critical'. The temperature region near $T \to T_c$ constitutes the 'critical region'. There exists a well defined prescription in equilibrium statistical mechanics for studying critical phenomena[44,46]. Let us consider first a specific example of second order thermodynamic phase transition and discuss the corresponding critical phenomena.

A well-known example is the paramagnet to ferromagnet transition which occurs at the critical temperature T_c. For $T < T_c$ it is the ferromagnetic phase and for $T > T_c$ it is the paramagnetic phase. The ferromagnetic phase has a net spontaneous magnetization $M = -(\partial F/\partial H)_T$ where F is the Helmholtz free energy of the system and H is the applied magnetic field, whereas in the paramagnetic phase the spontaneous magnetization M is always zero. The spontaneous magnetization M is known as the order parameter of the magnetic transition. As $T \to T_c$, the thermodynamic quantities exhibit singularities of a power law form. For example, M continuously goes to zero with a branch point singularity at $T = T_c$ characterized by the critical exponent β as

$$M \sim (T_c - T)^{\beta}. \tag{1.1}$$

The isothermal zero-field susceptibility $\chi(T)$ defined as $\chi(T) = (\partial M/\partial H)_T$ diverges as

$$\chi \sim |T - T_c|^{-\gamma}. \tag{1.2}$$

The specific heat $C = -T(\partial^2 F/\partial T^2)_H$ shows a singularity of the form

$$C \sim |T - T_c|^{-\alpha}. \tag{1.3}$$

Since the thermodynamic quantities are just different derivatives of the Helmholtz free energy F, it is then the most essential quantity to calculate in a thermodynamic system from its microscopic details. The free energy F of a system can be determined as

$$F = -k_{\mathrm{B}} T \ln Z \tag{1.4}$$

where Z is the canonical partition function, T is the absolute temperature and k_{B} is the Boltzmann constant. Knowing the Hamiltonian of a system, the partition function Z can be evaluated. Once the Helmholtz free energy F is known, the relevant thermodynamic quantities can be evaluated and their scaling behaviour can be studied. In general, the thermodynamic quantities Q exhibit singularities of the form

$$Q = |T - T_c|^{\pm\theta} \tag{1.5}$$

in the critical regime. The exponent θ is known as the critical exponent. The minus sign before θ indicates divergence and plus sign corresponds to branch point singularity.

The free energy function becomes a generalized homogeneous function in the

critical regime. A function is said to be a generalized homogeneous function if

$$f(\lambda^a x, \lambda^b y) = \lambda f(x, y) \tag{1.6}$$

for all values of the parameter λ, where a and b are two arbitrary numbers. Since the parameter λ is arbitrary, one can make a choice of λ as $\lambda = 1/x^{1/a}$ so that the above equation reduces to the form

$$\begin{aligned} & f(1, y/x^{b/a}) \equiv F(y/x^{b/a}) = \tfrac{1}{x^{1/a}} f(x, y) \\ \text{or} \quad & f(x, y) = x^{1/a} F(y/x^{b/a}). \end{aligned} \tag{1.7}$$

Most functions of two variables have the form of a generalized homogeneous function given in Eq. 1.7 if both x and y approach zero. In the case of magnetic phase transition, x represents the reduced temperature, $t = (T - T_c)/T_c$ and y is the reduced magnetic field h in units of energy. Thus, for the zero field behaviour as $T \to T_c$ both the parameters x and y tend to zero.

There are two important consequences of the free energy being a generalized homogeneous function. First, since the thermodynamic quantities Q are different derivatives of the free energy function F, the critical exponents θ are not all independent. The exponents α, β, γ, etc. can be defined in terms of a and b. Eliminating a and b, scaling relations between the critical exponents can be obtained and are verified experimentally. One such scaling relation between α, β, and γ is given by

$$\alpha + 2\beta + \gamma = 2. \tag{1.8}$$

Second, the scaling function $F(z) = f(x, y)/x^{1/a}$ can be obtained as a function of a scaled variable $z = y/x^{b/a}$. If Eq. 1.7 is valid, the plots of $F(z)$ versus z for different values of x and y all collapse into a single curve, the function $F(z)$. This is known as data collapse. The scaling assumption has also been verified experimentally through data collapse. In the case of magnetic transition, the scaling function of magnetization M is given by

$$M(t, h) \sim |t|^{\beta} \mathcal{M}(\pm 1, h|t|^{-\beta\delta}) \tag{1.9}$$

where t is the reduced temperature, h is the reduced magnetic field and β, δ are critical exponents. The scaled magnetization and magnetic field can be defined as

$$\mathcal{M}(\pm 1, z) = M(t, h)/|t|^{\beta}; \qquad z = h|t|^{-\beta\delta}. \tag{1.10}$$

Hence a plot of $\mathcal{M}$ against z should lie on the same curve for all values of temperature greater than or less than T_c respectively, provided that they lie in the critical regime. The data collapse of magnetization versus the scaled magnetic field was obtained for $CrBr_3$ by Ho and Lister in 1969[47]. A class of systems found to have the same values of the critical exponents (if the number of components of order parameter and dimension d of the embedding space are the same) consequently define a universality class. The values of the critical exponents, the scaling relations among them and the form of the scaling function then determine the universality class of a system.

In a magnetic system, fluctuations in the spin orientations occur in the critical region over all possible length scales, starting from atomic scale to the system size. The system becomes self similar. A part of it can not be distinguished from the whole lattice if enlarged to the appropriate scale. In the critical region, there are large patches of, say, up-spin domains containing down-spin domains which again contain still smaller domains of up-spins and so on. This has been verified by huge neutron scattering cross section at $T = T_c$. In fact, the enormous increase in the fluctuation in magnetization can be shown to be related to the divergence of susceptibility. The correlation length ξ, the distance between, say, two up spins in the same domain, diverges as $T \to T_c$ with a critical exponent ν as

$$\xi \sim |T - T_c|^{-\nu}. \tag{1.11}$$

The critical exponent ν is also related to other critical exponents by a hyperscaling relation

$$\gamma + 2\beta = d\nu \tag{1.12}$$

where d is the space dimension of the system. Relation 1.12 has also been verified experimentally. Many other such scaling relations exist between the critical exponents.

It has been observed that the critical exponents have identical values if the dimension d of the system is the same. The values of the critical exponents do not depend on the range of interaction or the lattice structure. The critical behaviour of widely different physical systems such as magnetic systems, fluid system, binary mixture then can be described by the same critical exponent in the same space dimension d. This defines a universality class.

A similar prescription is now essential to be established in order to study the percolation as critical phenomena. Before proceeding further, one should first identify the relevant geometrical or statistical quantities which exhibit critical behaviour at

the percolation threshold p_c. At p_c, a percolating system consists of an infinite (or spanning) percolating cluster and finite clusters of different possible sizes. Geometrical properties could be then classified into two groups, *i.e.*; properties of the infinite cluster and properties of the finite clusters. The probability that a site belongs to the infinite cluster P_∞ may be the most relevant quantity to look at which could serve the purpose of the order parameter of a percolating system. The geometry of the infinite cluster is found self-similar and fractal[19,48–51]. The relevant quantities associated with the finite clusters could be the average cluster size χ, the number of occupied sites present in a cluster on an average and the connectivity length ξ which is the mean distance between two occupied sites in the same cluster. In order to estimate these geometrical quantities, one can define a cluster generating function G similar to the partition function in thermodynamic critical phenomena. The generating function in the case of percolation is defined as

$$G = \sum_h \sum_s{}' n_s(p) e^{-sh} \tag{1.13}$$

where $n_s(p)$ is the number of s-sited clusters per lattice site at the site occupation probability p and h is a fictitious field with no physical meaning. The sum is over all finite clusters which is indicated by a prime. All the relevant cluster related quantities then can be extracted from different derivatives of the generating function G. The function G at $h = 0$, given by

$$G\Big|_{h=0} = \sum_s{}' n_s(p) \tag{1.14}$$

gives total number of finite clusters per lattice site. This is analogous to the free energy per site in the case of magnetic phase transition. For a small value of p below p_c, less number of sites will be occupied and the number of clusters per lattice site will also be small. On the other hand, for a high value of p above p_c, it will be again small due to less number of finite clusters appearing in the system. Most of the space will be occupied by the large percolating cluster. Only as $p \to p_c$, large number of finite clusters will appear and the quantity diverges from both sides of p_c as,

$$\sum_s{}' n_s(p) \sim |p - p_c|^{2-\alpha} \tag{1.15}$$

where α is a critical exponent.

The order parameter P_∞ of the percolation transition, defined as the probability

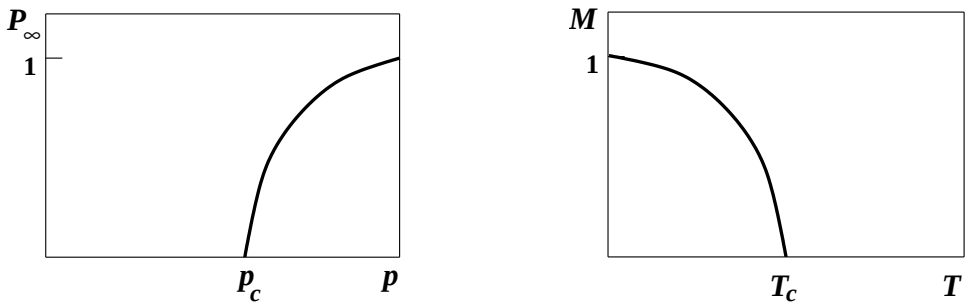

Figure 1.2: Order parameters P_∞ and M for the percolation and magnetic phase transitions respectively. Both of them go to zero continuously as the system approaches the critical point.

that a site belongs to the spanning cluster, can be obtained from the first derivative $(\partial G/\partial h)_{h=0} = \sum_s' s n_s(p)$ of the generating function as

$$P_\infty = p - \sum_s' s n_s(p). \tag{1.16}$$

The order parameter $P_\infty = 0$ for $p < p_c$ as $\sum_s' s n_s(p) = p$. At $p = 1$, $\sum_s' s n_s(p) = 0$ and thus $P_\infty = 1$. As p is decreased from a large value above p_c, P_∞ continuously goes to zero from $p = p_c$ with an exponent β defined as

$$P_\infty \sim (p - p_c)^\beta. \tag{1.17}$$

The scaling behaviour of P_∞ is similar to that of the spontaneous magnetization M, the order parameter in the case of ferromagnetic transition, as shown in Figure 1.2.

Another important geometrical quantity is the average cluster size χ. It can be obtained from the second derivative $(\partial^2 G/\partial h^2)_{h=0} = \sum_s' s^2 n_s(p)$ of the generating function. χ is defined as

$$\chi = \frac{\sum_s' s^2 n_s(p)}{\sum_s' s n_s(p)} = \frac{1}{p} \sum_s' s^2 n_s(p) \tag{1.18}$$

as $\sum_s' s n_s(p)$ represents the probability that a site belongs to any finite cluster and is therefore equal to p. Notice that, as p is small below p_c, only small clusters could appear and the average size would be small. As p increases, clusters of larger sizes will appear and χ will increase. As $p \to p_c$, the value of χ will diverge. The same behaviour will re-occur if p is reduced to p_c from a higher value above p_c. In Figure

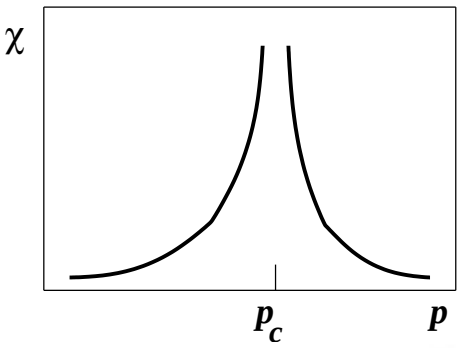

Figure 1.3: Behaviour of the average cluster size χ as $p \to p_c$. This behaviour is similar to the susceptibility in the magnetic phase transition as $T \to T_c$.

1.3, the behaviour is demonstrated as $p \to p_c$. χ is analogous to the susceptibility in the magnetic phase transition. It is then expected to diverge with an exponent γ as $p \to p_c$,

$$\chi \sim |p - p_c|^{-\gamma}. \tag{1.19}$$

Different geometrical quantities like order parameter, average cluster size are then just different moments of the cluster size distribution function $n_s(p)$. Since the critical exponents are not all independent and they satisfy certain scaling relations among them, it is important to know the scaling function form of the cluster size distribution function $n_s(p)$ and derive all the critical exponents in terms of the exponents related to $n_s(p)$. As the free energy function becomes generalized homogeneous function in the critical regime of thermodynamic phase transition, the cluster size distribution function $n_s(p)$ is then expected to be a generalized homogeneous function of two variables, *i.e.*; the inverse cluster size $1/s$ and $(p - p_c)$ in the critical regime here. Note that, as $p \to p_c$ both of the variables approach zero. The scaling function form of $n_s(p)$ is then given by

$$\begin{aligned} n_s(p) &= (1/s)^{\tau} \mathsf{f}[(p - p_c)/(1/s)^{\sigma}] \\ &= s^{-\tau} \mathsf{f}[s^{\sigma}(p - p_c)]. \end{aligned} \tag{1.20}$$

As all the geometrical quantities are just the different moments $n_s(p)$, the critical exponents associated with them are not all independent, rather they can be expressed in terms of the exponents τ and σ. Scaling relations among the critical exponents can also be established following the same procedure of thermodynamic phase transition.

The spin fluctuation in all possible length scales and the long range correlations in magnetic phase transition at the critical point is demonstrated by the divergence of correlation length. In the geometrical model like percolation, the linear size of the finite clusters, below and above p_c, is characterized by the connectivity length ξ

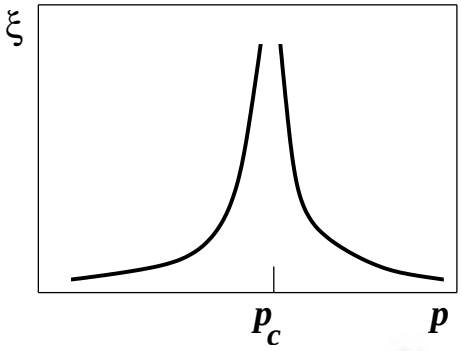

Figure 1.4: Behaviour of the connectivity length ξ as $p \to p_c$. Similar behaviour can be observed for the spin correlation length as $T \to T_c$ in the magnetic system.

which is similar to the correlation length in thermodynamic phase transition. Here ξ is defined as the root mean square distance between two sites on the same finite cluster and averaged over all finite clusters. It can be calculated by measuring the radius of gyration of a cluster

$$R_s^2 = \frac{1}{s^2} \sum_{i=1}^{s} |\mathbf{r_i} - \mathbf{r_0}|^2 \tag{1.21}$$

where $\mathbf{r}_0 = \sum_{i=1}^{s} \mathbf{r_i}/s$ is the position of the center of mass of the cluster and $\mathbf{r}_i$ is the position of ith site of the cluster. The connectivity length is the average radius of gyration over all finite clusters and given by

$$\xi^2 = \frac{2 \sum_s{}' R_s^2 s^2 n_s(p)}{\sum_s{}' s^2 n_s(p)}. \tag{1.22}$$

At p_c, clusters of all possible sizes, starting from a single sited cluster up to the cluster of system size, appear in the system and correspondingly there is a huge fluctuation in the cluster size. Due to the appearance of large finite clusters at the critical point, the connectivity length diverges as $p \to p_c$ (Figure 1.4) with an exponent ν given by

$$\xi \sim |p - p_c|^{-\nu}. \tag{1.23}$$

The connectivity length exponent ν is also found related to the moment exponents of $n_s(p)$ via hyperscaling relation. The infinite cluster at $p = p_c$ contains holes of all possible sizes and the percolation cluster is found to be self similar and fractal.

There are numerous analytical and numerical studies for estimating the values of the critical exponents in percolation[11,52–54]. The exact values of the critical exponents for $2D$ percolation model was obtained by mapping the model onto the q-state Potts model in limit $q \to 0$[52,53]. The values of some of the exponents are

Order parameter exponent β	5/36
Average cluster size exponent γ	43/18
Connectivity length exponent ν	4/3
Fractal dimension d_f	91/48

Table 1.1: Critical exponents of the ordinary percolation in $2D$ obtained by mapping it onto q-state Potts model in the limit $q \to 0$ [52,53].

listed in Table 1.1.

The values of the critical exponents are found the same on different lattices in the same space dimension. The critical exponents do not depend the site or the bond percolation problem on the same lattice in the same space dimension. This defines the universality class of the percolation model.

1.3 Effect of external bias on percolation

The universality in critical phenomena is a significant observation. The values of the critical exponents depend only on the dimensionality of the space, number of components in the order parameter and do not depend on the underlying lattice structure or range of interaction. Two widely different systems, *i.e.*; the Ising magnet and a liquid gas system in 3D with scalar order parameters, belong to the same universality class with the critical exponents having the same magnitude. However, application of external bias field on the percolation model leads to a new universality class. The individual effects of two different external bias fields on the percolation model are extensively studied. First is a global directional bias and the second is a local rotational bias. These external bias fields are implemented on the percolation model by assigning appropriate constraints on the occupation of lattice sites. The directional bias corresponds to a directional constraint and the rotational bias corresponds to a rotational or a spiral constraint. The percolation models under these external constraints are known as directed percolation (DP) [55,56] and spiral percolation (SP) [57–59] respectively. An example of directional constraint is the motion of a charged particle in the direction of applied electric field. Similarly, the motion of a charged particle in a plane in the presence of a magnetic field perpendicular to the plane of motion is an example of spiral constraint. Below, both the models and the main results obtained in these models are presented briefly.

1.3.1 Directed percolation

In directed percolation, a global directional constraint restricts the growth of the percolation cluster in a particular direction. For example, if the directional con-

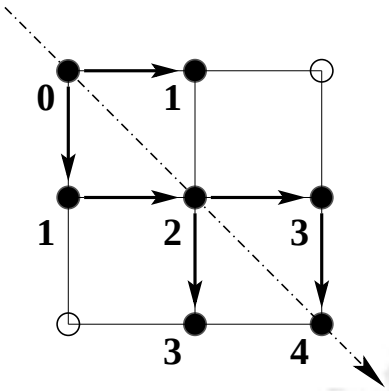

Figure 1.5: Growth of cluster in directed percolation. As the directional constraint in along the top left to right bottom diagonal, indicated by the dotted arrow, sites in the right or bottom are allowed to occupy. Black circles are the occupied sites. The numbers indicate the time steps at which they are occupied.

straint is along the top left to bottom right diagonal of the lattice, sites are allowed to occupy only in these two preferred directions, towards right or bottom. Percolation clusters in this model can also be generated by performing directed walk [60,61]. The model is illustrated in Figure 1.5. Due to the restriction in the cluster growth, the percolation threshold shifts to a higher value than that of ordinary percolation (OP). As a result of the clusters growth in the preferred direction, they become highly anisotropic in nature as shown in Figure 1.6. Consequently, unlike the ordinary percolation, two lenghtscales appear and the system behaves differently in these two directions. There are then two connectivity lengths, $\xi_{\parallel}$ along the preferred direction and $\xi_{\perp}$ in the direction perpendicular to that, which diverge with

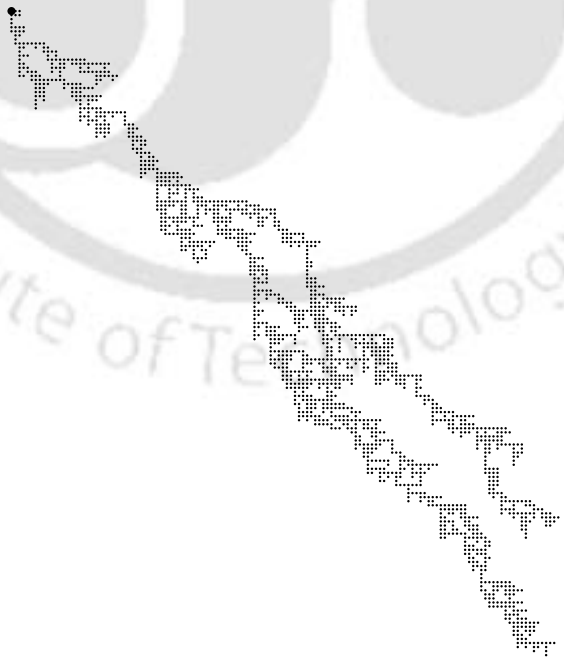

Figure 1.6: Typical spanning DP cluster generated on a $2^8 \times 2^8$ square lattice at the percolation threshold p_c.

Critical exponents	Values
β	0.277 ± 0.002
γ	2.2772 ± 0.0003
$\nu_{\parallel}$	1.7334 ± 0.001
$\nu_{\perp}$	1.0972 ± 0.0006
d_f	1.765 ± 0.010

Table 1.2: Critical exponents of the directed percolation in $2D$ obtained by series expansion and Monte Carlo methods[63,64,67].

two different connectivity exponents $\nu_{\parallel}$ and $\nu_{\perp}$ respectively as $p \to p_c$. This leads to anisotropic scaling and direction-dependent critical behaviour. The values of some of the critical exponents of this model are given in Table 1.2 for $2D$ lattices. All the critical exponents[62–67] in this model are different from those of OP. Thus the DP model belongs to a new universality class other than OP.

The DP model has a lot of applications in different fields like self-organized criticality[68–70], reaction diffusion systems[71–73], nonlinear random resistor networks[74,75], polymers[76–79] and many more[80–83]. Due to the connection with the motion of charged particle under electric field, the DP model is widely used to study the electrical transport properties of disordered systems[84,85].

1.3.2 Spiral percolation

In spiral percolation, a rotational constraint[86], say clockwise, present in the ordinary percolation model. In this model cluster can be grown starting from the central site of the lattice following the algorithm of Santra and Bose[58]. Due to the clockwisely rotational constraint present in the system, empty sites in the forward direction and in the clockwisely rotational direction are eligible for occupation. The

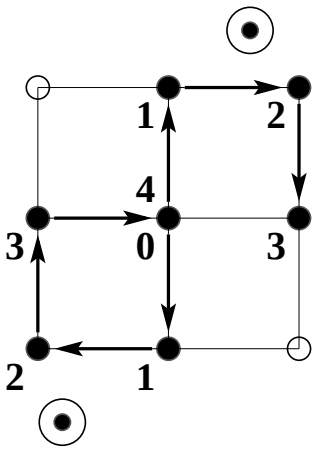

Figure 1.7: Growth of a cluster in spiral percolation. As the spiral constraint is in the clockwise direction, indicated by the encircled dots, sites in the forward and in the clockwise directions are allowed to occupy. Black circles are the occupied sites. The numbers denote the time steps of occupation.

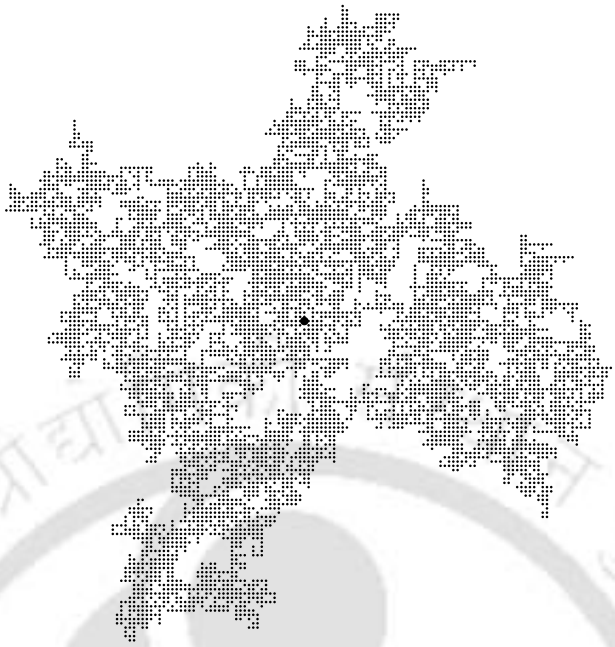

Figure 1.8: Typical spanning SP cluster generated on a $2^8 \times 2^8$ square lattice at the percolation threshold p_c.

forward direction is the direction from which the present site is occupied and the sense of rotational direction is defined with respect to the forward direction. This is illustrated in Figure 1.7. The eligible sites are then occupied with probability p and the clusters grow isotropically on the lattice [57,58]. In this model, due to the presence of rotational constraint, an occupied site can be reoccupied from different directions but forbidden for occupation from the same direction. Consequently, loops become an essential feature of the spirally grown clusters which make the clusters highly compact as compared to those of OP or DP. Unlike DP, the clusters are isotropic here, quite similar to OP, but they are much more compact as shown in Figure 1.8. As a consequence, critical properties of the SP model [57–59] are found different than that of the OP and DP model. The values of some of the critical exponents are given in Table 1.3.

The SP model has been applied in studying forest fire [87], pinning of interfaces [88] and diffusion under rotational bias in disordered systems [89]. As the rotational constraint is related to the behaviour of charged particle in a magnetic field, the SP model can also be used to study the hopping of electron in a strong magnetic field [90,91].

Therefore, it can be concluded that in the presence of an external constraint the critical properties of the system as well as the universality class of the OP model are

Critical exponents	Values
β	0.048 ± 0.011
γ	2.19 ± 0.07
ν	1.116 ± 0.003
d_f	1.957 ± 0.009

Table 1.3: Critical exponents of the spiral percolation in $2D$ [57–59].

changed [19]. The critical exponents associated with different cluster related quantities in the DP and SP models are not only different but also different from those in the case of the OP model. The DP and SP models then belong to two universality classes which are different from that of the OP model. It is thus intriguing to consider the effect of both the bias fields simultaneously on the OP model.

1.4 Percolation under crossed bias fields

In this section a motivation for constructing a new percolation model imposing both the directional constraints on the occupation of sites will be given. Recently, a great deal of interest has been focused on the electric and magnetic properties of disordered systems. Transport properties of electro-rheological and magneto-rheological fluids [92], magnetic semiconductors [93,94] and composite materials [95–105] have received a lot of attention due to their industrial applications. Transport of charged particles under crossed electric and magnetic fields in disordered systems is also an important field of study in recent times [89,106]. Disordered systems show anomalous behaviour depending on the external field strength and disorder of the medium [24]. A number of physical properties like electrical conductivity, magneto resistance, Hall effect etc. in disordered systems are not completely understood as a function of disorder, field strengths or other parameters. Disordered systems are generally modeled on the basis of percolation phenomenon [15,19,21]. The presence of external biases, *i.e.* the electric and magnetic fields, in the disordered system can be realized by applying suitable external constraints on the percolation model as described in the previous sections. In order to study the electro-magnetic properties of disordered systems in the presence of both the electric and magnetic fields, a new site percolation model called directed spiral percolation (DSP) is proposed in this thesis. The DSP model is constructed by imposing both the directional and rotational constraints simultaneously on the ordinary percolation model. If both the fields are present perpendicular to each other in a material system, due

to Lorentz force the electron will get deflected and a Hall field will appear in the system perpendicular to both the fields. This is known as Hall effect. The DSP model then can also be applied to study the Hall effect in such systems.

It is already mentioned that in the presence of an external constraint, the critical properties of the percolating systems as well as their universality class are changed[19,107]. The critical exponents associated with different cluster related quantities in both the biased percolation models DP and SP are not only different but also different from those in the case of the OP model. It is therefore interesting to study the critical properties of the percolation model in the presence of both the constraints simultaneously through the proposed DSP model. The DSP model has an academic interest and at the same time it could have several applications. In order to understand the static and dynamic critical properties of the model an extensive numerical study has been performed in $2D$. The findings are elaborated and discussed in the following chapters.

There are nine chapters in the thesis. In this chapter, a general introduction to percolation phenomena and the critical properties of different percolation models like OP, DP and SP are given. In the second chapter, the DSP model will be introduced and the Monte Carlo (MC) algorithm developed for cluster generation will be elaborated. The percolation threshold of the DSP model will be identified and the morphology of the spanning clusters will be discussed. A full scaling theory for the DSP model has been developed and the critical properties are verified in the third chapter. A finite-size scaling analysis of the cluster properties in support of the MC results will be given in the fourth chapter. Study of the critical properties of the DSP hull, the external perimeter, will be described in the fifth chapter. In the sixth chapter, effect of the field directions and the field intensities of the external biases on the critical properties of the DSP model will be reported. In the seventh chapter, the DSP model will be represented as a spin model and the multifractal aspects of DSP clusters will be presented. Finally, the study of the dynamical properties (diffusivity, conductivity, etc.) will be described in chapter eight. Chapter nine will contain the summary and conclusion of the whole work.

Bibliography

[1] P. J. Flory, J. Am. Chem. Soc. **63**, 3083, 3091, 3906 (1941).
[2] W. H. Stockmayer, J. Chem. Phys. **11**, 45 (1943).
[3] S. R. Broadbent and J. M. Hammersley, Proc. Cambridge Phill. Soc. **53**, 629 (1957).

[4] C. Domb, Nature **184**, 509 (1959).
[5] H. Sato, A. Arrott and R. Kikuchi, J. Phys. Chem. Solids **10**, 10 (1959).
[6] R. J. Elliott, B. R. Heap, D. J. Morgan and G. S. Rushbrooke, Phys. Rev. Lett. **5**, 306 (1960).
[7] M. B. Isichenko, Rev. Mod. Phys. **64**, 961 (1992).
[8] V. K. S. Shante and S. Kirkpatrick, Advances in Physics **20**, 325 (1971).
[9] S. Kirkpatrick, Phys. Rev. Lett. **27**, 1722 (1971).
[10] S. Kirkpatrick, Rev. Mod. Phys. **45**, 574 (1973).
[11] D. Stauffer, Phys. Rep. **54**, 1 (1979).
[12] J. W. Essam, Rep. Prog. Phys. **43**, 833 (1980).
[13] W. Kinzelin *Percolation Structure and Processes*, edited by G. Deutscher, R. Zallen and J. Adler, Adam Hilger, Bristol, 1983.
[14] E. Guyon et al., Rep. Prog. Phys. **53**, 373 (1990).
[15] D. Stauffer and A. Aharony, *Introduction to Percolation Theory*, Taylor and Francis, London, 2nd edition, 1994.
[16] B. Bollobás and O. Riordan, *Percolation*, Cambridge University Press, 2006.
[17] N. R. Moloney and K. Christensen, *Complexity And Criticality*, Imperial College Press, 2005.
[18] G. R. Grimmett, *Percolation*, Springer-Verlag, New York, 1999.
[19] A. Bunde and S. Havlin, *Fractals and Disordered Systems*, Springer-Verlag, Berlin, 1991.
[20] R. Zallen, *The Physics of Amorphous Solids*, Wiley, New York, 1983.
[21] M. Sahimi, *Applications of Percolation Theory*, Taylor and Francis, London, 1994.
[22] A. G. Hunt, *Percolation Theory for Flow in Porous Media*, Springer-Verlag, New York, 2005.
[23] A. Bovier, *Statistical Mechanics of Disordered Systems: a mathematical perspective*, Cambridge University Press, 2006.
[24] D. Ben-Avraham and S. Havlin, *Diffusion and Reactions in Fractals and Disordered Systems*, Cambridge University Press, UK, 2000.
[25] P. R. King et al., Physica A **274**, 60 (1999).
[26] P. R. King et al., Physica A **314**, 103 (2002).
[27] J. L. Cardy and P. Grassberger, J. Phys. A: Math. Gen. **18**, L267 (1985).
[28] R. Cohen, D. Ben-Avraham and S. Havlin, Phys. Rev. E **66**, 036113 (2002).
[29] A. Acin, J. I. Cirac and M. Lewenstein, Nature Physics **3**, 256 (2007).
[30] H. J. Herrmann and S. Roux, editors, *Statistical Models for the Fracture of Disordered Media*, North-Holland, 1990.
[31] Z. Ball, H. M. Phillips, D. L. Callahan and R. Sauerbrey, Phys. Rev. Lett. **73**, 2099 (1994).
[32] H. E. Roman, A. Bunde and W. Dieterich, Phys. Rev. B **34**, 3439 (1986).
[33] D. F. Fu, S. V. Buldyrev, M. A. Salinger and H. E. Stanley, Phys. Rev. E **74**, 036118 (2006).
[34] J. Brzychczyk, Phys. Rev. C **73**, 024601 (2006).

[35] M. Dolz, F. Nieto and A. J. Ramirez-Pastor, Phys. Rev. E **72**, 066129 (2005).
[36] N. I. Lebovka, S. Tarafdar and N. V. Vygornitskii, Phys. Rev. E **73**, 031402 (2006).
[37] I. Brovchenko, A. Krukau, A. Oleinikova and A. K. Mazur, Phys. Rev. Lett. **97**, 137801 (2006).
[38] I. Breskin, J. Soriano, E. Moses and T. Tlusty, Phys. Rev. Lett. **97**, 188102 (2006).
[39] K. Kosmidis and A. Bunda, Physica A **376**, 699 (2007).
[40] T. Chelidze and T. Matcharashvili, Tectonophysics **431**, 49 (2007).
[41] T. Abete, A. de Canadia, E. D. Gado, A. Fierro and A. Coniglio, Phys. Rev. Lett. **98**, 088301 (2007).
[42] A. Oleinikova and I. Brovchenko, Molecular Phys. **104**, 3841 (2006).
[43] K. H. Schatten, Astrophysical J. Suppl. Series **169**, 137 (2007).
[44] H. E. Stanley, *Introduction to Phase Transitions and Critical Phenomena*, Oxford University Press, New York, 1987.
[45] C. Domb and M. Green, editors, *Phase Transitions and Critical Phenomena*, Academic Press, London, 1976.
[46] J. M. Yeomans, *Statistical Mechanics of Phase Transitions*, Oxford University Press, New York, 1994.
[47] J. T. Ho and J. D. Lister, Phys. Rev. Lett. **22**, 603 (1969).
[48] H. E. Stanley, J. Phys. A **10**, L211 (1977).
[49] J. Feder, *Fractals*, Plenum Press and New York and London, 1998.
[50] J. F. Gouyet, *Physics and Fractal Structures*, Springer-Verlag, Berlin, New York, 1996.
[51] A. Bunde and S. Havlin, *Fractals in Science*, Springer-Verlag, Berlin, 2nd edition edition, 1995.
[52] M. P. M. den Nijs, J. Phys. A **12**, 1857 (1997).
[53] B. Nienhuis, J. Phys. A **15**, 199 (1982).
[54] R. M. Ziff and B. Sapoval, J. Phys. A **19**, L1169 (1987).
[55] S. P. Obukhov, Physica A **101**, 145 (1980).
[56] H. Hinrichsen, Brazilian Journal of Physics **30**, 69 (2000).
[57] P. Ray and I. Bose, J. Phys. A **21**, 555 (1988).
[58] S. B. Santra and I. Bose, J. Phys. A **24**, 2367 (1991).
[59] S. B. Santra and I. Bose, J. Phys. A **25**, 1105 (1992).
[60] M. Barma and D. Dhar, J. Phys. C: Solid State Phys. **16**, 1451 (1983).
[61] K. Debell, T. Lookman and D. L. Hunter, Phys. Lett. A **101**, 221 (1984).
[62] J. K. Williams and N. D. Mackenzie, J. Phys. A: Math. Gen. **17**, 3343 (1984).
[63] J. W. Essam, A. J. Guttmann and K. DéBell, J. Phys. A: Math. Gen. **21**, 3815 (1988).
[64] J. W. Essam, K. DéBell, J. Adler and F. M. Bhatti, Phys. Rev. B **33**, 1982 (1986).
[65] W. Kinzel and J. M. Yeomans, J. Phys. A: Math. Gen. **14**, L163 (1981).
[66] K. DéBell and J. W. Essam, J. Phys. A: Math. Gen. **16**, 385 (1983).
[67] B. Hede, J. Kertész and T. Vicsek, J. Stat. Phys. **64**, 829 (1991).
[68] S. P. Obukhov, Phys. Rev. Lett. **65**, 1395 (1990).

[69] H. M. Broker and P. Grassberger, Physica A **267**, 453 (1999).
[70] R. Dickman, Physica A **306**, 90 (2002).
[71] H. Hinrichsen, Adv. Phys. **49**, 815 (2000).
[72] N. Guisoni and M. J. de Oliveira, pre **74**, 061905 (2006).
[73] S. Lubeck, J. Stat. Phys. **123**, 193 (2006).
[74] H. K. Janseen and O. Stenull, Phys. Rev. E **63**, 025103 (2001).
[75] O. Stenull and H. K. Janssen, Phys. Rev. E **64**, 016135 (2001).
[76] E. Perlsman and S. Havlin, Eur. Phys. Lett. **46**, 13 (1999).
[77] E. Perlsman and S. Havlin, Eur. Phys. J. B **43**, 517 (2005).
[78] A. Hansen and J. Kertesz, Phys. Rev. E **53**, R5541 (1996).
[79] T. Halpin-Healy, Phys. Rev. E **58**, R4096 (1998).
[80] T. Vicsek, J. Kertész and J. Cserti, J. Phys. A: Math. Gen. **15**, L189 (1982).
[81] A. Jimenez-Dalmaroni, Phys. Rev. E **74**, 011123 (2006).
[82] S. Lubeck and R. D. Willmann, Nucl. Phys. B **718**, 341 (2005).
[83] Y. Timofeeva and S. Coombes, Phys. Rev. E **70**, 062901 (2004).
[84] I. Balberg and N. Binenbaum, Phys. Rev. B **33**, 2017 (1986).
[85] X. H. Wang, E. Perlsman and S. Havlin, Phys. Rev. E **67**, 050101 (2003).
[86] T. C. Li and Z. C. Zhou, J. Phys. A: Math. Gen. **18**, 67 (1985).
[87] S. B. Santra and I. Bose, Z. Phys. B **89**, 247 (1992).
[88] S. B. Santra, A. Paterson and S. Roux, Phys. Rev. E **53**, 3867 (1996).
[89] S. B. Santra and W. A. Seitz, Int. J. Mod. Phys. C **11**, 1357 (2000).
[90] S. N. Dorogovtsev, Sov. Phys. Solid State **28**, 1699 (1986).
[91] S. N. Dorogovtsev, arxiv: cond-mat , 9712042v2 (1997).
[92] M. V. Gandhi and B. S. Thompson, *Smart Materials and Structures*, Chapman and Hall, London, 1992.
[93] H. Ohno, Science **281**, 951 (1998).
[94] G. A. Prinz, Science **282**, 1660 (1998).
[95] D. J. Bergman and Y. M. Strelniker, Phys. Rev. B **59**, 2180 (1999).
[96] D. J. Bergman and Y. M. Strelniker, Phys. Rev. B **60**, 13016 (1999).
[97] K. K. Bardhan and R. K. Chakrabarty, Phys. Rev. Lett. **69**, 2559 (1992).
[98] R. K. Chakrabarty, K. K. Bardhan and A. Basu, J. Phys.: Condens. Matter **5**, 2377 (1993).
[99] K. K. Bardhan and R. K. Chakrabarty, Phys. Rev. Lett. **72**, 1068 (1994).
[100] U. N. Nandi, C. D. Mukherjee and K. K. Bardhan, Phys. Rev. B **54**, 12903 (1996).
[101] K. K. Bardhan, Physica A **241**, 267 (1997).
[102] C. D. Mukherjee, K. K. Bardhan and M. B. Heaney, Phys. Rev. Lett. **83**, 1215 (1999).
[103] U. N. Nandi, C. D. Mukherjee and K. K. Bardhan, Physica B **279**, 72 (2000).
[104] K. K. Bardhan and C. D. Mukherjee, Phys. Rev. B **65**, 212302 (2002).
[105] C. D. Mukherjee and K. K. Bardhan, Phys. Rev. Lett. **91**, 025702 (2003).
[106] R. Burioni, D. Cassi, G. Giusiano and S. Regina, Phys. Rev. E **67**, 016116 (2003).
[107] C. J. G. Evertsz and B. B. Mandelbrot, *in the appendix of* Chaos and Fractals *by H. O. Peitgen, H. Jürgens and D. Saupe*, Springer, New York, 1992.

Chapter 2

Directed Spiral Percolation Model

The Monte Carlo (MC) techniques[1–3] are generally used to generate percolation clusters. In order to calculate the expectation values of the physical quantities, two different MC sampling averaging methods are available: (i) random sampling average and (ii) importance sampling average. If the states of a system are restricted on certain portion of the phase space, importance sampling is applicable. On the other hand, if the states are uniformly distributed all over the phase space random sampling is more appropriate. In a geometrical model like percolation, random sampling is found suitable and produces good estimates of the expectation values. The expectation values of the cluster related geometrical quantities are then obtained here by random sampling average only. A lattice configuration in percolation is generated by occupying the sites of a lattice completely randomly with a probability p or remain unoccupied with a probability $q = 1 - p$[4–6]. In random sampling average, a large number of lattice configurations for a given p are generated and all the configurations are considered with equal probability. There are many algorithms available in the literature for generating percolation clusters via MC[4–14]. Hosen-Kopelman[15] and Leath[16] algorithms are the commonly used algorithms.

In the Hosen-Kopelman algorithm, all the lattice sites are called sequentially for occupation with a probability p. A cluster is a collection of occupied sites connected by nearest neighbour bonds. Occupied sites belonging to the same percolation cluster are then identified through Hosen-Kopelman algorithm and are labeled by the same number. Different labels are assigned to different clusters. The algorithm is quite tricky and the detailed description could be found in Ref. [15] and also in the other literature[4,5].

In the Leath algorithm[16], a single cluster is generated in a lattice configuration. The central site of the lattice is occupied with unit probability and the percolation

cluster grows starting from the central site of a lattice occupying the nearest neighbours of the already occupied sites with probability p. The growth of the cluster stops if no site is available for occupation. Details of the algorithm is discussed in Refs. [4,5].

In the presence of rotational constraint, it is easy to grow a percolation cluster following Leath algorithm than Hosen-Kopelman [17,18]. Implementation of rotational constraint after generating the cluster is found difficult than generating the cluster following the rotational constraint. In order to generate DSP clusters in the presence of both the directional and rotational constraints, a single cluster growth Monte Carlo (MC) algorithm is then developed following the original algorithm of Leath. In the following, the DSP model will be described and the new single cluster growth algorithm to generate the DSP clusters will be illustrated. Percolation threshold for the DSP model will be identified and the spanning cluster morphology will be discussed.

2.1 DSP model and single cluster growth algorithm

A single cluster growth Monte Carlo (MC) algorithm is developed for the DSP model in 2-dimensions ($2D$). The model will be demonstrated here on the square and triangular lattices of size $L \times L$. The $2D$ lattice is considered in the xy plane. A left to right directional constraint and a clockwise rotational constraint are considered. In this percolation model, both the directional and rotational constraints are present simultaneously. In the case of positively charged particles, the left to right directional constraint E represents an in-plane electric field in the positive x direction and the clockwise rotational constraint B represents a magnetic field perpendicular to the plane of the lattice and along the positive z direction of the right handed coordinate system. A possible path of a particle under both the constraints is shown in Figure 2.1.

In generating a percolation cluster, the directional and rotational constraints determine the eligibility of the empty nearest neighbours for occupation. In the single cluster growth algorithm, the central site of the lattice is occupied with unit probability. The nearest neighbours of the central site are occupied with equal probability p in the first MC time step. As soon as a site is occupied, the direction from which it was occupied is assigned to it. Lists of eligible sites for occupation in the next MC time steps are then prepared. Due to the directional constraint, an

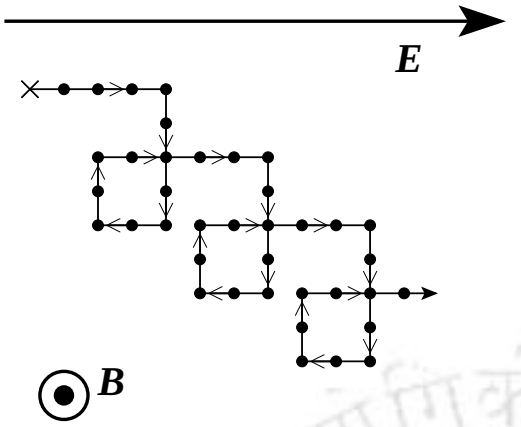

Figure 2.1: A possible path of a particle under the left to right directional (E) and the clockwisely rotational (B) constraints. The particle started from the site marked by a cross. The black dots represent the visited sites during the motion.

empty site on the right of an occupied site is always eligible for occupation. Due to the clockwise rotational constraint, empty sites in the forward direction and in the clockwise rotational direction (with respect to the forward direction) of an occupied site are eligible for occupation. However, a site index appears only once in the list of eligible sites at any time step. The eligible sites are then occupied with probability p. A random number r is called and compared with the occupation probability p. The pseudo-random number generator `ran2()`, developed by Press *et al* in Ref. [19] is used here. The algorithm is based on a multiplicative linear congruential generators by L'Ecuyer[20,21]. This has a period of more than 10^{18} which is far more than what is needed by the simulation here. If $r \leq p$, the site is occupied, otherwise it is rejected. In this algorithm, an occupied site can be reoccupied from a different direction but it is forbidden for occupation from the same direction. Once a site is rejected for occupation it is forbidden for occupation throughout the simulation from any possible direction. Each MC time step can be considered as a parallel update of nearest neighbours of already occupied sites. The growth of a cluster stops if there is no eligible site available for occupation.

Identification of eligible nearest neighbours for occupation at a MC step on the square lattice is illustrated in Figure 2.2. In the case of a square lattice, there are four nearest neighbours of a site and correspondingly, the coordination number $Z = 4$. The nearest neighbours are labeled accordingly. The directional constraint is represented by two long arrows from the left to the right. The presence of clockwise rotational constraint is shown by the encircled dots. The black circles represent the occupied sites and the open circles represent the empty sites. In the figures, the empty nearest neighbours of the central occupied site will be selected for occupation in this step. The direction from which the central site is occupied is represented by a short thick arrow. The dotted arrow indicates the eligible nearest neighbour due

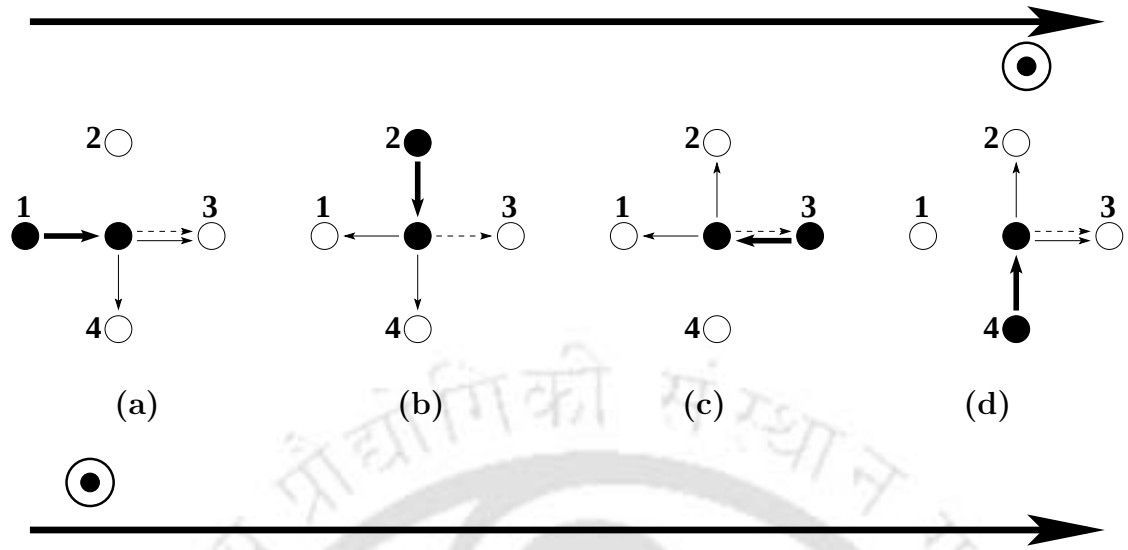

Figure 2.2: Selection of eligible empty nearest neighbors for occupation in a MC time step is demonstrated on the square lattice. Black circles are the occupied sites and open circles are the empty sites. Two thick long arrows from left to right represent the directional constraint. The presence of clockwise rotational constraint is shown by the encircled dots. The direction from which the central site is occupied is indicated by a short thick arrow. The dotted arrow indicates the sites allowed by the directional constraint and the thin arrows indicate the sites allowed by the rotational constraint.

to directional constraint and the thin arrows indicate the eligible nearest neighbours due to rotational constraint for occupation. Since the directional constraint is to the right, an empty site on the right of the occupied site is always eligible for occupation. Therefore, on the square lattice, site 3 is always eligible for occupation due to directional constraint (Figure 2.2). But as the rotational constraint acts in the forward and clockwise direction, the sites accessible for occupation due to the rotational constraint depend on the direction of approach to the present occupied site. On the square lattice, a site could be approached from 4 possible directions. In Figure 2.2(a), the central site is occupied from site 1 on the left. Thus, site 3 in the forward direction and site 4 in the clockwise direction are the eligible sites for occupation due to the rotational constraint. In this situation, sites 3 and 4 are then the only eligible sites for occupation in the next time step due to both the constraints. In Figure 2.2(b), as the central site is occupied from site 2 on the top, sites 4 and 1 are the eligible sites for occupation due to the rotational constraint. Therefore, the available sites for occupation are 1, 3 and 4 due to both the constraints in this case. In Figure 2.2(c), the eligible sites for occupation are 1 and 2 due to the rotational constraint and site 3 due to the directional constraint. Note that, site 3 is

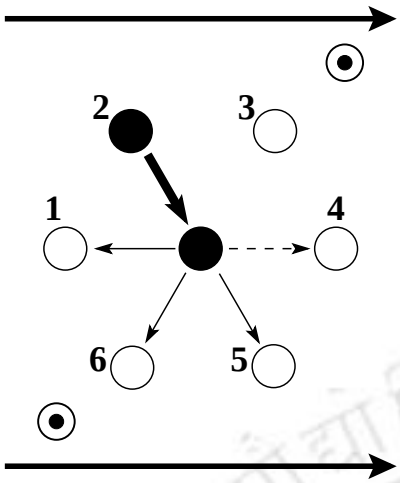

Figure 2.3: Selection of eligible empty nearest neighbors for occupation in a MC time step is demonstrated on the triangular lattice. The symbols have the same meaning as in Figure 2.2. There is one extra component due to the rotational constraint available on the triangular lattice than on the square lattice.

already an occupied site and could be reoccupied from a different direction. A site is forbidden for occupation from the same direction. On the square lattice, a site then could be occupied at most 4 times from 4 possible directions. This is unlike the case of the ordinary and directed percolations where a site is occupied only once. In Figure 2.2(d), sites 2 and 3 are eligible for occupation due to both the constraints. The eligible sites are then occupied with probability p. Once a site is rejected for occupation, it is not considered for occupation throughout the simulation.

Selection of eligible nearest neighbours for occupation on the triangular lattice is now illustrated in Figure 2.3. As the direction constraint is to the right, site 4 is always eligible for occupation due to the directional constraint. On the triangular lattice, there are six nearest neighbours of a site and correspondingly, the coordination number $Z = 6$ here which is higher than that of the square lattice. Due to this, there is an extra flexibility of selecting eligible sites by the spiral constraint on the triangular lattice than the square lattice. Here there are 6 possible directions of approach, from which a site can be occupied. In the configuration shown in Figure 2.3, the central site is approached from the nearest neighbour 2. In this situation, site 5 in the forward direction and sites 6 and 1 in the clockwisely rotational directions are eligible for occupation due to the spiral constraint. Thus, on the triangular lattice there are three empty nearest neighbours are available for occupation due to the rotational constraint whereas there are only two such sites available on the square lattice. The available sites for occupation are then 4, 5, 6 and 1 due to both the constraints in this case on the triangular lattice. It should be noted that the direction of the rotational constraint is not fixed in space and it depends on the previous time step whereas that of the directional constraint remains fixed in space. In that sense, the directional constraint is a global constraint and the rotational constraint

is a local constraint in the model. After selecting the eligible sites for occupation, they are occupied with probability p. In this way, the growth of the DSP cluster continues until no more site is available for occupation. Detailed description of the model on the square and triangular lattices have been elaborated in Refs. [22] and [23], respectively.

Algorithm:

A step wise algorithm for generating a DSP cluster is given here:

Step 1. Two arrays IOCC(INOW) and JVISIT(IV,INOW) are taken. INOW represents the lattice index. IV changes from 1 to Z, the coordination number of the lattice and it represents different directions of access to nearest neighbours on a given lattice. IOCC(INOW) represents the status of the lattice sites, unoccupied, occupied and rejected. JVISIT(IV,INOW) represents the direction from which a site is occupied.

Step 2. Initially all sites are set to IOCC(INOW) = 0 since they are unoccupied. Moreover since no direction assigned initially, JVISIT(IV,INOW) = 0 for all the sites.

Step 3. The central site of the lattice is occupied with probability $p = 1$ and IOCC(INOW) = 1 for the central site.

Step 4. A list of nearest neighbours of the central site is prepared which are eligible sites for occupation in the next step.

Step 5. The sites from the list of eligible sites for occupation are then occupied with probability p. A random number r is called and compared with p. If $r \leq p$, the site is occupied otherwise it is rejected. If a site is occupied its status is set as IOCC(INOW) = 1. If a site is called for occupation and not occupied (rejected) its status is made IOCC(INOW) = 2. As soon as a site is occupied the direction from which it is occupied is set as JVISIT(IV,INOW) = IV. On a square lattice, IV=1 means left, IV=2 means up, IV=3 means right, IV=4 means down. On the triangular lattice IV changes from 1 to 6.

Step 6. List of nearest neighbours of the sites occupied in the last time step which are eligible for occupation due to the rotational and directional constraints is then prepared. On a square lattice, two sites in the directions JVISIT(IV,INOW) and JVISIT(IV,INOW) + 1 from the present site INOW are eligible for occupation due

to the rotational constraint. The site on the right IV=3 of the present site is always eligible for occupation due to the left to right directional constraint. However, any site index appears only once in the list of eligible sites. {JNOW} is the list of eligible sites in a time step. The eligible sites should satisfy the condition either IOCC(JNOW) = 0 or IOCC(JNOW) = 1 and JVISIT(IV,JNOW) $\neq$ IV.

Step 7. If the length of the list is non-zero go to Step 5 otherwise stop.

Periodic boundary condition:

In order to study and predict the macroscopic properties of a real system through simulation, one needs to consider a lattice of linear size $L \to \infty$. However, computer simulations are performed only on small finite systems because of the limitations in the computer memory and computational time. In a finite system, a large number of sites are near the surface of the lattice imposing a surface effect in the simulation. This is so because, the sites at the boundaries have fewer bonds than those inside the lattice. In this situation, periodic boundary conditions (PBC) are generally used to eliminate the surface effects[24–26]. During the growth of a percolation cluster, it can reach the boundary of the actual lattice. By applying the periodic boundary condition it can be grown further inside the lattice through the opposite boundaries. In this way, the boundary effect could be eliminated in the simulation and only the cluster boundary can prevent further growth of the cluster. Though there is no rigid lattice boundary, the spatial extension of the cluster cannot be larger than the

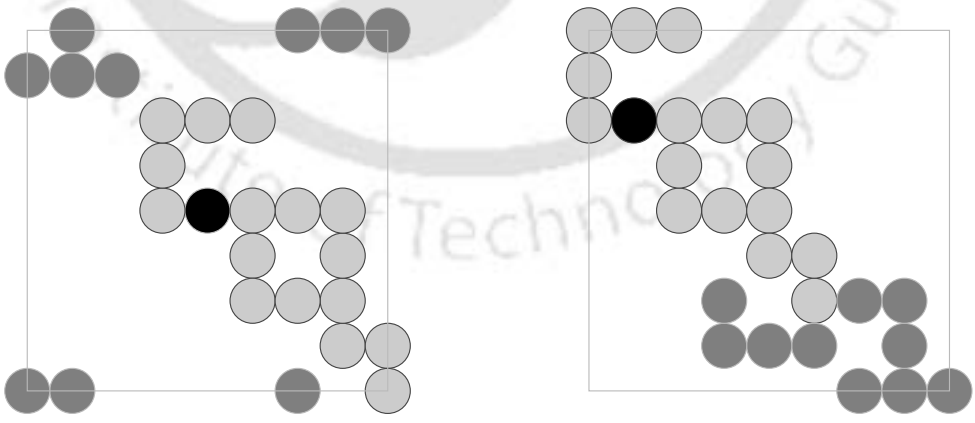

(a) (b)

Figure 2.4: DSP cluster grown on a 9×9 square lattice at $p = 0.5$ under periodic boundary conditions shown in (a) actual lattice coordinates and in (b) real spatial coordinates. The growth is started from the central black site. The gray circles are the occupied sites. Sites in the dark gray shade are occupied due to PBC.

linear size of the lattice as the cluster can only grow as large as the size of the whole lattice.

To illustrate the effect of periodic boundary conditions on the cluster growth, a small DSP cluster is grown on a 9×9 square lattice. Periodic boundary conditions are applied in both the x and y directions of the $2D$ lattice and demonstrated in Figure 2.4. The black circle represents the central site of the lattice from which the cluster is grown. Light gray circles represent the other occupied sites. Dark gray circles represent the sites occupied due to PBC. As the cluster grows, the coordinates (x,y) of the occupied sites are stored. The coordinates are adjusted accordingly whenever the boundary is crossed. After adjustment of the coordinates, the cluster in a shifted coordinate space is obtained. It is shown in Figure 2.4(b). At each time step the span of the cluster in the x direction $L_x = x_{max} - x_{min}$ and in the y direction $L_y = y_{max} - y_{min}$ are determined. If the extensions are found as L_x or $L_y \geq L$, the system size, then the cluster is considered to be a spanning cluster. At the critical percolation probability p_c, a spanning cluster appears in the system for the first time.

Computations are performed in a 64-bit (high performance computing) Linux cluster machine including a Xeon master node and 10 slave nodes each having 3GHz Intel P4 processors. Each slave node has 1GB of Random Access Memory. With this computational resource, maximum lattice size of $2^{11} \times 2^{11}$ was possible to consider for simulation.

2.2 Determination of percolation threshold

The percolation threshold or the critical probability p_c is defined as the maximum site occupation probability at which a spanning cluster appears for the first time in the system[27,28]. The percolation threshold is determined by generating a large number of clusters as a function of the occupation probability p and determining the probability to have a spanning cluster. The probability to have a spanning cluster is given by,

$$P_{sp}(p) = \frac{N_{sp}(p)}{N_{tot}} \tag{2.1}$$

where $N_{sp}(p)$ is the number of spanning clusters out of total N_{tot} clusters generated at a given site occupation probability p. The spanning probability $P_{sp} = 1$ at $p = 1$ and it goes continuously to zero at $p = p_c$ as p decreases. To determine p_c, clusters are generated on a large lattice of size $2^{11} \times 2^{11}$. Total $N_{tot} = 5 \times 10^4$ clusters

Square Lattice		Triangular Lattice	
p	P_{sp}	p	P_{sp}
0.6510	0.0105	0.5640	0.0014
0.6515	0.0180	0.5645	0.0039
0.6520	0.0262	0.5650	0.0066
0.6525	0.0361	0.5655	0.0106
0.6530	0.0489	0.5660	0.0175
0.6535	0.0694	0.5665	0.0282
0.6540	0.0953	0.5670	0.0416
0.6545	0.1270	0.5675	0.0658
0.6550	0.1656	0.5680	0.0889
0.6555	0.2089	0.5685	0.1239
0.6560	0.2466	0.5690	0.1619
0.6565	0.2842	0.5695	0.2049
0.6570	0.3219	0.5700	0.2522
0.6575	0.3539	0.5705	0.3054
0.6580	0.3878	0.5710	0.3515
0.6585	0.4141	0.5715	0.3994
0.6590	0.4442	0.5720	0.4445
0.6595	0.4687	0.5725	0.4792
0.6600	0.4876	0.5730	0.5123
0.6605	0.5045	0.5735	0.5440
0.6610	0.5158	0.5740	0.5664

Table 2.1: Values of spanning probability P_{sp} versus site occupation probability p for the DSP model measured on the square and the triangular lattices of linear size $L = 2^{11}$.

are generated at different occupation probabilities p in an interval of $\Delta p = 0.0005$. Values of P_{sp} measured at different occupation probabilities p on the square and triangular lattices are given in Table 2.1. P_{sp} is plotted against p in Figure 2.5(a) for the square lattice and in 2.5(b) for the triangular lattice. Note that, P_{sp} is not going to zero sharply at a particular value of p. This is due to the finite size of the lattice chosen here. The percolation threshold p_c then can be determined from the value of p at which the maximum rate of change of P_{sp} occurs. The numerical derivative dP_{sp}/dp of the series of data points P_{sp} with respect to p is evaluated using the central difference method[19],

$$\frac{dP_{sp}(p)}{dp} = \frac{P_{sp}(p+\Delta p) - P_{sp}(p-\Delta p)}{2\Delta p} + O\{(\Delta p)^2\} \tag{2.2}$$

where $O\{(\Delta p)^2\}$ is the order of error. The derivative of P_{sp} is then plotted against p in Figure 2.5(a) for the square lattice and for the triangular lattice in Figure 2.5(b). The maximum of the dP_{sp}/dp represents the maximum slope of the P_{sp} versus p plot.

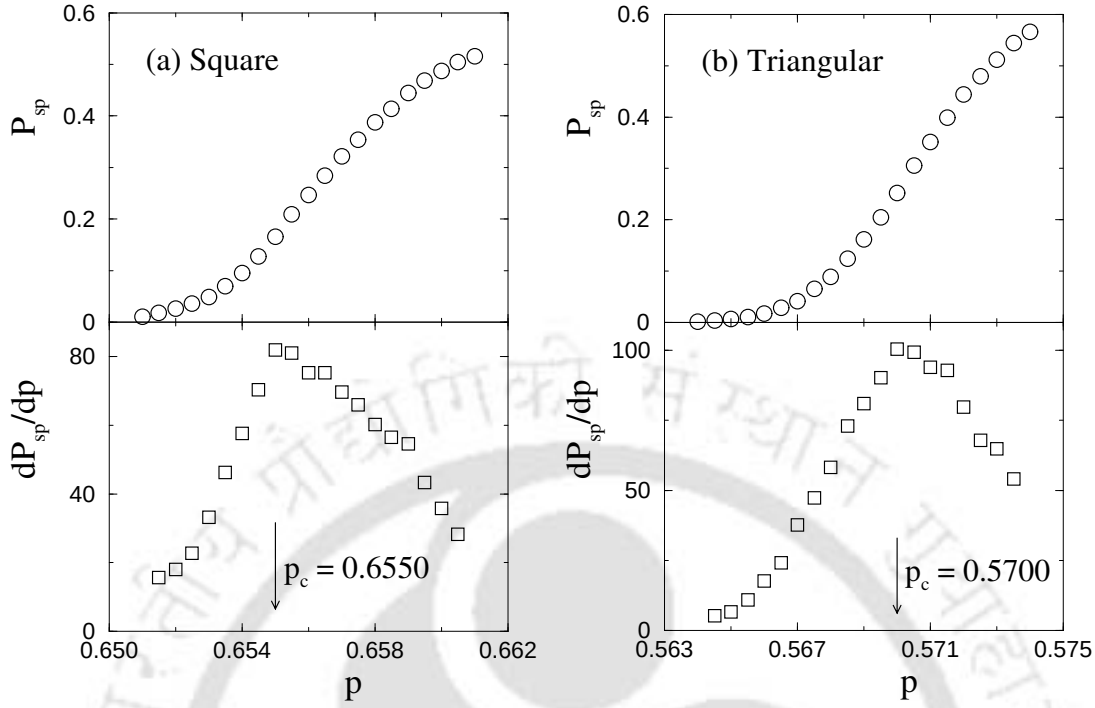

Figure 2.5: Plot of spanning probability P_{sp} (○) and the slope dP_{sp}/dp (□) versus p for the (a) square and (b) triangular lattices. The critical probability p_c is determined from the maximum slope. p_c is obtained as (a) 0.6550 ± 0.0005 for the square lattice and (b) 0.5700 ± 0.0005 for the triangular lattice.

The percolation threshold p_c is then identified from maximum of the dP_{sp}/dp versus p curve. p_c is obtained as 0.6550 ± 0.0005 on the square lattice and 0.5700 ± 0.0005 on the triangular lattice. The percolation threshold is a non-universal quantity and in general, it varies with the lattice structure. The values of p_cs obtained on the square and triangular lattices for the DSP model are reported in Ref. [23]. It should mentioned here that the percolation threshold for the DSP model on the square lattice was first identified by Santra[22] with lesser precision (± 0.001) on a smaller lattice of linear size $L = 2^{10}$. In Table 2.2, a comparison of the percolation thresholds of DSP model is made with that of other percolation models OP, DP and

Percolation model	Percolation threshold p_c	
	Square Lattice	Triangular Lattice
OP[27–31]	0.5927460	0.5(1/2)
DP[10,32–34]	0.705489	0.595646
SP[17,18,35]	0.712	0.667
DSP[22,23]	0.6550	0.5700

Table 2.2: Site percolation thresholds (p_c) for different percolation models on the square and triangular lattices.

SP. Similar to other models, in DSP also p_c is found less on the triangular lattice than that on the square lattice. This is due to the higher coordination number on the triangular lattice. Also notice that, on both the lattices, p_cs of DSP model are higher than the OP model and lesser than those of the other models DP and SP. In OP, as there is no constraint on the system, clusters can grow faster and consequently p_c is less than other constrained models. Since in DSP, both the directional and rotational constraints are present, more sites are eligible for occupation in a single MC step than in the cases of DP and SP where only one constraint is present. Due to this reason, the percolation thresholds of DSP model on both the square and triangular lattices are expected to be smaller than those of DP or SP model.

2.3 DSP spanning cluster morphology

Typical spanning DSP clusters on the square and triangular lattices of linear size $L = 2^8$ at $p = p_c$ are shown in Figures 2.6(a) and 2.6(b) respectively. There are few things to notice. First, the clusters are highly anisotropic in geometry similar to the DP clusters different from isotropic SP clusters. But the growth of the cluster is along the upper left to the lower right diagonal of the lattice and it is not along the applied directional field E as in the DP clusters. If one considers clustering of classical charged particles in the presence crossed electric field (directional constraint) and magnetic field perpendicular to the plane of motion (rotational constraint), then there will be a magnetic force E_H, shown in Figure 2.6, on the positively charged particle perpendicular to both the fields. Consequently, an effective field E_{eff} will develop in the system along the upper left to the lower right diagonal of the lattice. It is interesting to notice that the DSP clusters are growing along this effective direction. Though the DSP clusters grow along an effective field, geometrically it is very different from a DP cluster shown in Figure 1.6. It is to be noted that, in a material, during the transport of charged particles under crossed electric and magnetic fields, a Hall field develops perpendicular to both the fields. The deflection of charged particles in the transverse direction stops as soon an the Hall field becomes equal to the magnetic force on the particle. In the DSP model, it seems that a fictitious Hall field opposite to E_H appears in the system which in effect stops the growth of the cluster. This is a new observation in percolation theory. Second, the spanning clusters are highly rarefied. They contain holes of all possible sizes and seem to be self similar and fractal objects. As the clusters grow, more and more vacancies are generated into the cluster. This is because, the clockwise rotational

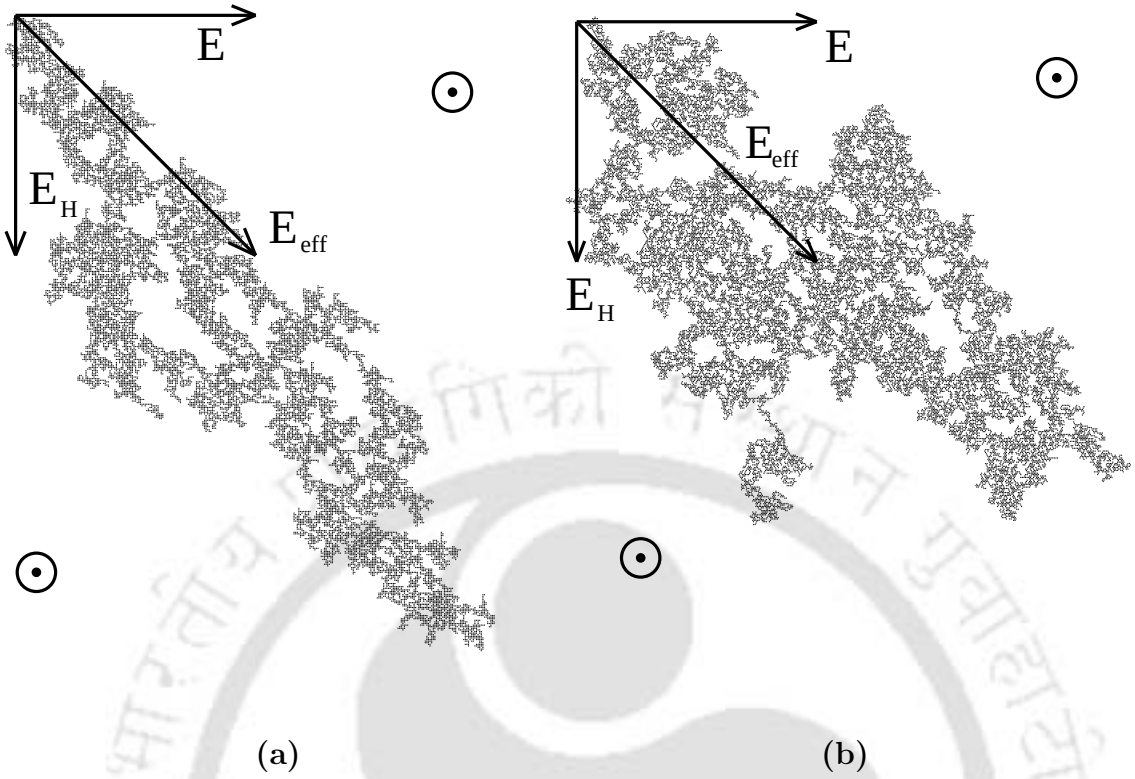

Figure 2.6: Spanning DSP clusters on the (a) square and (b) triangular lattices of size $2^8 \times 2^8$ generated at their respective percolation thresholds. The black dots are occupied sites. The clusters have holes of all possible sizes. The elongation of both the clusters are along the upper left to the lower right diagonal and not along the imposed directional constraint from left to right.

constraint tries to occupy sites away from the directional constraint whereas the directional constraint tries to occupy sites along itself in the x-direction. As a result, the clusters become rarefied and wider as it grows away from the origin (see Figure 2.6). Third, there exist chiral (clockwisely rotated) dangling ends on the perimeter of the clusters as in the case of SP clusters. This is due to the presence of rotational constraint in both the models. Forth, among the two clusters on the two lattices, it can be seen that the cluster on the triangular lattice is much more compact than that on the square lattice. Also, the anisotropy of the cluster on the triangular lattice is less than that on the square lattice.

Thus, a new type of percolation clusters are generated in the DSP model which contain some of the features of both the DP and SP clusters. The combined directed and spiral constraints produce highly rarefied anisotropic spiral clusters along with the development of Hall field in the system [23]. The effect of these three features *i.e.*; anisotropy [36], spiral constraint [35] and volume fraction [37], on the ordinary percolation clusters have been studied independently. Each of them corresponds to different

critical behaviour and consequently belongs to new universality classes. Here in DSP model, a new critical behaviour is expected at the percolation threshold because of the presence of all three features in the same cluster. It is then interesting to study the critical properties of the DSP clusters. Measuring the geometrical quantities related to the clusters generated in the DSP model at the critical regime, critical exponents will be estimated and the universality class of the DSP model will be identified in the following chapters.

2.4 Summary

In the presence of directional and rotational constraints simultaneously in a percolating system, a new site percolation model, the directed spiral percolation (DSP) is constructed. A single cluster growth Monte Carlo algorithm is developed to generate the DSP clusters on the square and triangular lattices in $2D$. The percolation threshold p_c at which a spanning cluster appears for the first time in the system has been determined for both the lattices. It is found to be higher than that of the OP model but less than that of the other models like DP and SP. Spanning clusters are generated at the percolation threshold. The morphology of the spanning clusters are found highly rarefied and contain holes of all possible sizes. They are self similar and fractal objects. The DSP clusters contain chiral dangling ends. Moreover, the DSP clusters are found anisotropic. The clusters grow in an effective direction different from the applied directional constraint. The presence of both the directional and rotational constraints simultaneously in the model leads to the development of a fictitious Hall field in the system. The new type of percolation clusters generated in the DSP model now need appropriate characterization. Critical properties of the DSP model will be studied from several different aspects and the results will be reported in the following chapters.

Bibliography

[1] D. P. Landau and K. Binder, *A Guide to Monte Carlo Simulations in Statistical Physics*, Cambridge University Press, 2005.

[2] K. Binder and D. W. Heermann, *Monte Carlo Simulation in Statistical Physics: an Introduction*, Springer Verlag, Berlin, 1992.

[3] M. E. J. Newman and G. T. Barkema, *Monte Carlo Methods in Statistical Physics*, Oxford University Press, USA, 1999.

[4] D. Stauffer and A. Aharony, *Introduction to Percolation Theory*, Taylor and Francis, London, 2nd edition, 1994.
[5] A. Bunde and S. Havlin, *Fractals and Disordered Systems*, Springer-Verlag, Berlin, 1991.
[6] B. Bollobás and O. Riordan, *Percolation*, Cambridge University Press, 2006.
[7] N. R. Moloney and K. Christensen, *Complexity And Criticality*, Imperial College Press, 2005.
[8] M. Sweeny, Phys. Rev. B **27**, 4445 (1983).
[9] K. Debell, T. Lookman and D. L. Hunter, Physics Letters A **101**, 221 (1984).
[10] J. K. Williams and N. D. Mackenzie, J. Phys. A: Math. Gen. **17**, 3343 (1984).
[11] M. Corsten, N. Jan and R. Jerrard, Physica A **156**, 781 (1989).
[12] L. A. Pugnaloni and F. Vericat, Journal of Chemical Physics **110**, 4028 (1999).
[13] C. K. Hu, J. A. Chen, N. S. Izmailian and P. Kleban, Computer Physics Communications **126**, 77 (2000).
[14] R. M. Ziff and M. E. J. Newman, Phys. Rev. E **64**, 016706 (2001).
[15] J. Hosen and R. Kopelman, Phys. Rev. B **14**, 3426 (1976).
[16] P. L. Leath, Phys. Rev. B **14**, 5046 (1976).
[17] P. Ray and I. Bose, J. Phys. A **21**, 555 (1988).
[18] S. B. Santra and I. Bose, J. Phys. A **24**, 2367 (1991).
[19] W. H. Press, *Numerical Recipes in FORTRAN: The Art of Scientific Computing*, Cambridge University Press, 1992.
[20] P. L'Ecuyer, Communications of the ACM **31**, 742 (1988).
[21] S. K. Park and K. W. Miller, Communications of the ACM **31**, 1192 (1988).
[22] S. B. Santra, Eur. Phys. J. B **33**, 75 (2003).
[23] S. Sinha and S. B. Santra, Eur. Phys. J. B **39**, 513 (2004).
[24] L. J. Chen, C. K. Hu and K. S. Mak, Computer Physics Communications **66**, 377 (1991).
[25] P. J. Forrester, J. Stat. Phys. **63**, 491 (1991).
[26] M. S. Watanabe, Phys. Rev. E **51**, 3945 (1995).
[27] D. Stauffer, Phys. Rep. **54**, 1 (1979).
[28] J. W. Essam, Rep. Prog. Phys. **43**, 833 (1980).
[29] M. P. M. den Nijs, J. Phys. A **12**, 1857 (1997).
[30] B. Nienhuis, J. Phys. A **15**, 199 (1982).
[31] R. M. Ziff and B. Sapoval, J. Phys. A **19**, L1169 (1987).
[32] J. W. Essam, A. J. Guttmann and K. DéBell, J. Phys. A: Math. Gen. **21**, 3815 (1988).
[33] J. W. Essam, K. DéBell, J. Adler and F. M. Bhatti, Phys. Rev. B **33**, 1982 (1986).
[34] S. P. Obukhov, Physica A **101**, 145 (1980).
[35] S. B. Santra and I. Bose, J. Phys. A **25**, 1105 (1992).
[36] D. Dhar and M. Barma, J. Phys. C: Solid State Phys. **14**, L1 (1981).
[37] J. Kertész, J. Phys. France **42**, L393 (1981).

Chapter 3

DSP Cluster Properties and Scaling

Just as the thermodynamic quantities become singular at the critical point[1,2], geometrical quantities like average cluster size, correlation length, etc. in percolation become singular at the percolation threshold p_c. The singularities of the geometrical quantities in percolation are also characterized by well-defined critical exponents. The critical exponents satisfy certain scaling relations among them[3–6] similar to those in thermodynamic critical phenomena. This is a consequence of the fact that the thermodynamic potential functions become generalized homogeneous function at the critical point. A new type of percolation clusters are generated in the DSP model. DSP clusters are found highly rarefied and anisotropic in nature with chiral dangling ends. It is now essential to define the singularities associated with the geometrical quantities defined for these highly rarefied and anisotropic clusters. In order to characterize the singularities associated with the cluster related quantities a scaling theory is needed to be developed. The scaling theory for the DSP model is developed assuming the cluster size distribution function $P_s(p)$ as a generalized homogeneous function of the site occupation probability p and the cluster size s.

In the following, the values of the critical exponents associated with cluster properties will be measured via Monte Carlo simulation following the algorithm defined in the previous chapter. The proposed scaling theory will then be verified using the measured critical exponents.

3.1 Scaling theory for the DSP model

In order to study the cluster related quantities of a percolation model generally a generating function or cluster size distribution function, analogous to the partition function in statistical mechanics, is constructed[3,4]. The cluster size distribution

function $P_s(p)$ is the probability to have a s-sited cluster if the lattice sites are occupied with a probability p. A cluster is a collection of occupied lattice sites connected by nearest neighbour bonds. For a given system of linear size L, the cluster size distribution function $P_s(p)$ can be defined as,

$$P_s(p) = \frac{N_s(p)}{N_{tot}} \tag{3.1}$$

where $N_s(p)$ is the number of s-sited clusters in a total of N_{tot} clusters generated with site occupation probability p. In the DSP model, clusters are generated under both the directed and rotational constraints using a single cluster growth algorithm developed in the previous chapter. In the single cluster growth method, the origin (the central site of the lattice) is occupied with unit probability. It is expected that the cluster size distribution function $P_s(p)$ becomes a generalized homogeneous function of two variables, namely inverse cluster size $1/s$ and $(p-p_c)$, as the percolation threshold p_c is approached, like the thermodynamic functions in critical phenomena. The scaling function form of the cluster size distribution is then assumed to be

$$\begin{aligned} P_s(p) &= s(1/s)^{\tau}\mathsf{f}[(p-p_c)/(1/s)^{\sigma}] \\ &= s^{-\tau+1}\mathsf{f}[s^{\sigma}(p-p_c)] \end{aligned} \tag{3.2}$$

where τ and σ are two exponents. All the relevant cluster related quantities then can be calculated by taking appropriate moments of the cluster size distribution function given in Eq. 3.2. As $p \to p_c$, the cluster related quantities become singular with specific critical exponents. Since the cluster related quantities are different moments of $P_s(p)$, the exponents describing their singularities at $p = p_c$ can be expressed in terms of τ and σ only. In other words, all the critical exponents associated with different cluster related quantities are not independent and will be related to τ and σ through different scaling relations. In the following, different geometrical quantities will be defined and the singularities associated with them will be identified. The scaling relations between the critical exponents will then be established.

A. Order parameter

The most distinguishing property of a phase transition is the order parameter which continuously goes to zero in the disordered phase from a non-zero value in the ordered phase. In the percolation transition, the order parameter is defined as the probability P_∞ that a site belongs to an infinite (spanning) cluster and it can be obtained from the zeroth moment of the cluster size distribution function $P_s(p)$.

The order parameter P_∞ is analogous to the spontaneous magnetization in ferro to para magnetic transition. The order parameter P_∞ then can be expressed as,

$$P_\infty = p - p\sum_s{}' P_s(p). \tag{3.3}$$

The leading singularity of P_∞ will be governed by $\sum_s' P_s(p)$, the zeroth moment of the cluster size distribution. The primed sum indicates that the spanning or infinite clusters are excluded from the sum. Below the percolation threshold p_c, there is no spanning cluster appears in the system and consequently $P_\infty = 0$ for all values of $p < p_c$. On the other hand, at $p = 1$ all the sites of the system are occupied with unit probability and the order parameter becomes $P_\infty = 1$. As $p \to p_c$ from above, P_∞ continuously goes to 0 as a power law given by

$$P_\infty \sim (p - p_c)^\beta, \quad \text{for} \quad p > p_c \tag{3.4}$$

where β is a critical exponent.

B. Average cluster size

An important cluster related quantity is the average cluster size χ which is analogous to the magnetic susceptibility. It is the average number of occupied lattice sites in a cluster, generated at a given site occupation probability p. In the single cluster growth method, it can be obtained from the first moment of the cluster size distribution function. The average cluster size χ is given as

$$\chi = \sum_s{}' sP_s(p). \tag{3.5}$$

Since for small values of p, only few small clusters appear, the average cluster size is expected to be small. As p approaches close to p_c, many large finite clusters will appear and consequently the average cluster size will be large. On the other hand, above p_c, for the large value of p, the probability to have a finite cluster is going to be small and consequently χ will be small. As $p \to p_c$, the average cluster size χ diverges from both sides of p_c with a critical exponent γ defined as,

$$\chi \sim |p - p_c|^{-\gamma}. \tag{3.6}$$

Next two higher moments of $P_s(p)$ can also be defined as

$$\chi_1 = \sum_s{}' s^2 P_s(p) \quad \text{and} \quad \chi_2 = \sum_s{}' s^3 P_s(p) \tag{3.7}$$

which are the second and third moments of $P_s(p)$. In the present context these higher moments have no physical meaning but might be useful in particular situations. The moments χ_1 and χ_2 also diverge with their respective critical exponents δ and η as $p \to p_c$. The critical exponents δ and η are defined as

$$\chi_1 \sim |p - p_c|^{-\delta} \text{ and } \chi_2 \sim |p - p_c|^{-\eta}. \tag{3.8}$$

C. Scaling relations

Since the cluster related quantities are just different moments of the cluster size distribution function $P_s(p)$, studying the singularity of the kth moment M_k of $P_s(p)$, the associated critical exponents can be expressed in terms of the exponents τ and σ appear in $P_s(p)$ (Eq. 3.2). The kth moment M_k of the cluster size distribution $P_s(p)$ is defined as,

$$M_k = \sum_s{}' s^k P_s(p) \tag{3.9}$$

where k is an integer. In the continuum limit, the summation can be replaced by an integration and the kth moment M_k of $P_s(p)$ can be written as

$$M_k = \int_0^\infty s^k P_s(p) ds = \int_0^\infty s^{-\tau+1+k} \mathsf{f}[(p - p_c)s^\sigma] ds. \tag{3.10}$$

Defining a scaled variable $z = s^\sigma(p - p_c)$, M_k can be obtained in terms of z as

$$M_k = (p - p_c)^{-(2+k-\tau)/\sigma} \frac{1}{\sigma} \int_z z^{-1+(2+k-\tau)/\sigma} \mathsf{f}(z) dz. \tag{3.11}$$

Since the integral will contribute a constant, it is then possible to obtain M_k without knowing the exact form of $\mathsf{f}(z)$. M_k then can be written directly as

$$M_k = \sum_s{}' s^k P_s(p) \sim |p - p_c|^{-(2+k-\tau)/\sigma}. \tag{3.12}$$

Different cluster related geometrical quantities can be obtained from Eq. 3.12 putting appropriate values of k. For $k = 0$, the 0th moment of cluster size distribution describes the singularity of the order parameter P_∞ as, $M_0 = \sum_s{}' P_s(p)$.

Therefore from Eq. 3.12, $P_\infty \sim (p-p_c)^{(\tau-2)/\sigma}$ for $p > p_c$. Hence the scaling relation between the order parameter exponent β and the cluster size distribution exponents τ and σ can be obtained as,

$$\beta = (\tau - 2)/\sigma. \tag{3.13}$$

Similarly, the average cluster size χ and next two higher moments χ_1 and χ_2 of $P_s(p)$ can be obtained for $k = 1$, 2 and 3 respectively as

$$\begin{aligned} M_1 &= \chi &&= \sum_s{}' sP_s(p) &&\sim |p-p_c|^{-(3-\tau)/\sigma} \\ M_2 &= \chi_1 &&= \sum_s{}' s^2P_s(p) &&\sim |p-p_c|^{-(4-\tau)/\sigma} \\ M_3 &= \chi_2 &&= \sum_s{}' s^3P_s(p) &&\sim |p-p_c|^{-(5-\tau)/\sigma}. \end{aligned} \tag{3.14}$$

Since, as $p \to p_c$, χ, χ_1 and χ_2 diverge with their respective critical exponents γ, δ and η, the following scaling relations can be obtained as,

$$\gamma = (3-\tau)/\sigma, \;\; \delta = (4-\tau)/\sigma \;\text{ and }\; \eta = (5-\tau)/\sigma. \tag{3.15}$$

Eliminating τ and σ from the above scaling relations in Eq. 3.13 and 3.15, scaling relations between β, γ, δ and η could be obtained as,

$$\delta = 2\gamma + \beta \quad \text{and} \quad \eta = 2\delta - \gamma. \tag{3.16}$$

Therefore, if the kth moment M_k of $P_s(p)$ become singular with a critical exponent q_k as

$$M_k \sim |p-p_c|^{-q_k} \tag{3.17}$$

then a general scaling relation between the moment exponents can be obtained as

$$q_{k+1} = 2q_k - q_{k-1} \tag{3.18}$$

for $k = 1, 2, 3, \cdots$ and note that $\beta = -q_0$.

D. Connectivity lengths

In the case of DSP model, the clusters generated are anisotropic in nature. Thus, two length scales, $\xi_\parallel$ and $\xi_\perp$, are needed to describe the connectivity of the occupied sites in a cluster. $\xi_\parallel$ is the connectivity length along the elongation of the cluster and $\xi_\perp$ is the connectivity length along the perpendicular direction to the elongation. To measure $\xi_\parallel$ and $\xi_\perp$, the moment of inertia tensor $\mathbf{T}$, a 2×2 matrix here, is calculated.

For a s-sited cluster, the xy component of the tensor $\mathbf{T}$ is given by

$$T_{xy} = \sum_{\ell=1}^{s} (x_\ell - x_0)(y_\ell - y_0) \tag{3.19}$$

where x_ℓ and y_ℓ are the x and y coordinates of the ℓth site and (x_0,y_0) is the coordinate of the center of mass of the cluster. The radii of gyration $R_\parallel(s)$ and $R_\perp(s)$ with respect to two principal axes are obtained as $R_\parallel^2(s) = \lambda_1/s$ and $R_\perp^2(s) = \lambda_2/s$ where λ_1 is the largest eigenvalue and λ_2 is the smallest eigenvalue of the 2×2 moment of inertia matrix $\mathbf{T}$. $R_\perp$ is about the axis passing through (x_0,y_0) and parallel to the elongation of the cluster and $R_\parallel$ is about the axis perpendicular to the elongation of the cluster and passing through (x_0,y_0). The connectivity lengths now can be determined as

$$\xi_\parallel^2 = \frac{2\sum_s' R_\parallel^2(s) s P_s(p)}{\sum_s' s P_s(p)} \quad \text{and} \quad \xi_\perp^2 = \frac{2\sum_s' R_\perp^2(s) s P_s(p)}{\sum_s' s P_s(p)}. \tag{3.20}$$

Note that, the connectivity lengths are weighted by the cluster size. For small value of p below p_c, the clusters generated are small, their elongation is less and thin as well. As p increases, the clusters elongation as well as thickness, the perpendicular extent also increases. Consequently, the connectivity lengths $\xi_\parallel$ and $\xi_\perp$ diverge with two different critical exponents $\nu_\parallel$ and $\nu_\perp$ as $p \to p_c$. The critical exponents $\nu_\parallel$ and $\nu_\perp$ are defined as

$$\xi_\parallel \sim |p - p_c|^{-\nu_\parallel} \quad \text{and} \quad \xi_\perp \sim |p - p_c|^{-\nu_\perp}. \tag{3.21}$$

E. Hyperscaling relations

The cluster mass is given by the number of sites s in the cluster and is expected to scale as $s \approx R_\parallel R_\perp^{(d_f-1)}$ at $p = p_c$ and above p_c, it should go as $s \approx R_\parallel R_\perp^{(d-1)}$ where d is the spatial dimension of the lattice and d_f is the fractal dimension of the infinite clusters generated on the same lattice. The percolation probability P_∞ is the ratio of the number of sites on the infinite cluster to the total number of sites,

$$P_\infty = \frac{R_\parallel R_\perp^{(d_f-1)}}{R_\parallel R_\perp^{(d-1)}} \tag{3.22}$$

for $R_\parallel < \xi_\parallel$ and $R_\perp < \xi_\perp$. Assuming $R_\parallel \sim \xi_\parallel$ and $R_\perp \sim \xi_\perp$, the above equation can

be expressed in terms of $|p - p_c|$ as,

$$P_\infty \sim \xi_\perp^{d_f - d} \sim |p - p_c|^{-\nu_\perp (d_f - d)}. \tag{3.23}$$

As $P_\infty \sim |p - p_c|^\beta$, the hyperscaling relation is obtained as,

$$\beta = (d - d_f)\nu_\perp. \tag{3.24}$$

Another hyperscaling relation can be obtained from $\xi_\perp$ as follows. In integral form, $\xi_\perp$ can be written as,

$$\xi_\perp^2 = \frac{2\int_0^\infty R_\perp^2 s P_s(p) ds}{\int_0^\infty s P_s(p) ds}. \tag{3.25}$$

Writing the integral in terms of the scaled variable $z = s^\sigma (p - p_c)$ and assuming

$$R_\perp^2 = \frac{s^{2/(d_f - 1)}}{R_\parallel^{2/(d_f - 1)}} \tag{3.26}$$

one has

$$\begin{aligned} \xi_\perp^2 &= 2R_\parallel^{-2/(d_f-1)} \frac{\int_z s^{\frac{2}{d_f-1} - \tau + 3} z^{-1} \mathsf{f}(z) dz}{\int_z s^{-\tau+3} z^{-1} \mathsf{f}(z) dz} \\ &\sim 2R_\parallel^{-2/(d_f-1)} (p - p_c)^{-2/(\sigma(d_f-1))}. \end{aligned}$$

Since $R_\parallel \sim \xi_\parallel \sim |p - p_c|^{-\nu_\parallel}$,

$$\xi_\perp^2 \sim (p - p_c)^{2(\nu_\parallel - 1/\sigma)/(d_f - 1)}$$

Again, since $\xi_\perp \sim |p - p_c|^{-\nu_\perp}$, the following hyperscaling relation can be obtained as,

$$\nu_\perp (d_f - 1) + \nu_\parallel = \frac{1}{\sigma} \tag{3.27}$$

Eliminating d_f from the above relations in Eq. 3.24 and 3.27, another scaling relation could be obtained as

$$\begin{aligned} (d-1)\nu_\perp + \nu_\parallel &= \gamma + 2\beta = 2\delta - 3\gamma = 3\eta - 4\delta & (3.28) \\ &= k q_k - (k+1) q_{k-1} & (3.29) \end{aligned}$$

where $k = 1, 2, 3, \cdots$ and $\beta = -q_0$. In the following, the values of the critical exponents will be determined and the scaling relations will be verified.

3.2 Results and discussion

To determine the fractal dimension and other critical exponents associated with different cluster related quantities of the DSP model, simulations are performed on the square and triangular lattices of size $L \times L$ in $2D$. In this chapter, a single large lattice of linear size $L = 2^{11}$ has been considered for estimating the values of the critical exponents. An average over 5×10^4 samples have been taken to measure any geometrical quantity. In the following sections, the results obtained on the square lattice will be present first. A comparison of the results obtained on the square lattice will be made with that of the other percolation models OP, DP and SP in order to determine the universality class of DSP model. Estimates of the critical exponents on the triangular lattice will then be reported and the results will be compared with that of the square lattice.

3.2.1 The square lattice results

A. Fractal dimension

It is already observed from the cluster geometry given in Figure 2.6 that, at the percolation threshold p_c, the spanning DSP clusters are rarefied and contain holes of all possible sizes (see Chapter 2). They seem to be self-similar on all length scales (larger than the unit size and smaller than the lattice size) and can be regarded as fractals. It was first noticed by Stanley[7] that the structure of the percolation clusters can be well described by the fractal concept[4,8,9]. The dimensionality of a fractal object is characterized by the fractal dimension d_f which is defined as,

$$M(r) \sim r^{d_f} \tag{3.30}$$

where, $M(r)$ is the mass of the object within a sphere of radius r.

The fractal dimension of the DSP cluster is determined here employing the box-counting method[8–13]. The method is widely used to determine the fractal dimension of many physical systems[14–19]. The algorithm used is briefly discussed here. In the box counting algorithm, the spanning percolation cluster at p_c on a single large lattice is considered. The $2D$ lattice of linear size L, which contains the cluster, is

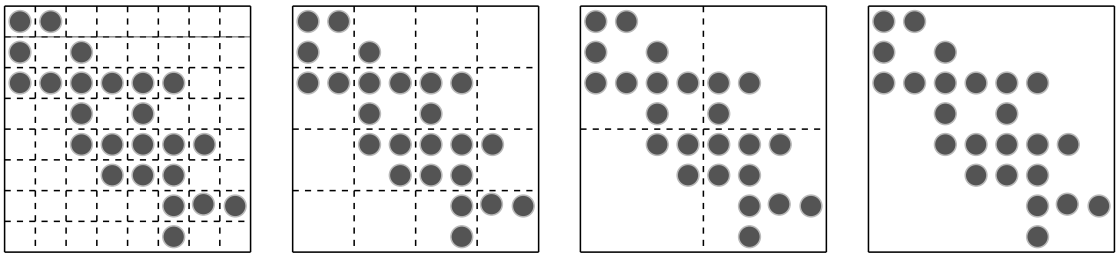

$\epsilon = 1$ $N_B(\epsilon) = 24$ | $\epsilon = 2$ $N_B(\epsilon) = 10$ | $\epsilon = 4$ $N_B(\epsilon) = 4$ | $\epsilon = 8$ $N_B(\epsilon) = 1$

Figure 3.1: Demonstration of box counting method for the determination of fractal dimension. The black circles represent the occupied sites of a spanning cluster generated on a $L = 8$ square lattice. The lattice is divided into smaller boxes of linear size $\epsilon = 1$, 2, 4 and 8, as shown by dotted lines. Corresponding number of occupied boxes are $N_B(\epsilon) = 24$, 10, 4 and 1 respectively.

then divided into $(L/\epsilon)^2$ number of smaller boxes of linear size ϵ. The number of boxes $N_B(\epsilon)$, which contain at least one occupied site of the cluster is then counted for a given box of dimension ϵ. The linear size ϵ of the box is then varied and the numbers of the occupied boxes $N_B(\epsilon)$ are counted as a function of the box size ϵ. The method is demonstrated in Figure 3.1 for a spanning cluster generated on a square lattice of size $L = 8$. The fractal dimension d_f can then be calculated using the scaling relation,

$$N_B(\epsilon) \sim \epsilon^{-d_f} \tag{3.31}$$

which is equivalent to the definition in Eq. 3.30. To determine the fractal dimension using this method, spanning DSP clusters are generated on the square lattice of

Box size (ϵ)	$N_B(\epsilon)$
1	0.607059×10^6
2	0.232126×10^6
4	0.706185×10^5
8	0.207980×10^5
16	0.611780×10^4
32	0.181782×10^4
64	0.550103×10^3
128	0.170391×10^3
256	0.535693×10^2
512	0.154015×10^2
1024	0.400000×10^1
2048	0.100000×10^1

Table 3.1: Number of the occupied boxes $N_B(\epsilon)$ versus box size ϵ measured using box counting algorithm for the spanning DSP clusters on the square lattice of linear size $L = 10^{11}$. Data are averaged over 5×10^4 spanning clusters.

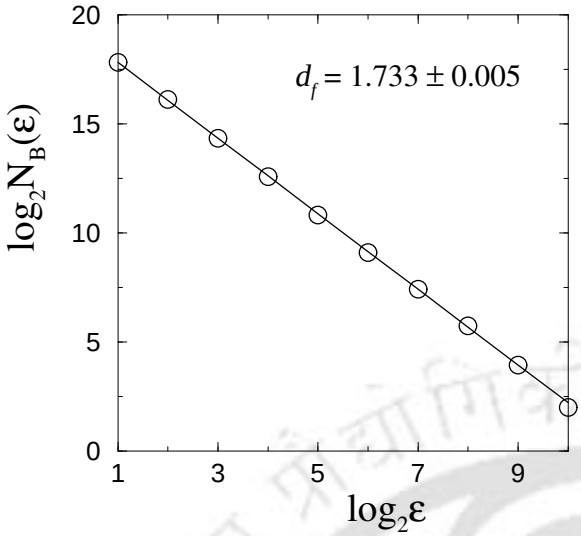

Figure 3.2: Number of boxes $N_B(\epsilon)$ is plotted against the box size ϵ measured for the DSP model on the square lattice of $L = 2^{11}$. From the slope, the fractal dimension is found as $d_f = 1.733 \pm 0.005$.

linear size $L = 2^{11}$ at the percolation threshold. The number of boxes $N_B(\epsilon)$ with at least one occupied site is then counted using box counting algorithm. The data are averaged over 5×10^4 samples. The values of $N_B(\epsilon)$ are listed in Table 3.1 as a function of box size ϵ. In Figure 3.2, $N_B(\epsilon)$ is plotted against the box size ϵ. A reasonably good straight line is obtained in the double logarithmic scale. From the slope, the fractal dimension d_f is found as $d_f = 1.733 \pm 0.005$ [20]. The error is due to the least squares fitting of the data points taking into account the statistical error of each point. The fractal dimension $d_f \approx 1.733$ obtained here is the smallest among the fractal dimensions obtained in other percolation models OP, DP and SP. The values of d_f in other percolation models are: $d_f(\mathrm{OP}) = 91/48$ [21,22], $d_f(\mathrm{DP}) \approx 1.765$ [23] and $d_f(\mathrm{SP}) \approx 1.957$ [24]. Also, the fractal dimension $d_f(\mathrm{DSP})$ obtained here is little higher than the fractal dimension 1.64 of ordinary lattice animals [25], large OP clusters below p_c. The infinite cluster generated in the DSP model on the square lattice is then the most rarefied one among the infinite clusters obtained in all four models. This is because, the clockwise rotational constraint tries to occupy sites away from the directional constraint whereas the directional constraint tries to occupy sites along itself in the x-direction. The effects of these two counter acting constraints are the following: the cluster with spiral dangling ends become rarefied and wider as it is away from the origin (see Chapter 2, Figure 2.6) and elongated along a clockwisely rotated direction from the original globally fixed directional constraint in the x-direction.

The fractal dimension of the DSP clusters can also be estimated by measuring the mass of the infinite cluster as a function of the linear size L of the system. It

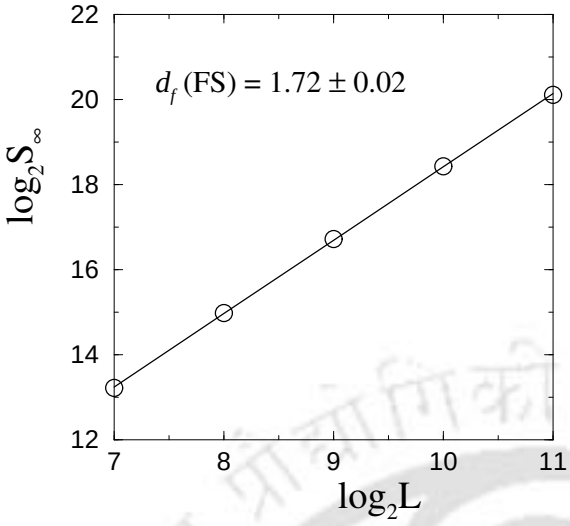

Figure 3.3: The mass of the largest spanning cluster S_∞, measured at p_c, is plotted against the system size L. From the slope, the fractal dimension is obtained as $d_f(\mathrm{FS}) = 1.72 \pm 0.02$ for the square lattice.

is expected that the mass of the largest infinite cluster S_∞ should scale with the system size L as

$$S_\infty \sim L^{d_f} \tag{3.32}$$

where d_f is the fractal dimension of the cluster. To determine d_f using this method, spanning clusters are generated on lattices of linear size L ranging from 2^7 to 2^{11} in the multiple of 2. For each lattice size, at least 5×10^4 spanning clusters are generated. In Figure 3.3, S_∞ is plotted against the system size L for the square lattice. Reasonably good straight line is obtained in log-log scale. The fractal dimension obtained from the slope of the plot is $d_f = 1.72 \pm 0.02$ [20]. Thus the value of the fractal dimension obtained using finite-size scaling method is within error bar with the other estimate using box counting algorithm.

Since the value of d_f is found different from that of the other percolation models, the values of the other critical exponents of the DSP model are also expected be different from those of other percolation models in order to satisfy the scaling relations among the critical exponents. It is then essential to measure all the critical exponents in order to determine the universality class of this model.

B. Moment exponents

To estimate the values of the critical exponents γ, δ and η, the average cluster size χ and two other higher moments χ_1 and χ_2 of cluster size distribution are measured generating 5×10^4 finite clusters below p_c on the square lattice of linear size $L = 2^{11}$ at different values of p. Measured values of χ, χ_1 and χ_2 are tabulated in Table 3.2. In Figure 3.4, χ, χ_1 and χ_2 are plotted against $|p - p_c|$. The circles represent χ, the squares represent χ_1 and the triangles represent χ_2. The exponent values are

p	χ	χ_1	χ_2
0.405	0.79047509×10^1	0.11337509×10^3	0.29781485×10^4
0.478	0.14638948×10^2	0.41716664×10^3	0.22515018×10^5
0.530	0.26835540×10^2	0.16804191×10^4	0.18960124×10^6
0.567	0.51334360×10^2	0.68754898×10^4	0.17009391×10^7
0.593	0.10065892×10^3	0.29612493×10^5	0.14943824×10^8
0.611	0.19383622×10^3	0.12440329×10^6	0.13960914×10^9
0.624	0.37697502×10^3	0.52592128×10^6	$0.13028068 \times 10^{10}$
0.633	0.72462980×10^3	0.19710049×10^7	$0.11316431 \times 10^{11}$
0.639	0.12755467×10^4	0.68987330×10^7	$0.79657988 \times 10^{11}$
0.644	0.25046616×10^4	0.29350871×10^8	$0.76295129 \times 10^{12}$
0.647	0.44208252×10^4	0.10083352×10^9	$0.44395805 \times 10^{13}$

Table 3.2: Values of the average cluster size χ and the next two higher moments χ_1 and χ_2 of the cluster size distribution for the DSP model measured on the square lattice of size $2^{11} \times 2^{11}$ for different site occupation probabilities p.

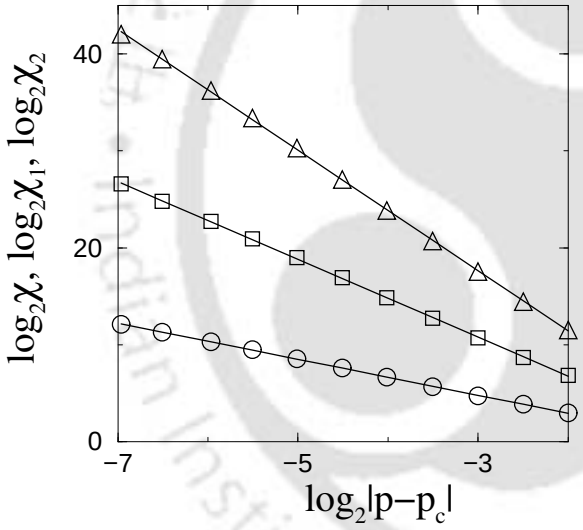

Figure 3.4: Plot of the first, second and third moments χ, χ_1 and χ_2 of the cluster size distribution versus $|p - p_c|$ for the square lattice. Different symbols are: circles for χ, squares for χ_1 and triangles for χ_2. The solid lines represent the best fits through the data points.

then obtained from the respective slopes as $\gamma = 1.85 \pm 0.01$, $\delta = 4.01 \pm 0.02$ and $\eta = 6.21 \pm 0.04$. The errors quoted here are the standard least squares fit error taking into account the statistical error of each single data point. Because of the error bar $\Delta p_c = 0.0005$ in the threshold, all the exponents have also been estimated for two other critical probabilities $p_c \pm \Delta p_c$. The values of the exponents obtained for $p = 0.6545$ are $\gamma \approx 1.84$, $\delta \approx 3.99$ and $\eta \approx 6.15$ whereas for $p = 0.6555$ they are $\gamma \approx 1.86$, $\delta \approx 4.04$ and $\eta \approx 6.26$. The values of the critical exponents for the square lattice are then taken as: $\gamma = 1.85 \pm 0.01$, $\delta = 4.01 \pm 0.04$ and $\eta = 6.21 \pm 0.08$. The error bars quoted now include the systematic errors as well as the statistical errors.

These values of exponents are now used to verify the scaling relations obtained in

section 3.1. The order parameter exponent β are estimated at first using the scaling relation $\delta = \beta + 2\gamma$ (Eq. 3.16). Since $\gamma = 1.85 \pm 0.01$ and $\delta = 4.01 \pm 0.04$, the value of β is obtained as $\beta = 0.31 \pm 0.06$. The error has propagated from the errors of γ and δ. Independent estimation of the exponent β becomes difficult because of the presence of curvature in the plot of P_∞ versus $(p - p_c)$ in the log-log scale for $p > p_c$. This may be due to dominating corrections to scaling to the leading singularity of P_∞. Next the scaling relations $\eta = 2\delta - \gamma$ obtained in Eq. 3.16 are considered for verification. The value of $2\delta - \gamma$ is approximately 6.17 which is very close to the value of the exponent $\eta = 6.21$ obtained here. Thus the scaling relation holds true within error bar.

C. Connectivity exponents

To measure the connectivity exponents $\nu_\parallel$ and $\nu_\perp$ for the DSP model, the connectivity lengths $\xi_\parallel$ along the growth of a cluster and $\xi_\perp$ along the transverse direction are measured on the square lattice of linear size $L = 2^{11}$. The data are given in Table 3.3. In Figure 3.5, they are plotted against $|p - p_c|$. The squares represent $\xi_\parallel$ and the circles represent $\xi_\perp$. The exponents $\nu_\parallel$ and $\nu_\perp$ are then measured from the respective slopes in the log-log plot as $\nu_\parallel = 1.33 \pm 0.01$ and $\nu_\perp = 1.12 \pm 0.02$. The errors quoted here are the least squares fit errors. The values of the exponents are also estimated at $p_c \pm \Delta p_c$. For $p = 0.6545$, the values obtained are $\nu_\parallel \approx 1.33$ and $\nu_\perp \approx 1.11$ and for $p = 0.6555$, the values obtained are $\nu_\parallel \approx 1.34$ and $\nu_\perp \approx 1.14$. There is a little variation in the values of the critical exponents over Δp_c. The values of $\nu_\parallel$ and $\nu_\perp$ are then taken as: $\nu_\parallel = 1.33 \pm 0.01$ and $\nu_\perp = 1.12 \pm 0.03$ on the square lattice incorporating the systematic errors.

p	$\xi_\parallel$	$\xi_\perp$
0.405	0.27853433×10^1	0.13546952×10^1
0.478	0.43234738×10^1	0.20641067×10^1
0.530	0.67828777×10^1	0.31871720×10^1
0.567	0.10827833×10^2	0.47676392×10^1
0.593	0.17362069×10^2	0.72476485×10^1
0.611	0.27661932×10^2	0.10767936×10^2
0.624	0.44735245×10^2	0.15892448×10^2
0.633	0.75290641×10^2	0.22890713×10^2
0.639	0.11689895×10^3	0.31522011×10^2
0.644	0.20247780×10^3	0.45612197×10^2
0.647	0.28951196×10^3	0.59608695×10^2

Table 3.3: Values of the connectivity lengths $\xi_\parallel$ and $\xi_\perp$ for DSP model measured on the square lattice of linear size $L = 2^{11}$.

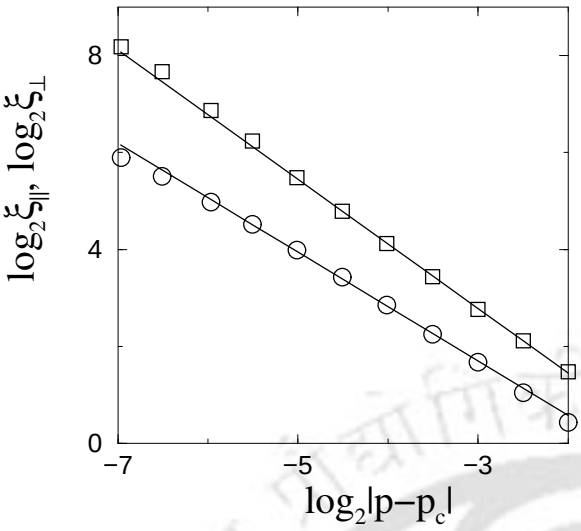

Figure 3.5: The connectivity lengths $\xi_{\parallel}$ and $\xi_{\perp}$ are plotted against $|p-p_c|$ for DSP model on the square lattice. The circles represent $\xi_{\perp}$ and the squares represent $\xi_{\parallel}$. The solid lines represent the best fits through the data points.

The hyperscaling relations $2\delta-3\gamma=(d-1)\nu_{\perp}+\nu_{\parallel}$ and $(d-d_f)\nu_{\perp}=\beta=\delta-2\gamma$ in Eq. 3.28 are verified now. Here, $(d-1)\nu_{\perp}+\nu_{\parallel}=2.45\pm0.04$ for $d=2$ and $2\delta-3\gamma=2.47\pm0.05$. Hence the hypersacling relation $2\delta-3\gamma=(d-1)\nu_{\perp}+\nu_{\parallel}$ in Eq. 3.28 is satisfied within error bars for the square lattice. The other hyperscaling relation $(d-d_f)\nu_{\perp}=\beta=\delta-2\gamma$ is also satisfied within error bars: $(d-d_f)\nu_{\perp}=0.30\pm0.02$ and $\delta-2\gamma=0.31\pm0.05$. However, it should be noted that the hyperscaling relation is violated in the case of directed percolation [26].

D. Comparison of critical exponents of different percolation models

Morphological differences and development of a Hall like field in DSP model are already mentioned in the previous chapter. Now, a comparison between the values of the critical exponents obtained in different percolation models is made here in Table 3.4. The values of the critical exponents obtained on the square lattice are reported in Refs. [27,28]. It can be seen that the values of the exponents obtained in this model are very different from those obtained in other percolation models like OP, DP and SP. The fractal dimension of the infinite spanning clusters is the lowest in the DSP model. The magnitude of the order parameter exponent β is the largest and the magnitude of average cluster size exponent γ is the smallest among the four models. The DSP model then belongs to a new universality class.

The DSP clusters are anisotropic and need two connectivity length exponents to characterize. There are now few things to notice. First, the value of $\nu_{\parallel}$ is almost equal to the connectivity exponent of ordinary percolation, $\nu(\mathrm{OP})=4/3$ [21,22]. Recently, a study of magnetoresistance of a three-component composites consisting of cylindrical insulator and perfect conductors in a metallic host film was made

Percolation Models	β	γ	τ	σ	ν	d_f
OP [21,22]	5/36	43/18	187/91	36/91	4/3	91/48
DP [23,29,30]	0.277 ±0.002	2.2772 ±0.0003	2.108 ±0.001	0.3915 ±0.0004	$\nu_\perp = 1.0972$ ±0.0006 $\nu_\parallel = 1.733$ ±0.001	1.765
SP [24]	0.048 ±0.011	2.19 ±0.07	2.022 ±0.004	0.447 ±0.014	1.116 ±0.003	1.957 ±0.009
DSP [20] (Square lattice)	0.31 ±0.01	1.85 ±0.01	2.16 ±0.20	0.459 ±0.004	$\nu_\perp = 1.12$ ±0.03 $\nu_\parallel = 1.33$ ±0.01	1.733 ±0.005

Table 3.4: Comparison of the values of the critical exponents β, γ, τ, σ, ν and d_f in the case of ordinary (OP), directed (DP), spiral (SP) and directed spiral (DSP) percolation models on the square lattice. The values of the critical exponents of the DSP model are found different from the other models. The DSP model then belongs to a new universality class.

by Barabash *et al*[31]. Since the Hall effect will generate an electric field with a component perpendicular to the plane of the film with an in-plane applied current, their system appears inherently three dimensional ($3D$). However, the electric field perpendicular to the film plane vanishes because of the presence of columnar perfect conductor. Thus, their $3D$ problem reduces to that of calculating the effective conductivity of a $2D$ composites of perfect insulator and perfect conductor[31,32]. The results obtained in the model of composite material by Barabash *et al*[31] then could be compared with the results of the present DSP model in 2 dimensions. It is found by Barabash *et al*[31] that the correlation length exponent is 4/3 independent of anisotropy. The correlation length exponent quoted there is equivalent to the connectivity exponent $\nu_\parallel$ of the DSP model considered here. The results of the DSP model is thus in good agreement with the results obtained in the model calculation of magnetoresistance of composite materials. Second, the values of $\nu_\parallel$ and $\nu_\perp$ are different from those obtained in the DP model, $\nu_\parallel(\mathrm{DP}) = 1.733 \pm 0.001$ and $\nu_\perp(\mathrm{DP}) = 1.0972 \pm 0.0006$[29,30] (see Table 3.4 also). Third, the ratio of the connectivity lengths goes as $\xi_\parallel/\xi_\perp \sim |p - p_c|^{-\Delta\nu}$ where $\Delta\nu = \nu_\parallel - \nu_\perp$. Here in the case of DSP, $\Delta\nu$ is approximately 0.21 for the square lattice whereas it is approximately 0.64 for DP which is much larger than that of the DSP model. This means that clusters in the DSP model are less anisotropic than the clusters in the DP model at any p. This is due to the presence of the rotational constraint which tries to make

the clusters isotropic. It is thus important to note that even the DSP clusters grow along an effective field direction they are not merely DP cluster. The DSP clusters exhibit distinct critical properties on its own. Fourth, Barabash *et al*[31] assumed that $\Delta\nu = 0$. The effective aspect ratio of their problem might vary as $|p - p_c|^{-\Delta\nu}$ with $\Delta\nu = 0.21$ as obtained here in the DSP model.

It should be mentioned here that, Santra in Ref. [28] estimated the values of the critical exponents with higher error bars on smaller system size and less accurate p_c. Certain rational fractions were proposed in Ref. [28] for the values of the critical exponents as $\beta = 1/3$, $\gamma = 11/6$, $\delta = 24/6$, $\eta = 37/6$, $\tau = 28/13$ and $\sigma = 6/13$. Interestingly they satisfy all the scaling relations in Eq. 3.15 and Eq. 3.16 exactly.

3.2.2 The triangular lattice results

It is already discussed that critical exponents are independent of most of the parameters of the model such as the range of interaction or the lattice structure in the same space dimension. In order to verify the universality of the critical exponents in the DSP model, one therefore needs to study the same model on a different lattice in the same space dimension. DSP model is then studied on the triangular lattice in $2D$ and all the critical exponents are estimated. In the following, the values of the critical exponents will be reported and a comparison with that of the square lattice will be made.

A. Fractal dimension

The fractal dimension d_f of the spanning DSP clusters on the triangular lattice is

Box size (ϵ)	$N_B(\epsilon)$
1	0.644535×10^6
2	0.241445×10^6
4	0.707675×10^5
8	0.206879×10^5
16	0.604461×10^4
32	0.173399×10^4
64	0.500420×10^3
128	0.145549×10^3
256	0.428929×10^2
512	0.130097×10^2
1024	0.383521×10^1
2048	0.100000×10^1

Table 3.5: Number of the occupied boxes $N_B(\epsilon)$ versus box size ϵ measured using box counting algorithm for the spanning DSP clusters on the triangular lattice of linear size $L = 10^{11}$. Data are averaged over 5×10^4 spanning clusters.

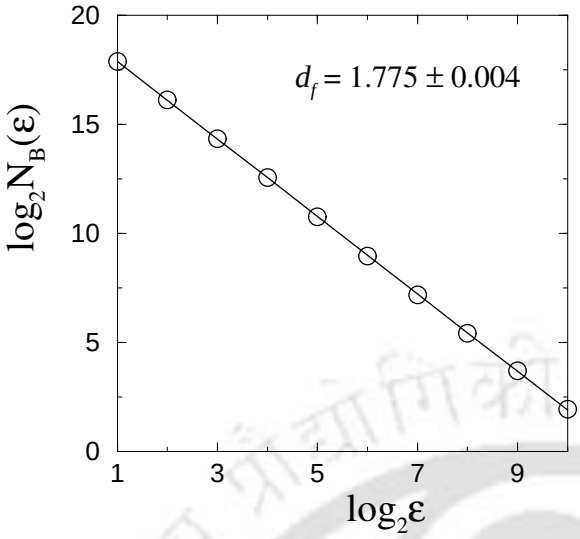

Figure 3.6: Number of boxes $N_B(\epsilon)$ is plotted against the box size ϵ measured for the DSP model on the triangular lattice. From the slope, the fractal dimension is found as $d_f = 1.775 \pm 0.004$.

measured using the box counting method as in the case of square lattice. The lattice size is taken as $2^{11} \times 2^{11}$. The number of boxes $N_B(\epsilon)$ with at least one occupied site are counted and listed in Table 3.5 as a function of box size ϵ. Data are averaged over 5×10^4 samples. In Figure 3.6, $N_B(\epsilon)$ is plotted against the box size ϵ. From the slope, the fractal dimension d_f is obtained as 1.775 ± 0.004. Surprisingly it is little higher than that of the square lattice data 1.733 ± 0.005. It has already been observed from the spanning cluster morphology that they are less anisotropic and more compact on the triangular lattice than on the square. The little higher value of the fractal dimension d_f on the triangular lattice as compared to that of the square lattice is in support of this observation from the morphological point of view. This is because of the fact that, due to the higher number of branching of the rotational constraint on the triangular lattice the cluster penetrates into itself more and more than on the square lattice. As a result, the infinite clusters become less rarefied on the triangular lattice than on the square lattice.

To verify the result obtained using box counting method, the fractal dimension of the DSP spanning cluster on the triangular lattice is also measured by measuring the mass of the spanning cluster as a function of L. Spanning clusters are generated on lattices of linear size L ranging from 2^7 to 2^{11} in the multiple of 2. For each lattice size, at least 5×10^4 spanning clusters are generated. In Figure 3.7, S_∞ is plotted against the system size L for the triangular lattice. From the slope, the fractal dimension is obtained as $d_f = 1.80 \pm 0.03$. The value of the fractal dimension obtained using finite-size scaling method is within error bar with the other estimate using box counting algorithm. Moreover, the difference in the values of d_f for the

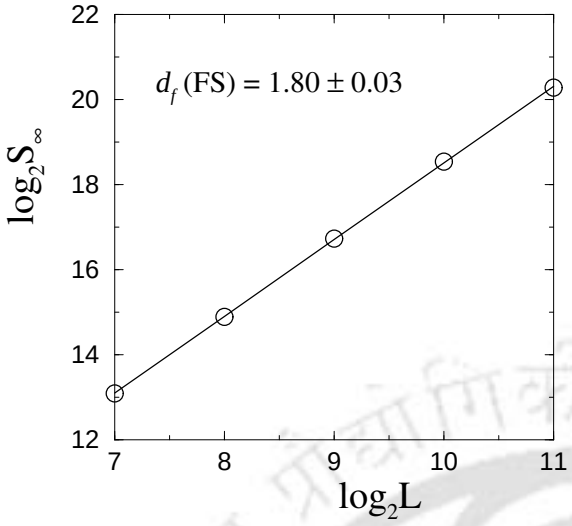

Figure 3.7: The mass of the largest spanning cluster S_∞, measured at p_c, is plotted against the system size L. From the slope, the fractal dimension is obtained as $d_f(\mathrm{FS}) = 1.80 \pm 0.03$ for the triangular lattice.

square and triangular lattices are much more distinct in the finite-size estimate. However, this has serious consequences. Since the critical exponents are related to the fractal dimension via scaling relations, other critical exponents on the two lattices may also be different which is unusual in critical phenomena. One should then analyze the data on the two lattices with extreme care in order to very the universality property of the model.

B. Moment exponents

The average cluster size χ and two other higher moments χ_1 and χ_2 of cluster size distribution are measured on the triangular lattice of linear size $L = 2^{11}$ generating 5×10^4 finite clusters below p_c at different values of p. Measured values of χ, χ_1 and χ_2 are tabulated in Table 3.6. The exponents γ, δ and η are then estimated from the respective slopes of χ, χ_1 and χ_2, plotted against $|p - p_c|$ in Figure 3.8. The circles represent χ, the squares represent χ_1 and the triangles represent χ_2. The exponents are obtained as $\gamma = 1.98 \pm 0.01$, $\delta = 4.30 \pm 0.02$ and $\eta = 6.64 \pm 0.04$ for the critical probability $p_c = 0.5700$. The values of the exponents have also obtained for $p_c \pm \Delta p_c$. For $p = 0.5695$, the values of the exponents are obtained as $\gamma \approx 1.96$, $\delta \approx 4.27$ and $\eta \approx 6.60$ whereas for $p = 0.5705$ they are $\gamma \approx 2.00$, $\delta \approx 4.33$ and $\eta \approx 6.71$. The values of the critical exponents for the triangular lattice are then taken as[20]: $\gamma = 1.98 \pm 0.02$, $\delta = 4.30 \pm 0.04$ and $\eta = 6.66 \pm 0.08$. The values of the critical exponents and error bars quoted now include the variations due to $p_c \pm \Delta p_c$. It is important to note that, the exponent values are found very different (beyond the error bars) than the square lattice values. The values of the exponents on the triangular lattice are little higher than that of the square lattice. The clusters then

p	χ	χ_1	χ_2
0.216	0.34015832×10^1	0.17906942×10^2	0.13318638×10^3
0.337	0.77906618×10^1	0.10326947×10^3	0.21538387×10^4
0.416	0.17189426×10^2	0.59382844×10^3	0.32198730×10^5
0.468	0.37892542×10^2	0.32571153×10^4	0.45300532×10^6
0.503	0.86928144×10^2	0.19765670×10^5	0.74916010×10^7
0.526	0.20216754×10^3	0.12129475×10^6	0.12338671×10^9
0.541	0.47526574×10^3	0.76788675×10^6	$0.21959875 \times 10^{10}$
0.551	0.11235081×10^4	0.49494125×10^7	$0.38166985 \times 10^{11}$
0.557	0.23793046×10^4	0.25994451×10^8	$0.46896410 \times 10^{12}$

Table 3.6: Values of the average cluster size χ and next two higher moments χ_1 and χ_2 of the cluster size distribution function for the DSP model on the triangular lattice of size $2^{11} \times 2^{11}$ at different site occupation probabilities p.

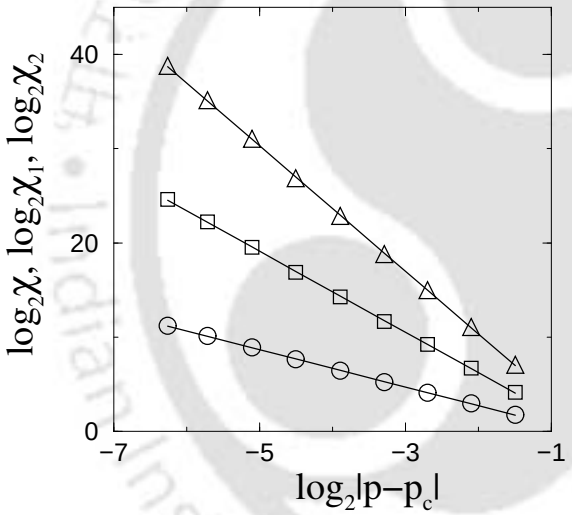

Figure 3.8: Plot of the first, second and third moments χ, χ_1 and χ_2 of the cluster size distribution versus $|p-p_c|$ for the triangular lattice. Different symbols are: circles for χ, squares for χ_1 and triangles for χ_2. The solid lines represent the best fits through the data points.

grow much larger in size on the triangular lattice than on the square lattice for the same $\Delta p = |p - p_c|$. This might be due to higher number of branching possibilities on the triangular lattice.

The scaling relation $\eta = 2\delta - \gamma$ given in Eq. 3.16, which is satisfied for the square lattice, can now be verified for the triangular lattice. Here, $2\delta - \gamma = 6.62$ which is very close to the value of the exponent $\eta = 6.66$. The scaling relation is then satisfied within error bars for both the lattices. Employing the scaling relation $\delta = \beta + 2\gamma$ (Eq. 3.16) the value of the exponent β is also obtained as 0.34 ± 0.08 for the triangular lattice. The error here is due to the propagation error from the errors of γ and δ.

C. Connectivity exponents

The connectivity lengths $\xi_\parallel$ and $\xi_\perp$ are measured generating 5×10^4 finite clusters below p_c on the triangular lattice of size $2^{11} \times 2^{11}$. The estimates are given in Table 3.7. At $p_c = 0.5700$, the exponents $\nu_\parallel$ and $\nu_\perp$, obtained from the slopes of the plots in Figure 3.9 are $\nu_\parallel = 1.36 \pm 0.02$ and $\nu_\perp = 1.23 \pm 0.02$. The errors quoted here are the least squares fit errors. The values of the exponents are also estimated at $p_c \pm \Delta p_c$ where $\Delta p_c = 0.0005$. For $p = 0.5695$, the values of the exponents obtained are $\nu_\parallel \approx 1.35$ and $\nu_\perp \approx 1.21$ and for $p = 0.5705$, the values obtained are $\nu_\parallel \approx 1.37$ and $\nu_\perp \approx 1.24$. Hence, the exponents are taken as $\nu_\parallel = 1.36 \pm 0.02$ and $\nu_\perp = 1.23 \pm 0.02$ for the triangular lattice incorporating the systematic errors. It can be noticed that the value of $\nu_\parallel$ is close to that of the square lattice but $\nu_\perp$ seem

p	$\xi_\parallel$	$\xi_\perp$
0.216	0.15048887×10^1	0.65193397×10^0
0.337	0.26814429×10^1	0.13130013×10^1
0.416	0.45949644×10^1	0.22910127×10^1
0.468	0.77088567×10^1	0.38135457×10^1
0.503	0.13620342×10^2	0.64458421×10^1
0.526	0.24082634×10^2	0.10742666×10^2
0.541	0.44126752×10^2	0.17945790×10^2
0.551	0.82078017×10^2	0.29641358×10^2
0.557	0.14274342×10^3	0.45212104×10^2
0.562	0.28709794×10^3	0.76705135×10^2

Table 3.7: Values of the connectivity lengths $\xi_\parallel$ and $\xi_\perp$ for DSP model measured on the triangular lattice at different site occupation probabilities p.

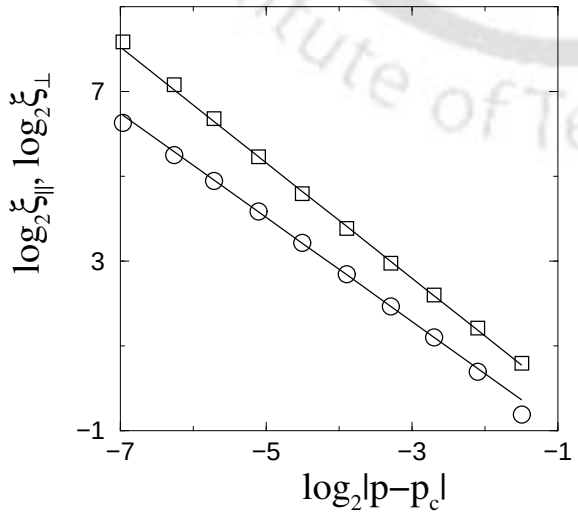

Figure 3.9: The connectivity lengths, $\xi_\parallel$ and $\xi_\perp$, are plotted against $|p - p_c|$ for the triangular lattice of linear size $L = 2^{11}$. The circles represent $\xi_\perp$ and the squares represent $\xi_\parallel$. The solid lines represent the best fits through the data points.

to be different beyond the error bar for the two lattices.

On the triangular lattice, both the hyperscaling relations described in Eq. 3.28 are satisfied marginally: $2\delta - 3\gamma = 2.66 \pm 0.06$ whereas $(d-1)\nu_\perp + \nu_\parallel = 2.59 \pm 0.04$ and $\delta - 2\gamma = 0.34 \pm 0.06$ whereas $(d - d_f)\nu_\perp = 0.28 \pm 0.03$. However, both of them were satisfied within error bar on the square lattice.

D. Comparison of the square and the triangular lattice results

The values of the critical exponents and the fractal dimension obtained in the above study on the triangular lattice are summarized and compared with the square lattice data in Table 3.8. The values of the critical exponents obtained on the square and triangular lattices are reported in Ref. [20,33]. It is observed here that, most of the critical exponents and the fractal dimensions are considerably different on the square and triangular lattices for the DSP model. According to the theory of critical phenomena, the values of the critical exponents are independent of the underlying lattice structure in the same spatial dimension. As a consequence, the systems defined on different lattices in the same space dimension then belong to the same universality class. Since the values of the critical exponents of the DSP model differ on the square and the triangular lattices in $2D$, the DSP model then seems to exhibit a breakdown of universality between the square and triangular lattices. This is the first percolation model which shows breakdown of universality in their cluster properties on two different lattices in the same spatial dimension. It is already mentioned in the above discussion that the flexibility in the spiraling constraint makes the clusters compact and less anisotropic. Note that on the triangular lattice, $\Delta\nu = \nu_\parallel - \nu_\perp$ is approximately 0.13 which is much less than the square lattice value (≈ 0.21). This observation supports the spanning cluster morphology, described in Chapter 2, that they are less anisotropic on the triangular lattice than on the square lattice. It may be due to the additional flexibility given to the rotational constraint which makes the cluster not only compact but also less anisotropic. A possible reason for different critical behaviour on the square and triangular lattices may be due to different scaling behaviour of the finite clusters below percolation threshold on the two lattices. Below p_c, the finite clusters are called lattice animals[25]. Lattice animals without any loop are known as lattice trees. Though the spiral lattice animals have the same scaling form on the square and triangular lattices, it has been found that the spiral trees (lattice animals without loops) follow two different scaling relations on the square and triangular lattices and belong to two different universality classes[34]. In the asymptotic $n \to \infty$ limit, the number of spiral lattice

Lattice	d_f	γ	δ	η	$\nu_{\parallel}$	$\nu_{\perp}$
Square [20,28]	1.733 ± 0.005	1.85 ± 0.01	4.01 ± 0.04	6.21 ± 0.08	1.33 ± 0.01	1.12 ± 0.03
Triangular [20]	1.775 ± 0.004	1.98 ± 0.02	4.30 ± 0.04	6.66 ± 0.08	1.36 ± 0.02	1.23 ± 0.02

Table 3.8: Comparison of the critical exponents and fractal dimension measured for the DSP model on the square and triangular lattices. The exponents are significantly different on the two lattices.

site trees (a_n) of n-sites on the triangular lattice obey the scaling relation given by [34] $a_n \approx \lambda^{n^\delta} n^{-\theta}$ whereas on the square lattice it is given by [35–38] $a_n \approx \lambda^n n^{-\theta}$, where δ and θ are two exponents and λ is known as the growth parameter. The origin of different scaling forms for the spiral lattice site trees on the square and triangular lattices is due to the fact that they can not have branching on the triangular lattice except at the origin whereas on the square lattice branching is possible at any point. The radius of gyration exponent of spiral trees was also found different on the square ($\nu \approx 0.653$) and triangular ($\nu \approx 0.618$) lattices [34]. Another lattice statistical model, the spiral self-avoiding walks (SAW) also exhibits breakdown of universality on the square and triangular lattices. The asymptotic (large n) behaviour of the number of walks S_n is given by $S_n \approx An^{-\gamma} \exp(\lambda\sqrt{n})$, where $A = 2^{-2} \times 3^{-5/4}\pi$, $\gamma = 7/4$ and $\lambda = 2\pi/\sqrt{3}$ for the square lattice [39] and $A = 2^{1/4} \times 3^{-7/4}\pi$, $\gamma = 5/4$ and $\lambda = \pi/\sqrt{2/3}$ for the triangular lattice [40]. Notice that the scaling relation for the spiral lattice site trees is similar to that of the spiral SAWs. It should be mentioned here that the values of the critical exponents and the scaling behaviour of the cluster related quantities in the SP model are the same on the square and triangular lattices and no breakdown of universality was observed [24]. This may be due to the fact that the spiral lattice trees are minority in number at the percolation threshold of SP and unable to change the universality class of the SP model. In the DSP model, the presence of the directional constraint on top of the rotational constraint might increase the number of spiral lattice trees. It might be possible that, the higher number of tree like structures in the clusters generated has a non-trivial effect on the critical properties of the DSP model at the percolation threshold and leads to breakdown of universality of the critical exponents.

3.2.3 Scaling function form

The scaling function form assumed for the cluster size distribution, given by, $P_s(p) = s^{-\tau+1}\mathsf{f}[s^\sigma(p-p_c)]$ is verified in this section for both the square and triangular lattices. The values of the exponents τ and σ are estimated using the scaling relations in Eq.

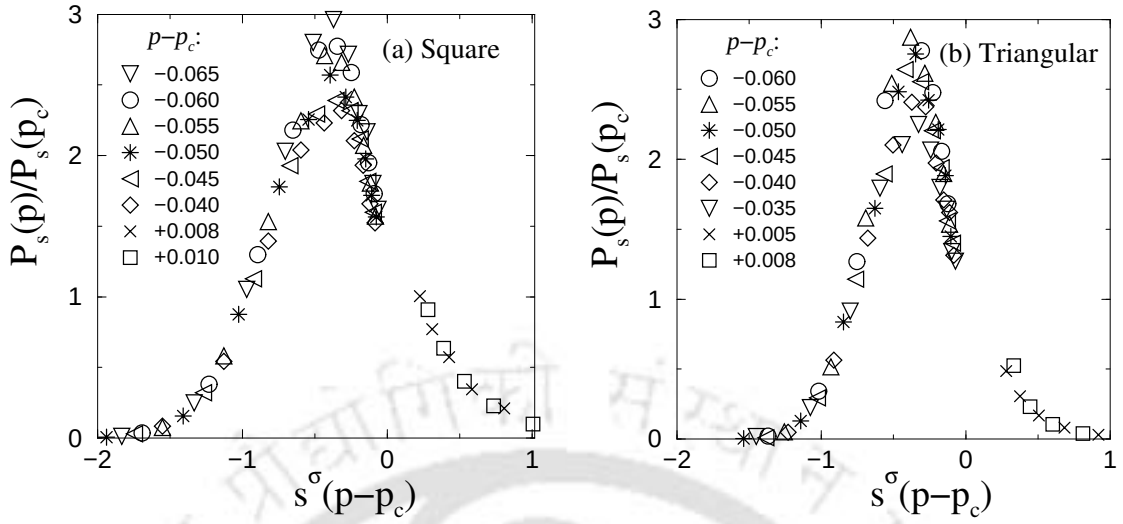

Figure 3.10: Plot of the scaled cluster size distribution $P_s(p)/P_s(p_c)$ versus the scaled variable $s^\sigma(p-p_c)$ for the (a) square and (b) triangular lattices for different values of p. The value of σ is taken as 0.459 for the square lattice and 0.427 for the triangular lattice. The cluster size s changes from 64 to 16384. Reasonable data collapse is observed for both the lattices.

3.15. For the square lattice, the value of $\tau = 2.16 \pm 0.20$ is obtained from the average of $\tau_1 = (3\delta - 4\gamma)/(\delta - \gamma) = 2.14 \pm 0.18$, $\tau_2 = (4\eta - 5\delta)/(\eta - \delta) = 2.18 \pm 0.28$ and $\tau_3 = (3\eta - 5\gamma)/(\eta - \gamma) = 2.15 \pm 0.11$. Similarly $\sigma = 0.459 \pm 0.015$ is determined from $\sigma_1 = 1/(\delta - \gamma) = 0.463 \pm 0.011$, $\sigma_2 = 1/(\eta - \delta) = 0.455 \pm 025$ and $\sigma_3 = 2/(\eta - \gamma) = 0.459 \pm 0.009$. The errors quoted here are the propagation errors. The values of τ and σ for the triangular lattice has also been estimated in the similar way and obtained as $\tau = 2.16 \pm 0.20$ and $\sigma = 0.427 \pm 0.003$ respectively. Note that the value of τ is almost same for the two lattices whereas σ differs slightly from the square to triangular lattice. The scaling function form $\mathsf{f}(z)$ can be verified defining a scaled cluster size distribution $P_s(p)/P_s(p_c)$ as function of a scaled variable $z = s^\sigma(p - p_c)$. It is expected that the data for different p or s should collapse onto a single curve $\mathsf{f}(z)$. In Figure 3.10, $P_s(p)/P_s(p_c)$ is plotted against z. It is assumed that $\mathsf{f}[0]$ is a constant. Distribution of 10^4 clusters over the bins of width $2^{i-1} - (2^i - 1)$ with $i = 1$ to $L^2 = 2^{22}$ is considered for each value of p. The cluster size s changes from 64 to 16384 and $(p - p_c)$ changes from 0.010 to -0.065 for the two different lattices. Data for different values of s and $(p - p_c)$ collapse reasonably well onto a single curve for the individual lattices. This means that the scaling function form assumed for the cluster size distribution is appropriate for this model. It is found that the maximum value of $P_s(p)/P_s(p_c)$ for DSP model (≈ 3) is different from that of OP

model (≈ 4.5)[3]. The height of the function for the two lattices almost the same but the width of the function for the triangular lattice is slightly smaller than that of the square lattice function. The lesser width of the scaling function $P_s(p)$ is just a consequence of the lesser value σ on the triangular lattice.

3.3 Conclusion

The critical properties of the directed spiral percolation (DSP) model under both directional and rotational constraints are studied on the square and triangular lattices in $2D$. A completely new type of percolation clusters are generated in the DSP model along with the development of a Hall like field. The clusters produced under these two combined directed and rotational constraints have three important features: the clusters are rarefied, they contain spiral dangling ends and most importantly they are anisotropic. The critical properties of the cluster related quantities in this model are very different from the other percolation models like OP, DP and SP. In the above study, it is found that the fractal dimension d_f and the values of the critical exponents (τ, σ, β, γ, $\nu_{\parallel}$, $\nu_{\perp}$, etc.) of the DSP model are different from that of the other percolation models. For both the lattices, it is found that the critical exponent γ of the average cluster size χ is the smallest and the exponent β of P_∞ is the largest among the four models. The exponent $\nu_{\parallel}$ is found approximately equal to the connectivity exponent $\nu = 4/3$ of the OP model which is also in good agreement with the correlation length exponent ν obtained by Barabash *et al*[31] in the study of magnetoresistance of a model composite material. Both $\nu_{\parallel}$ and $\nu_{\perp}$ are different from those obtained in the DP model. The order of anisotropy $\xi_{\parallel}/\xi_{\perp}$ is higher in the DP clusters than that of the clusters in the DSP model at any p. Note that the OP and SP clusters are isotropic and they are characterized by a single connectivity length exponent ν. Therefore, it can be concluded that the DSP model belongs to a new universality class, different from that of OP, DP or SP.

Another surprising and unusual observation in this model is the breakdown of universality between the square and triangular lattices in $2D$. In the DSP model, the clusters on the triangular lattice are found more compact and less anisotropic than the clusters on the square lattice. Consequently, it is found to be that the values of the fractal dimension and some of the critical exponents are significantly different on the two lattices. Though this is very unusual in critical phenomena, several features like the cluster morphology, scaling relations and the data collapse support the values of the critical exponents obtained on the individual lattices. It

should be noted here that the critical exponents on both the lattices satisfy the scaling relations between the moment exponents (γ, δ, η) whereas the hyperscaling relations are satisfied on the square lattice but they are only "marginally" satisfied on the triangular lattice. The breakdown of universality of the critical exponents on the square and triangular lattices might be due to different scaling behaviour of the finite clusters below the percolation threshold on the two lattices as already discussed.

Apart from the new geometrical features like development of Hall like field, anisotropy, rarefaction and chiral dangling ends in the cluster morphology, the DSP clusters then exhibit two important characteristics such as new universality class and breakdown of universality in the same space dimension from the critical phenomena point of view. These two aspects will be further considered and discussed in the following chapters after performing finite size scaling analysis, measuring hull critical exponents, varying the applied field directions and intensities, looking into the multifractal aspects of the DSP spanning clusters and also determining the dynamical scaling exponents.

Bibliography

[1] H. E. Stanley, *Introduction to Phase Transitions and Critical Phenomena*, Oxford University Press, New York, 1987.

[2] J. M. Yeomans, *Statistical Mechanics of Phase Transitions*, Oxford University Press, New York, 1994.

[3] D. Stauffer and A. Aharony, *Introduction to Percolation Theory*, Taylor and Francis, London, 2nd edition, 1994.

[4] A. Bunde and S. Havlin, *Fractals and Disordered Systems*, Springer-Verlag, Berlin, 1991.

[5] N. R. Moloney and K. Christensen, *Complexity And Criticality*, Imperial College Press, 2005.

[6] B. Bollobás and O. Riordan, *Percolation*, Cambridge University Press, 2006.

[7] H. E. Stanley, J. Phys. A **10**, L211 (1977).

[8] J. Feder, *Fractals*, Plenum Press and New York and London, 1998.

[9] B. B. Mandelbrot, *The Fractal Geometry of Nature*, Freeman, San Francisco, 1982.

[10] A. Giorgilli, D. Casati, L. Sironi and L. Galgani, Physics Letters A **115**, 202 (1986).

[11] L. S. Liebovitch and T. Toth, Physics Letters A **141**, 387 (1989).

[12] P. Grassberger, Phys. Lett. **97A**, 224 (1983).

[13] P. Grassberger, Int. J. Mod. Phys. C **4**, 515 (1993).

[14] A. Block, W. Vonblow and H. J. Schellnhuber, Phys. Rev. A **42**, 1869 (1990).

[15] F. H. Ling and G. Schmidt, J Comp. Phys. **99**, 196 (1992).

[16] B. Dubrulle and M. Lachiezerey, Astronomy and Astrophysics **289**, 667 (1994).
[17] M. Osaka and N. Ito, Int. J. Mod. Phys. C **11**, 1519 (2000).
[18] M. Tanaka, Y. Kimura, L. Chouanine, R. Kato and J. Taguchi, J Material Sc. Lett. **22**, 1279 (2003).
[19] L. Lorenzo and R. A. Mosquera, Journal of Computational Chemistry **24**, 707 (2003).
[20] S. Sinha and S. B. Santra, Eur. Phys. J. B **39**, 513 (2004).
[21] M. P. M. den Nijs, J. Phys. A **12**, 1857 (1997).
[22] B. Nienhuis, J. Phys. A **15**, 199 (1982).
[23] B. Hede, J. Kertész and T. Vicsek, J. Stat. Phys. **64**, 829 (1991).
[24] S. B. Santra and I. Bose, J. Phys. A **25**, 1105 (1992).
[25] T. C. Lubensky and J. Isaacson, Phys. Rev. Lett. **46**, 871 (1981).
[26] M. Henkel and V. Privman, Phys. Rev. Lett. **65**, 1777 (1990).
[27] S. B. Santra, Int. J. Mod. Phys. B **17**, 5555 (2003).
[28] S. B. Santra, Eur. Phys. J. B **33**, 75 (2003).
[29] J. W. Essam, A. J. Guttmann and K. DéBell, J. Phys. A: Math. Gen. **21**, 3815 (1988).
[30] J. W. Essam, K. DéBell, J. Adler and F. M. Bhatti, Phys. Rev. B **33**, 1982 (1986).
[31] S. V. Barabash, D. J. Bergman and D. Stroud, Phys. Rev. B **64**, 174419 (2001).
[32] D. J. Bergman and Y. M. Strelniker, Phys. Rev. B **59**, 2180 (1999).
[33] S. Sinha and S. B. Santra, in *Proceedings - 46th DAE Solid State Phys. Symp., Jiwaji Univ, Gwalior, India, Dec., 2003*, page 33.
[34] S. B. Santra, J. Phys. I France **5**, 1573 (1995).
[35] I. Bose and P. Ray, Phys. Rev. B **35**, 2071 (1987).
[36] I. Bose, P. Ray and D. Dhar, J. Phys. A **21**, L219 (1988).
[37] I. Bose, P. Ray and S. Mukhopadhyay, J. Phys. A **21**, L979 (1988).
[38] S. B. Santra and I. Bose, J. Phys. A **22**, 5043 (1989).
[39] H. J. W. Blöte and H. J. Hilhorst, J. Phys. A **17**, L111 (1984).
[40] K. Y. Lin, J. Phys. A **18**, L145 (1985).

Chapter 4

Finite-Size Scaling for DSP

The universality class of a lattice statistical model is defined by the values of the critical exponents and by the form of the scaling function at the critical point [1,2]. The values of the critical exponents are determined so far for the DSP model considering finite lattice systems. Simulations have been performed on a single large lattice of size $L \times L$ considering the maximum size of the lattice equal to $2^{11} \times 2^{11}$ in the previous chapters. However, the singularities that occurr at the critical point in the second order phase transitions are generally described by power laws characterized by well defined critical exponents in the thermodynamic limit of the system size ($L \to \infty$). In a finite system, there is rounding off and shifting of critical singularities depending on the ratio of correlation length ξ to the linear size L of the system. It is then essential to verify whether the values of the critical exponents obtained and the conclusions drawn from them for the DSP model in the previous chapters are free from finite size effect or not. In order to obtain the behavior of the infinite system, the results of finite systems are generally extrapolated using finite-size scaling (FSS) [3–10] anstaz.

Extrapolation of the results of finite systems to that of an infinite system can be made in two possible ways. One is by obtaining the values of L-dependent critical exponents for different finite systems of linear size L studying the critical properties on a given lattice as a function of occupation probability p below p_c as usual. Then, the L-dependent critical exponents are extrapolated to the limit $L \to \infty$ corresponding to the infinite network [11]. The other way is to develop an L-dependent scaling function for the cluster properties and to study them by varying the system size L right at the percolation threshold p_c. From the study of L-dependent scaling function against the system size L, one could extract a set of new exponents as ratio of an exponent to the correlation length exponent ν.

Knowing the value of ν of the infinite system from some other method, the values of the critical exponents of infinite system are possible to be obtained from the study of finite systems.

In the following, the effect of finite system size on the values of critical exponents is verified in both the ways and the values of critical exponents are identified for the infinite systems.

4.1 Extrapolation of critical exponents

In order to obtain the size dependent critical behaviour, the percolation threshold p_c of the DSP model for an infinite system should be obtained first. Determining $p_c(L)$s on the finite systems and extrapolating them in the $L \to \infty$ limit, p_c of an infinite system is obtained here. The critical behaviour of the finite systems are then studied around this size independent threshold p_c varying the system size L only.

4.1.1 L - dependent percolation threshold

Percolation threshold at which a spanning cluster appears for the first time in the system is a non-universal quantity and depends on the system size L. The percolation threshold $p_c(L)$ is then determined for different system sizes ranging from $L = 2^7$ to 2^{11} in multiple of 2 both for the square and triangular lattices. In Figure 4.1, $p_c(L)$ is plotted against the inverse system size $1/L$ for the (a) square and (b)

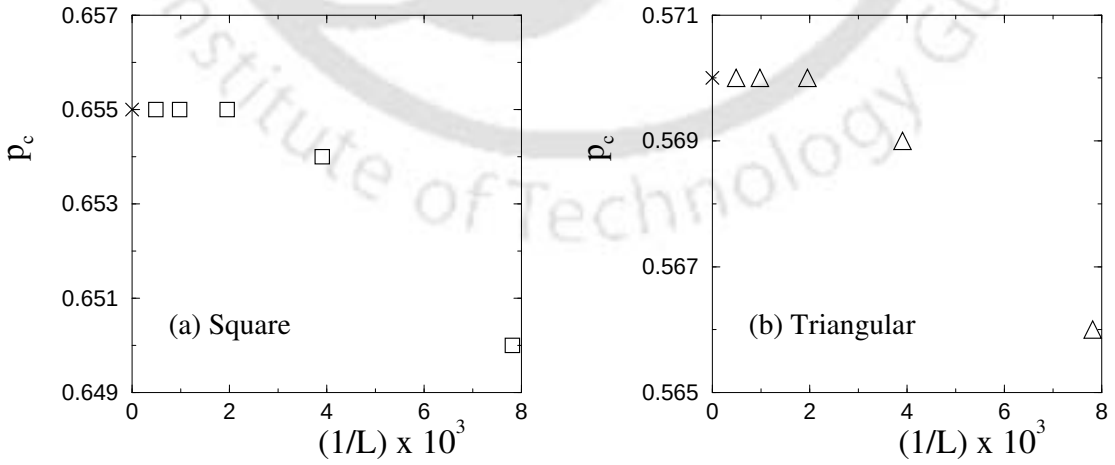

Figure 4.1: Plot of critical probability $p_c(L)$ versus $1/L$ measured on the (a) square ($\square$) and (b) triangular ($\triangle$) lattices in 2D. The values of $p_c(L)$ are extrapolated to $L \to \infty$ and it is found that $p_c \approx 0.6550$ for the square lattice and ≈ 0.5700 for the triangular lattice.

triangular lattices in 2D. It can be seen that, for both the lattices, the critical probabilities of the smaller systems converge to the value of p_cs of the large systems. The plot is extrapolated to the infinite network ($1/L = 0$) and the percolation threshold p_c of DSP model is identified as ≈ 0.6550 on the square lattice and ≈ 0.5700 on the triangular lattice. Note that, the values of p_c identified for infinite system size of different lattices are used for estimating the critical exponents.

4.1.2 L - dependent critical exponents

In this section, the values of the critical exponents corresponding to an infinite system are obtained by extrapolating the values of the critical exponents obtained on the finite systems of linear size L to the $L \to \infty$ limit. The values of the critical exponents are estimated for the finite system of linear sizes L ranging from $L = 2^7$ to 2^{11} (in multiple of 2) for both the square and triangular lattices in $2D$ at their respective p_cs. The cluster properties like average cluster size $\chi = \sum_s' sP_s(p)$ and two higher moments of the cluster size distribution $P_s(p)$, $\chi_1 = \sum_s' s^2 P_s(p)$ and $\chi_2 = \sum_s' s^3 P_s(p)$ are measured for each finite system of size L as it was done previously. In order to measure χ, χ_1 and χ_2 for a given L, at least 5×10^4 finite clusters are generated at different p values below the percolation threshold. For each system size L, the corresponding exponents γ_L, δ_L and η_L are determined from the slope of the plots of χ, χ_1 and χ_2 against $|p - p_c|$ in the double logarithmic scale. In Figure 4.2 the average cluster size χ is plotted against $|p - p_c|$ for different L. The same range of $|p - p_c|$ is chosen for all system sizes. It can be noticed that for smaller systems, the critical regime is found more and more away from the threshold. At the same time, the range of $|p - p_c|$ for which the power law behaviour is observed

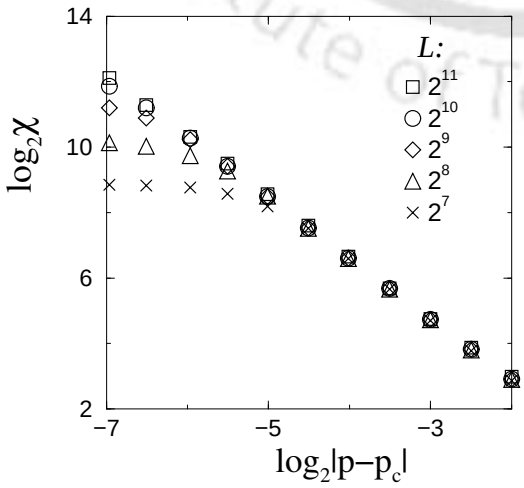

Figure 4.2: Plot of average cluster size χ of the DSP clusters on the square lattices of different sizes. Lattice sizes are taken as $L = 2^{11}$, 2^{10}, 2^9, 2^8 and 2^7.

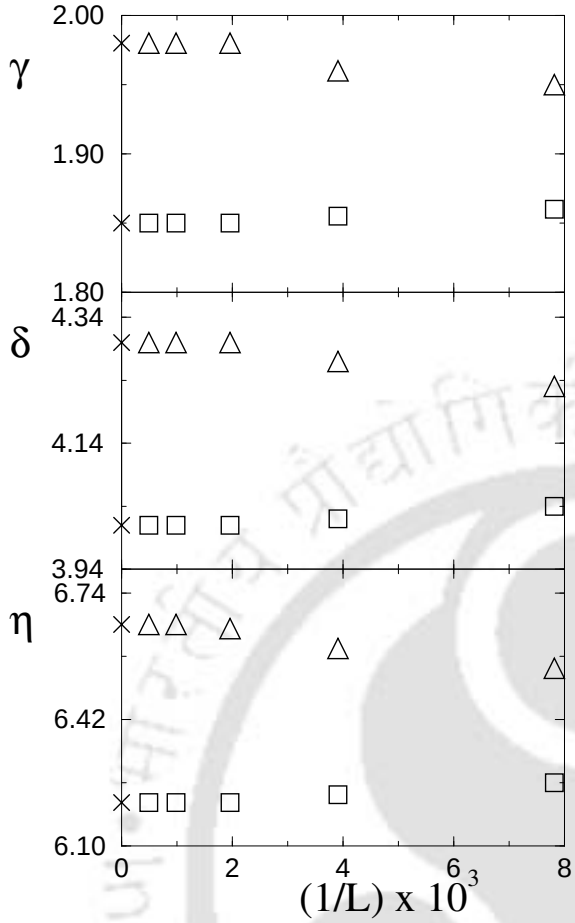

Figure 4.3: Plot of the average cluster size exponent γ and the exponents δ and η corresponding to the other two higher moments of cluster size distribution against the inverse system size $1/L$ for the square (□) and triangular (△) lattices. The extrapolated values of the exponents to $L \to \infty$ are marked by crosses. It can be seen that the exponents are significantly different on the two lattices.

becomes smaller and smaller for small systems. For these reasons, determination of the values of the critical exponents for smaller system sizes become difficult. Performing linear fit to the data points in the linear regime of each system size L, the size dependent critical exponents are obtained. The functional dependence of the exponents γ_L, δ_L and η_L on the system size L are shown in the Figure 4.3. The squares represent the square lattice data and the triangles represent the triangular lattice data. The maximum error to the exponents obtained here are ± 0.02 for γ, ± 0.04 for δ and ± 0.08 for η. The errors are least squares fit errors taking into account the statistical error of each data point. The values of the critical exponents converge to that of large systems like $L = 2^{10}$ and $L = 2^{11}$. The results are then extrapolated up to $L \to \infty$, the infinite system size. The extrapolated values of the exponents are marked by crosses and the numerical values obtained are $\gamma \approx 1.85$, $\delta \approx 4.01$ and $\eta \approx 6.21$ for the square lattice and $\gamma \approx 1.98$, $\delta \approx 4.30$ and $\eta \approx 6.66$ for the triangular lattice. The exponents values are the same as obtained in MC simulation on a large system of linear size $L = 2^{11}$ obtained in Chapter 3. The values of the critical exponents are found very different (beyond the error bars) on

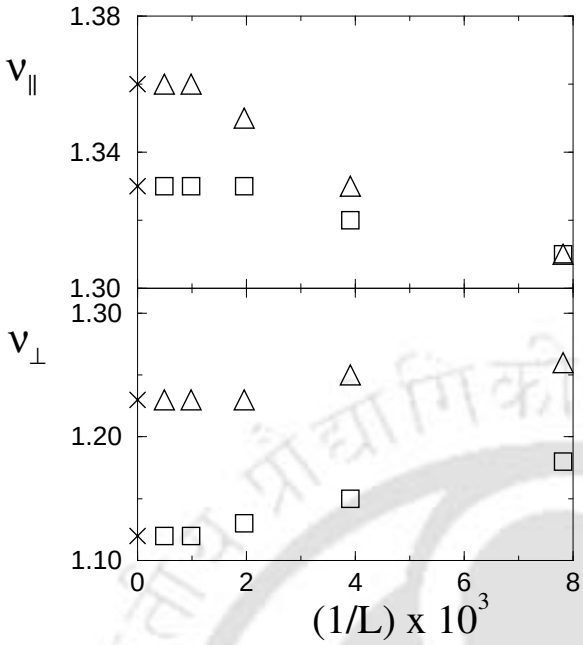

Figure 4.4: The connectivity exponents $\nu_{\parallel}$ and $\nu_{\perp}$ are plotted against the inverse system size $1/L$ for the square (□) and triangular (△) lattices. Extrapolated values to the infinite system size ($1/L = 0$) are marked by crosses.

the square and triangular lattices. Moreover, the difference is much more distinct as the system size is approaching to infinity. All the exponents are also different from those of the other percolation models like OP[3,12,13], DP[14,15] and SP[16–18]. The extrapolation of critical exponents then confirms the differenence in the values of critical exponents on the square and triangular lattices in $2D$. The observation has been reported in the Ref. [19].

The connectivity lengths $\xi_{\parallel}$ along the elongation of the cluster and $\xi_{\perp}$ along the transverse direction defined as,

$$\xi_{\parallel}^2 = \frac{2\sum_s' R_{\parallel}^2 s P_s(p,L)}{\sum_s' s P_s(p,L)} \quad \text{and} \quad \xi_{\perp}^2 = \frac{2\sum_s' R_{\perp}^2 s P_s(p,L)}{\sum_s' s P_s(p,L)} \tag{4.1}$$

are also measured for different system sizes. Here $R_{\parallel}$ and $R_{\perp}$ are radii of gyration with respect to two principal axes of the cluster. Corresponding connectivity exponents, $\nu_{\parallel,L}$ and $\nu_{\perp,L}$ are then determined from the slope of the plots of $\log \xi_{\parallel}$ and $\log \xi_{\perp}$ against $\log |p - p_c|$. In Figure 4.4, $\nu_{\parallel,L}$ and $\nu_{\perp,L}$ are plotted against the inverse system size $1/L$ for the square and triangular lattices. In both the plots, the squares represent the square lattice data and the triangles represent the triangular lattice data. The exponents are extrapolated to $L \to \infty$ and found as $\nu_{\parallel} \approx 1.33$ and $\nu_{\perp} \approx 1.12$ on the square lattice and $\nu_{\parallel} \approx 1.36$ and $\nu_{\perp} \approx 1.23$ on the triangular lattice. There are few things to notice. First, the values of the exponents converge to the corresponding values of the large system sizes. The extrapolated values also

match with those already obtained on the $L = 2^{11}$ lattices. Second, the exponents for both the lattices are different from those of other percolation models OP, DP and SP. Third, though the exponent $\nu_{\parallel}$ for the triangular lattice is very close to that of the square lattice value, $\nu_{\perp}$ is significantly different on the two lattices.

According to the above study, the values of the critical exponents for the DSP model obtained in the $L \to \infty$ limit on the square and triangular lattices are found same with the already obtained values on the large systems reported in the previous chapter. Most of the exponents are found significantly different on the two lattices. Also, it is found that the difference is much more distinct for the larger systems. The exponents on both the lattices are found different from other percolation models OP, DP and SP also. Therefore, this finite size scaling study also supports the arguments made earlier that the DSP model belongs to a new universality class other than OP, DP and SP. The study also confirms that the model exhibits a breakdown of universality in the cluster properties on the square and triangular lattices in 2D [19].

4.2 Anisotropic FSS theory

FSS functions for isotropic percolation models such as OP [3] and SP [17] are already available. According to the isotropic FSS theory, a cluster related Q, which scales as $Q \sim |p - p_c|^{-q}$ as $p \to p_c$, should obey the FSS scaling function form

$$Q(L, p) = L^{q/\nu} F[(p - p_c)L^{1/\nu}] \tag{4.2}$$

in the finite geometry ($L < \xi$). Here ν is the connectivity length exponent. Since DSP is an anisotropic percolation model, there are two connectivity lengths $\xi_{\parallel}$ and $\xi_{\perp}$, both of which become singular at the percolation threshold with two different critical exponents $\nu_{\parallel}$ and $\nu_{\perp}$. Therefore, the usual FSS theory for the isotropic percolation models is not applicable for the anisotropic DSP and as well as for the DP model. However, there are very few FSS theories available for anisotropic models in statistical physics [5–8]. Considering DP as a minimal stochastic Markovian process represented by Langevin equation, a FSS theory has been developed by Janssen *et al* [9] below the upper critical dimension $d_c = 4$ and above d_c by Lübeck and Janssen [20]. For the 3-state Potts model, finite size scaling theory was studied by Cardy [5,6] on the 2D strip like systems having finite dimension only in x direction and infinite dimension along y. A detailed study on the finite size effects on the systems of rectangular geometry ($L_{\parallel} \times L_{\perp}$) with anisotropic correlations had been

performed by Binder *et al*[8]. The anisotropy in the system is due to different exchange interactions between the spins in different directions. Bhattacharjee *et al*[21] studied the finite-size effects of anisotropic dimer model of domain walls in the strip like and rectangular systems. Finite size scaling theory was also developed for the directed self-avoiding walks on the square lattice of rectangular geometry with cylindrical boundary condition[22]. Thus, the anisotropy considered in the FSS theory generally is either in the interaction between the constituent particles[8] or in the topology of the system (strip like structure)[5–7]. However, in a geometrical model like percolation, the particles are simply occupied with a probability p in absence of any interaction between them. The models are generally defined on topologically isotropic systems of size $L \times L$. For such non-interacting anisotropic models defined on topologically isotropic systems, a simple phenomenological FSS theory is developed here considering the cluster size distribution function as a generalized homogeneous function[1]. The scaling function is then function of the occupation probability p and the ratios of connectivity lengths with the system size L.

A system is said to be finite if the system size $L < \xi$, the connectivity length. In the case of anisotropic percolation models, there are two connectivity lengths $\xi_{\parallel}$ and $\xi_{\perp}$ where $\xi_{\parallel}$ always greater than $\xi_{\perp}$. The finiteness of the system size is then defined in terms of $\xi_{\parallel}$, *i.e.* if $L < \xi_{\parallel}$, the system is finite. According to the theory of critical phenomena, thermodynamic functions become generalized homogeneous functions at the critical point[1]. The cluster size distribution function $P_s(p, L)$ describing the geometrical quantities here in percolation is then expected to be a generalized homogeneous function at the percolation threshold p_c. In order to develop a FSS theory, the scaling of the order parameter of the percolation transition P_∞, probability to find a site in the spanning cluster, with the system size L is considered first. At the end, the scaling form will be generalized for arbitrary cluster related quantity Q.

In the case of an infinite system, the order parameter P_∞ becomes singular at $p = p_c$ as

$$P_\infty \sim (p - p_c)^\beta \tag{4.3}$$

with a critical exponent β. In a finite geometry with topologically isotropic dimension $L \times L$, the critical singularity of P_∞ for anisotropic percolation clusters depends not only on $(p - p_c)$ but also on the the ratios $\xi_{\parallel}/L$ and $\xi_{\perp}/L$. The functional dependence of P_∞ on these parameters is then given by

$$P_\infty(L, p) = \mathcal{F}[(p - p_c), \frac{\xi_{\parallel}}{L}, \frac{\xi_{\perp}}{L}]. \tag{4.4}$$

For an infinite system, $\xi_{\parallel}$ is infinitely large at $p = p_c$ and the system properties become independent of the system size L. Accordingly, two parameters $\xi_{\parallel}/L$ and $\xi_{\perp}/L$ in P_∞ given in Eq. 4.4 can be reduced to a single parameter $\xi_{\parallel}/\xi_{\perp}$. Thus, P_∞ in Eq. 4.4 can be expressed as

$$P_\infty = \mathcal{G}[(p - p_c), \xi_{\parallel}/\xi_{\perp}]. \tag{4.5}$$

It is now important to know how $\xi_{\parallel}$ and $\xi_{\perp}$ scale with the lattice dimension L of the finite system at the percolation threshold p_c. Two new scaling relations for $\xi_{\parallel}$ and $\xi_{\perp}$ with L are assumed as,

$$\xi_{\parallel} \approx L^{\theta_{\parallel}} \quad \text{and} \quad \xi_{\perp} \approx L^{\theta_{\perp}} \tag{4.6}$$

where $\theta_{\parallel}$ and $\theta_{\perp}$ are two new exponents. It is now possible to define P_∞ in terms of the system size L as

$$P_\infty = F[(p - p_c), L^{\theta_{\parallel} - \theta_{\perp}}]. \tag{4.7}$$

If the scaling function F is a generalized homogeneous function of $(p - p_c)$ and L, then

$$F[\lambda^a (p - p_c), \lambda^b L^{\theta_{\parallel} - \theta_{\perp}}] = \lambda P_\infty \tag{4.8}$$

where a and b are arbitrary numbers and λ is a parameter[1]. The above relation is valid for any value of λ. For $\lambda = L^{-(\theta_{\parallel} - \theta_{\perp})/b}$, P_∞ takes the form

$$P_\infty = L^{A(\theta_{\parallel} - \theta_{\perp})} F[(p - p_c) L^{-B(\theta_{\parallel} - \theta_{\perp})}, 1] \tag{4.9}$$

where $A = 1/b$ and $B = a/b$ are two exponents to be determined. However, as $L \to \infty$, the L-dependence of P_∞ will vanish. Therefore, $F[z]$ should go as $z^{A/B}$ in the limit $L \to \infty$ where $z = (p - p_c) L^{-B(\theta_{\parallel} - \theta_{\perp})}$. In that case,

$$\begin{aligned} P_\infty &\approx L^{A(\theta_{\parallel} - \theta_{\perp})} \left[L^{-B(\theta_{\parallel} - \theta_{\perp})} (p - p_c) \right]^{A/B} \\ &\approx (p - p_c)^{A/B}. \end{aligned} \tag{4.10}$$

The order parameter exponent β is then given by $\beta = A/B$.

The percolation probability P_∞ is the ratio of the number of sites on the infinite cluster to the total number of sites and can be given as

$$P_\infty = \frac{R_{\parallel} R_{\perp}^{(d_f - 1)}}{R_{\parallel} R_{\perp}^{(d-1)}} = R_{\perp}^{(d_f - d)} \tag{4.11}$$

where $R_\parallel$ and $R_\perp$ are two radii of gyrations with respect to two principal axes of the cluster. Assuming $R_\perp \approx \xi_\perp \approx L^{\theta_\perp}$ at p_c, Eq. 4.11 leads to $P_\infty \sim L^{\theta_\perp(d_f-d)}$. Also at $p = p_c$, the functional form of P_∞, given in Eq. 4.9, reduces to $P_\infty \sim L^{A(\theta_\parallel-\theta_\perp)}$, assuming $F[0]$ is a constant. Therefore, exponent A can be obtained in terms of the new exponents $\theta_\parallel$ and $\theta_\perp$ as

$$A = \frac{\theta_\perp(d_f - d)}{\theta_\parallel - \theta_\perp}. \tag{4.12}$$

Inserting the value of A in Eq. 4.9 at $p = p_c$ it reduces to

$$P_\infty = L^{\theta_\perp(d_f-d)}F[0] = \xi_\perp^{(d_f-d)}F[0] = \xi_\parallel^{(d_f-d)\theta_\perp/\theta_\parallel}F[0] \tag{4.13}$$

where $F[0]$ is a constant. For an infinite system, at $p = p_c$, the connectivity lengths diverge as

$$\xi_\parallel \sim |p - p_c|^{-\nu_\parallel} \quad \text{and} \quad \xi_\perp \sim |p - p_c|^{-\nu_\perp} \tag{4.14}$$

where $\nu_\parallel$ and $\nu_\perp$ are connectivity exponents. The following scaling relations then can easily be extracted as

$$\beta = \nu_\perp(d - d_f) \quad \text{and} \quad \beta = \nu_\parallel(d - d_f)\theta_\perp/\theta_\parallel. \tag{4.15}$$

The first one of these relations is the well known hyperscaling relation[3] and the second one is a new scaling relation connecting the exponents $\theta_\perp$ and $\theta_\parallel$. From the above scaling relations it can be seen that $\nu_\perp = \nu_\parallel\theta_\perp/\theta_\parallel$. Consequently, one can define the anisotropy exponent

$$\theta = \frac{\theta_\parallel}{\theta_\perp} = \frac{\nu_\parallel}{\nu_\perp} \tag{4.16}$$

as suggested in Refs. [23,24]. Using the above scaling relations and eliminating $(d - d_f)$, the values of the exponents A and B can be obtained as

$$\begin{aligned} A &= -\frac{\theta_\perp\beta}{(\theta_\parallel-\theta_\perp)\nu_\perp} = -\frac{\theta_\parallel\beta}{(\theta_\parallel-\theta_\perp)\nu_\parallel} = -\frac{\beta}{(\theta-1)\nu_\perp} = -\frac{\theta\beta}{(\theta-1)\nu_\parallel} \\ B &= -\frac{\theta_\perp}{(\theta_\parallel-\theta_\perp)\nu_\perp} = -\frac{\theta_\parallel}{(\theta_\parallel-\theta_\perp)\nu_\parallel} = -\frac{1}{(\theta-1)\nu_\perp} = -\frac{\theta}{(\theta-1)\nu_\parallel} \end{aligned} \tag{4.17}$$

which reduces to $B = A/\beta$. Since the clusters are elongated along the diagonal of the lattice, $\xi_\parallel$ should be $\approx \sqrt{2}L$ for large clusters and accordingly $\theta_\parallel$ is expected to be 1. Consequently, the anisotropic exponent $\theta \approx 1/\theta_\perp$. The numerical value of $\theta_\perp$ has to be determined in order to verify Eq. 4.16. This is interesting to note that Eq.

4.16 is always valid even if the hyperscaling relations in Eq. 4.15 are not exactly satisfied. It is known that hyperscaling relations are not satisfied in case of DP [25].

Since the values of A and B are now known, the finite-size scaling form of P_∞ can be given as

$$P_\infty(L,p) = L^{-\beta/(\theta\nu_\perp)} F[(p-p_c)L^{1/(\theta\nu_\perp)}]. \tag{4.18}$$

A finite-size scaling relation is thus obtained in terms of the transverse connectivity length exponent $\nu_\perp$ and the anisotropic exponent θ.

Now, the finite size scaling form of the order parameter P_∞ can be generalized for any cluster related quantity Q. Suppose that in an infinite system, as $p \to p_c$ the cluster related quantity Q scales as

$$Q \sim |p-p_c|^{-q} \tag{4.19}$$

where q is a critical exponent. In a finite geometry, it is then expected that the cluster related quantities in general will obey the finite size scaling law given by

$$Q(L,p) = L^{q/(\theta\nu_\perp)} F[(p-p_c)L^{1/(\theta\nu_\perp)}]. \tag{4.20}$$

It should be noticed that the finite-size scaling relation obtained here describes the scaling of cluster related quantities in the transverse direction. This is obtained without varying the system size in the transverse direction. The FSS relation in Eq. 4.20 is different from those of Binder and Wang [8] obtained for the Ising system and of Szpilka and Privman [22] obtained for directed self-avoiding walks both on the rectangular geometry $L_\parallel \times L_\perp$. Therefore, the FSS relation obtained here in terms of anisotropic exponent θ and connectivity exponent $\nu_\perp$ in the transverse direction is a new scaling relation.

In the following, the proposed anisotropic FSS theory will now be verified numerically for the DSP model. As the theory is developed for anisotropic percolation models in general, it should also be applicable to the DP model. Therefore, the anisotropic FSS theory is also verified for the DP model which will also be reported here.

4.2.1 Verification of anisotropic FSS theory

In order to verify the proposed FSS theory for the DSP model, simulations are performed on the square and triangular lattices of various sizes. Different system sizes are considered as $L = 2^7$ to 2^{11} in multiple of 2. Average has been taken

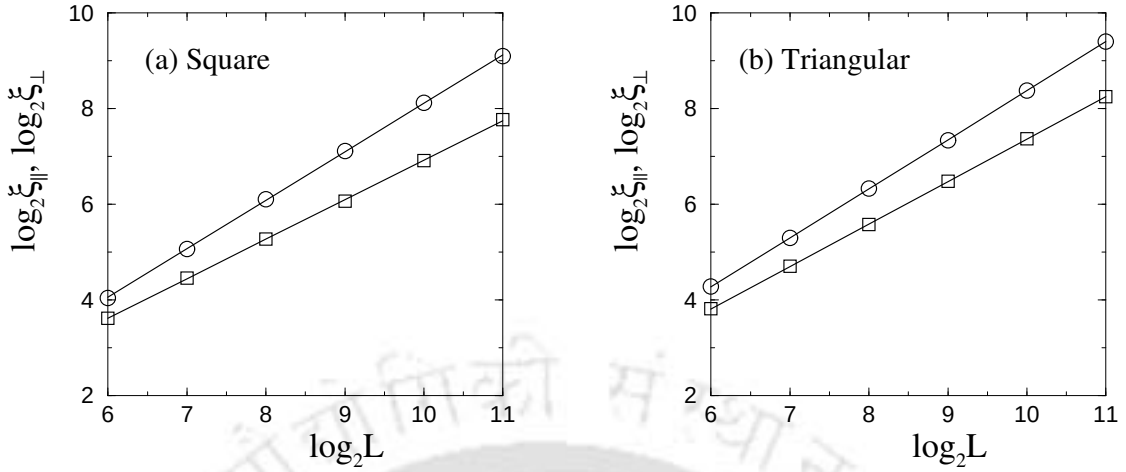

Figure 4.5: Plot of $\xi_\parallel$ (○) and $\xi_\perp$ (□) versus system size L for the DSP clusters on the (a) square and (b) triangular lattices at their respective percolation thresholds. From the slopes, value of $\theta_\parallel$ is obtained as $\theta_\parallel = 1.01 \pm 0.01$ for the square lattice and $\theta_\parallel = 1.02 \pm 0.01$ for the triangular lattice. Value of $\theta_\perp$ is obtained as $\theta_\perp = 0.83 \pm 0.01$ and $\theta_\perp = 0.89 \pm 0.01$ for the square and triangular lattices respectively.

over 5×10^4 large finite clusters. First, the exponents $\theta_\parallel$ and $\theta_\perp$ which describe the dependence of connectivity lengths with the system size L are determined by measuring $\xi_\parallel$ and $\xi_\perp$ on lattices of different sizes L at $p = p_c$. In Figure 4.5, $\xi_\parallel$ and $\xi_\perp$ are plotted against the system size L for the (a) square and (b) triangular lattices. The circles represent the data for $\xi_\parallel$ and the squares represent the data for $\xi_\perp$. From the slopes, the values of $\theta_\parallel$ and $\theta_\perp$ are obtained as 1.01 ± 0.01 and 0.83 ± 0.01 respectively for the square lattice. For the triangular lattice, corresponding values are 1.02 ± 0.01 and 0.89 ± 0.01 respectively. There are few things to notice. First, the exponent $\theta_\perp$ is found different on the square and triangular lattices. Second, as expected, the exponent $\theta_\parallel$ is found ≈ 1 for both the lattices. Assuming $\theta_\parallel = 1$, one should have $\theta_\perp = \nu_\perp/\nu_\parallel$ (Eq. 4.16). Since for DSP, the connectivity exponents are different on the square and triangular lattices[19], exponent $\theta_\perp$ is also expected to be different on the two lattices. On the square lattice, $\nu_\perp = 1.12 \pm 0.03$ and $\nu_\parallel = 1.33 \pm 0.01$[19,26] the expected value of $\theta_\perp$ is 0.84 ± 0.03. On the triangular lattice, expected value of $\theta_\perp$ should be 0.90 ± 0.03 as $\nu_\perp = 1.23 \pm 0.02$ and $\nu_\parallel = 1.36 \pm 0.02$[19]. Thus the measured values of $\theta_\perp$ on both the lattices are found close to the expected values. Also they are different on the two lattices as expected. The scaling relation in Eq. 4.16 is then verified within error bar. The anisotropy exponent θ then can be estimated as $\theta = 1/\theta_\perp \approx 1.20$ for the square lattice and ≈ 1.11 for the triangular lattice. It should be noticed that, the anisotropy exponent θ is higher for the square

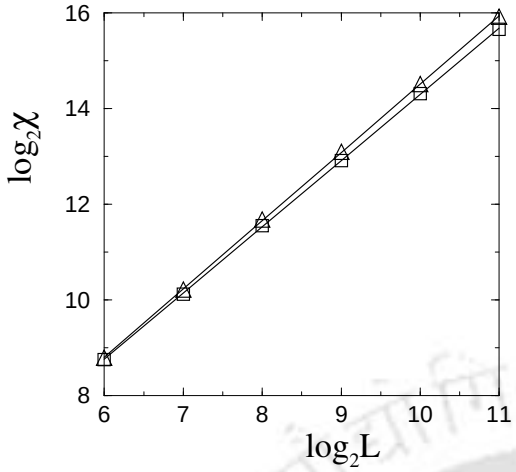

Figure 4.6: Plot of average cluster size χ versus system size L for the DSP clusters on the square (□) and triangular (△) lattices at respective percolation thresholds p_c. From the slopes, the ratio of $\gamma/(\theta\nu_\perp)$ is obtained as 1.38 ± 0.01 and 1.43 ± 0.01 for the square and triangular lattices respectively.

lattice than for the triangular lattice. Consequently the DSP clusters on the square lattice are more anisotropic than on the triangular lattice.

Knowing the value of the anisotropic exponent θ, the proposed FSS theory is verified for the average cluster size χ at the percolation threshold (p_c). According to the FSS theory, the average cluster size χ should behave as $\chi(L) \sim L^{\gamma/(\theta\nu_\perp)}$ at $p = p_c$. The average cluster size χ is then measured on the lattices of different sizes at the percolation threshold. In Figure 4.6, χ plotted against the system size L. The cluster size χ follows a power law with the system size L. The obtained slopes are 1.38 ± 0.01 for the square lattice and 1.43 ± 0.01 for the triangular lattice. According to the proposed FSS theory, the expected values of the ratio of the exponents are $\gamma/(\theta\nu_\perp) \approx 1.38$ for the square lattice and $\gamma/(\theta\nu_\perp) \approx 1.45$ for the triangular lattice as $\gamma = 1.85 \pm 0.01$ and 1.98 ± 0.02 [19,26] on the two lattices respectively. It can be seen that the measured values are in agreement with the expected values within error bars. It confirms that, at percolation threshold, the cluster properties follow the proposed finite size scaling theory. Moreover, the exponents measured on the large $L = 2^{11}$ lattices earlier, are free from the finite size effects as the ratio $\gamma/(\theta\nu_\perp)$ gives the same exponent when scaled with the system size L. The propegation errors are found very high in the case of higher moments.

Finally, the FSS function form has been verified. According to the developed FSS theory, the average cluster size χ should obey the scaling function form,

$$\chi(L, p) = L^{\gamma/(\theta\nu_\perp)} F[(p - p_c)L^{1/(\theta\nu_\perp)}] \tag{4.21}$$

for different values of the system size L. To verify the scaling function form, the average cluster size χ is measured on the lattices of different sizes L at different

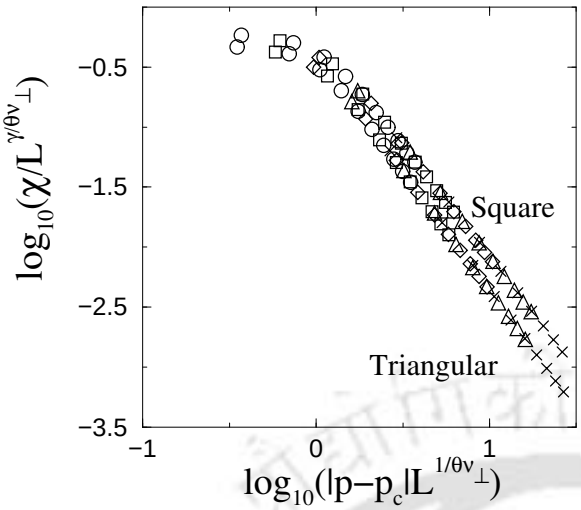

Figure 4.7: Plot of scaled average cluster size $\chi(p,L)/L^{\gamma/(\theta\nu_\perp)}$ versus scaled variable $|p-p_c|L^{1/(\theta\nu_\perp)}$ for the DSP clusters at different values of L and p. The data plotted correspond to different system sizes of $L = 2^7$ (○), 2^8 (□), 2^9 (◇), 2^{10} (△) and 2^{11} (×). The $|p-p_c|$ values here are 0.01 to 0.10 in the interval of 0.01.

percolation probabilities p. Here L is taken from 2^7 up to 2^{11} in the multiple of 2. The $|p-p_c|$ values are 0.01 to 0.10 in the interval of 0.01. In Figure 4.7, the scaled average size $\chi/L^{\gamma/(\theta\nu_\perp)}$ is plotted against the scaled variable $z = (p-p_c)L^{1/(\theta\nu_\perp)}$. It can be seen that a reasonable data collapse is obtained. Thus, the cluster properties obey the proposed L-dependent scaling function form not only at $p = p_c$ but also as $p \to p_c$. Interestingly, the scaling function form is found to be different for the square and triangular lattices. The tail of the scaling function $F(z)$ shows a power law behavior with different scaling exponents, approximately 1.86 for the square lattice and 1.99 for the triangular lattice. It can be noticed that, these exponents are close to the respective average cluster size critical exponent γ measured earlier on the large $L = 2^{11}$ lattices. It is expected because as $p \to p_c$, $\log F(z)/\log z = -\gamma$. It again confirms that the exponents obtained earlier on the large finite lattices are free from the finite size effects or they are within error bar of the exponents for the infinite systems.

4.3 Verification of FSS theory for DP model

The proposed anisotropic finite-size scaling theory has also been verified for the anisotropic directed percolation model also. It is found that, the DP cluster properties also obey the FSS theory as well as the FSS scaling function form. DP clusters are generated on the square lattice varying the system size L. The exponents $\theta_\parallel$ and $\theta_\perp$ are obtained as 1.01 ± 0.01 and 0.64 ± 0.01 for DP. Here also $\theta_\parallel \approx 1$ as expected. As the connectivity exponents $\nu_\perp = 1.0972 \pm 0.0006$ and $\nu_\parallel = 1.7334 \pm 0.001$ [14,23] for the DP model, the expected value of $\theta_\perp$ is 0.633 ± 0.001 which is in good agreement

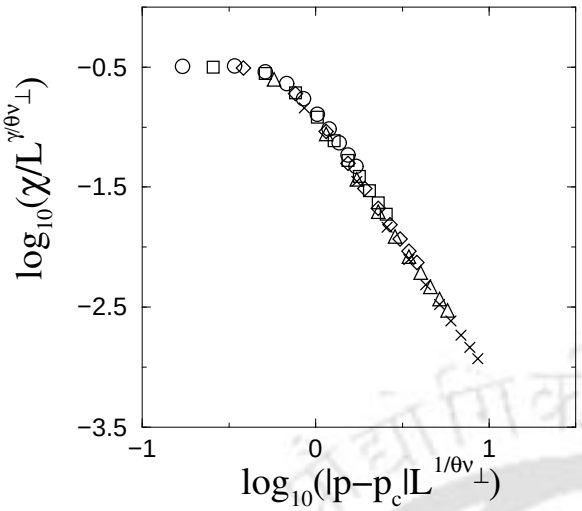

Figure 4.8: Plot of scaled average cluster size $\chi(p,L)/L^{\gamma/(\theta\nu_\perp)}$ versus scaled variable $|p-p_c|L^{1/(\theta\nu_\perp)}$ for the DP clusters for different values of L and p. The data plotted correspond to different system sizes of $L = 2^7$ (○), 2^8 (□), 2^9 (◇), 2^{10} (△) and 2^{11} (×). The $|p-p_c|$ values here are 0.01 to 0.10 in the interval of 0.01.

with the measured value. The anisotropic exponent $\theta = 1/\theta_\perp$ is estimated as ≈ 1.56 here which is much higher than that of the DSP model. It is expected as DP clusters are more anisotropic than DSP clusters.

The average cluster size χ of the DP clusters is measured for different system sizes L at the percolation threshold (≈ 0.705) [14]. The scaling function form at p_c given by $\chi(L) = L^{\gamma/(\theta\nu_\perp)}$ is then verified. The ratio of the exponents $\gamma/(\theta\nu_\perp)$ is obtained as 1.31 ± 0.01. This is close to the expected value ≈ 1.33, as $\gamma = 2.2772 \pm 0.0003$ [14,15] for the DP model. Thus the proposed FSS theory is valid for the DP model at p_c with the standard DP exponents available in the literature [14,15].

The FSS function form has also been verified for the average cluster size of the DP model. In Figure 4.8, the scaled average size $\chi/L^{\gamma/(\theta\nu_\perp)}$ is plotted against the scaled variable $z = (p-p_c)L^{1/(\theta\nu_\perp)}$. A reasonable data collapse is obtained. The scaling function form is different from those of the DSP model. Here, the tail of the scaling function $F(z)$ also shows a power law with an exponent ≈ 2.23. This is again close to the average cluster size exponent $\gamma = 2.2772 \pm 0.0003$ [14,15]. The method of anisotropic FSS and its validity has been reported in Refs. [27,28].

Thus, both the DSP and DP follow the proposed anisotropic finite size scaling theory and belong to two different universality classes.

4.4 Conclusion

The effect of finite system size on the Monte Carlo results of the DSP model has been studied by finite size scaling techniques. Two different methods have been adopted to verify the previous MC results obtained on a single large but finite lattice. First,

the exponents are calculated as a function of the system size L and extrapolated to $L \to \infty$. It is found that the values of the critical exponents converge to the values for larger systems like $L = 2^{10}$ and 2^{11}. Exponents in the $L \to \infty$ limit are same with the values already obtained on a single large lattice of size $2^{11} \times 2^{11}$. Second, a finite size scaling theory is proposed for anisotropic percolation models. In this theory the cluster size distribution is assumed to be a generalized homogeneous function of $(p - p_c)$ and the ratios of the connectivity lengths $\xi_{\parallel}$ and $\xi_{\perp}$ to the system size L. The scaling function form of the cluster properties is obtained in terms of the anisotropic exponent θ and connectivity exponent $\nu_{\perp}$ in the transverse direction. Through numerical simulation, the proposed scaling relations as well as the scaling function form are verified for the DSP model and also for the DP model. The results obtained here through the FSS study also confirm the breakdown of universality observed in the DSP cluster properties. This is an unusual property of the DSP model in the context of critical phenomena. This property will be analyzed critically again later in this thesis by performing multifractal analysis of spanning infinite clusters. However, the immediate aim is to look for universal properties of the model. In the next chapter the properties of external perimeter or hull of the DSP clusters will be analyzed in the search of universality.

Bibliography

[1] H. E. Stanley, *Introduction to Phase Transitions and Critical Phenomena*, Oxford University Press, New York, 1987.

[2] J. M. Yeomans, *Statistical Mechanics of Phase Transitions*, Oxford University Press, New York, 1994.

[3] D. Stauffer and A. Aharony, *Introduction to Percolation Theory*, Taylor and Francis, London, 2nd edition, 1994.

[4] V. Privman, *Finite Size Scaling and Numerical Simulation of Statistical Systems*, World Scientific Publication, Singapore, 1990.

[5] J. L. Cardy, *Finite Size Scaling*, North Holland, Amsterdam, 1988.

[6] J. L. Cardy, J. Phys. A: Math. Gen. **17**, L961 (1984).

[7] J. L. Cardy, J. Phys. A: Math. Gen. **25**, L201 (1992).

[8] K. Binder and J. S. Wang, J. Stat. Phys. **55**, 87 (1989).

[9] H. K. Janssen, B. Schaub and B. Schmittmann, Z. Phys. B - Condensed Matter **71**, 377 (1988).

[10] J. F. Nagle, C. S. O. Yokoi and S. M. Bhattacharjee, Dimer models on anisotropic lattices, in *Phase transitions and Critical Phenomena*, edited by C. Domb and J. Lebowitz, Academic Press, 1989.

[11] S. B. Santra, Int. J. Mod. Phys. B **17**, 5555 (2003).
[12] M. P. M. den Nijs, J. Phys. A **12**, 1857 (1997).
[13] B. Nienhuis, J. Phys. A **15**, 199 (1982).
[14] J. W. Essam, A. J. Guttmann and K. DéBell, J. Phys. A: Math. Gen. **21**, 3815 (1988).
[15] J. W. Essam, K. DéBell, J. Adler and F. M. Bhatti, Phys. Rev. B **33**, 1982 (1986).
[16] P. Ray and I. Bose, J. Phys. A **21**, 555 (1988).
[17] S. B. Santra and I. Bose, J. Phys. A **24**, 2367 (1991).
[18] S. B. Santra and I. Bose, J. Phys. A **25**, 1105 (1992).
[19] S. Sinha and S. B. Santra, Eur. Phys. J. B **39**, 513 (2004).
[20] S. Lübeck and H. K. Janssen, Phys. Rev. E **72**, 016119 (2005).
[21] S. M. Bhattacharjee and J. Nagle, Phys. Rev. A **31**, 3199 (1985).
[22] A. M. Szpilka and V. Privman, Phys. Rev. B **28**, 6613 (1983).
[23] W. Kinzel and J. M. Yeomans, J. Phys. A: Math. Gen. **14**, L163 (1981).
[24] J. K. Williams and N. D. Mackenzie, J. Phys. A: Math. Gen. **17**, 3343 (1984).
[25] M. Henkel and V. Privman, Phys. Rev. Lett. **65**, 1777 (1990).
[26] S. B. Santra, Eur. Phys. J. B **33**, 75 (2003).
[27] S. Sinha and S. B. Santra, Indian J. Phys. **(communicated)** (2007).
[28] S. Sinha and S. B. Santra, in *Abstracts - Condensed Matter Days 2006, Tezpur Univ., Assam, India, Aug., 2006.*

Chapter 5

DSP Hull Properties and Scaling

The hull of a percolation cluster is the continuous path of occupied sites at the external perimeter of the cluster. The hull has important significance of its own apart from being a part of the percolation cluster. It has connection with a large number of physical and chemical problems[1,2]. The hull of ordinary percolation cluster is closely related to the diffusion front resulting in a diffusion from a source[3–5], kinetic growth[6], surface growth[7–9], interacting surfaces[10], aggregation[11], image processing[12], biological evolution[13], fragmentation of random solid[14,15] and many others. Several other physical phenomena like nucleation[16,17], surface reaction[18–20] etc. are also connected to the percolation hull.

The hull exhibits scaling behaviour, different from that of the clusters, characterized by its own critical exponents at the percolation threshold[21–24]. It has already been shown that the DSP clusters are anisotropic with chiral dangling ends. Anisotropic hulls are less characterized in the literature of percolation except the hull of DP clusters[24–26]. The DP hull has similar scaling properties as that of the interfaces in the surface growths[27]. The critical properties of the DSP clusters were already found to be significantly different from that of the other percolation models OP, DP and SP. It is also observed that the critical exponents related to the DSP cluster properties differ on the square and triangular lattices. It is then important to search for the universal characteristics of this model and the critical properties of hull could be considered as an relevant quantity in this regard. The critical behaviour of the anisotropic-chiral hulls associated with the DSP clusters is then studied at the percolation threshold and the critical properties are characterized.

5.1 Extraction of hull from the DSP clusters

In order to study the DSP hull properties, clusters are generated on the square and triangular lattices using the same single cluster growth algorithm developed in Chapter 2. As soon as a cluster is generated, the continuous path of occupied sites, connected by nearest neighbour bonds, at the external boundary of the cluster called the percolation hull can be identified. The DSP cluster hull is determined by the method of Ziff *et al*[28] developed to extract the hull of the OP clusters. The algorithm of hull determination consists of the following steps:

(1) Pick a pair of occupied and empty nearest neighbour sites at one point on the external boundary or hull. An arrow is drawn from the empty site to the occupied site to define a direction and one moves to the occupied site.

(2) Facing the direction of the arrow, a search is made for an occupied nearest neighbour from the left and following the order left, front, right and back. As soon as an occupied site is encountered an arrow is drawn from the present site to the new occupied site and one moves to the new occupied site.

(3) The process is continued until the path passes the starting point in the same direction as it had first passed. All the distinct occupied sites encountered during this walk are listed in an array called the hull of the cluster.

The algorithm takes one on a walk around the external perimeter of the cluster. The size of the hull is determined by the distinct occupied sites encountered during the walk. Since an occupied site can be encountered more than once, it is necessary to remember whether a site has been previously counted. The above algorithm had been generalized further by Ziff *et al*[29] which generates the perimeter independent of the cluster itself. However, this generalization is not possible in the case of DSP.

Typical percolation clusters and their hulls at the $p = p_c$ on the square and triangular lattices are shown in Figures 5.1 and 5.2, respectively. The sites on the hull are marked by red dots and the interior cluster sites are marked by black dots. The hulls are found anisotropic on both the lattices though the percolation cluster as well as the hull are more anisotropic on the square lattice than on the triangular lattice. However, both the hulls contain chiral dangling ends and look very similar on small length scales. Apart from the external perimeter or hull, there are holes of all possible sizes inside the percolation cluster. These holes or cavities have perimeters called internal perimeter. It has been demonstrated by Blaudeck *et al*[30] after computing both external and internal perimeters that both of them follow the same scaling behaviour.

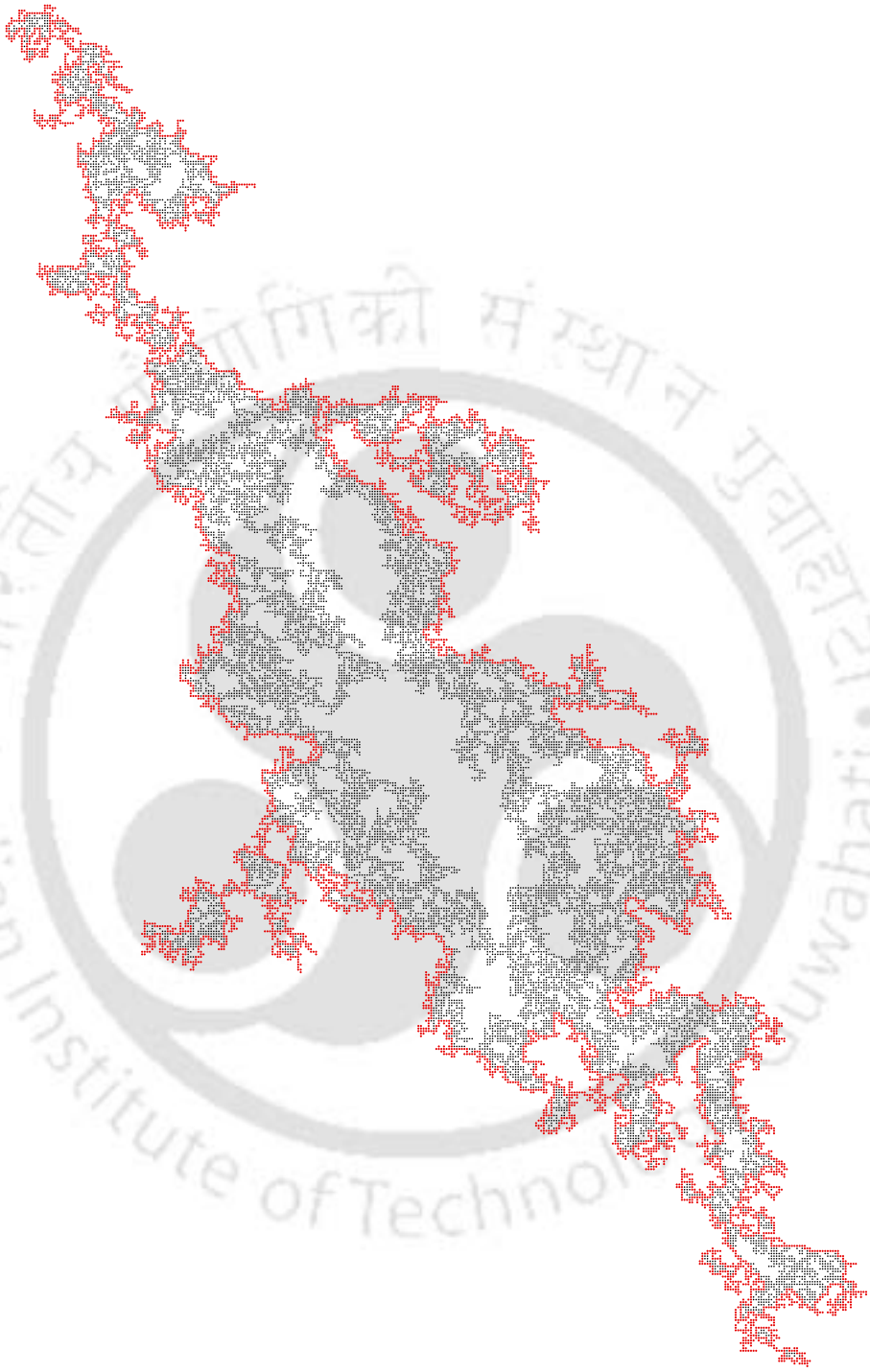

Figure 5.1: Hull of a spanning cluster of size $S = 23964$ on a $2^8 \times 2^8$ square lattice at the percolation threshold $p_c = 0.655$. The size of the hull is $H = 7938$. It could be seen that the dangling ends are clockwisely rotated and the cluster is anisotropic.

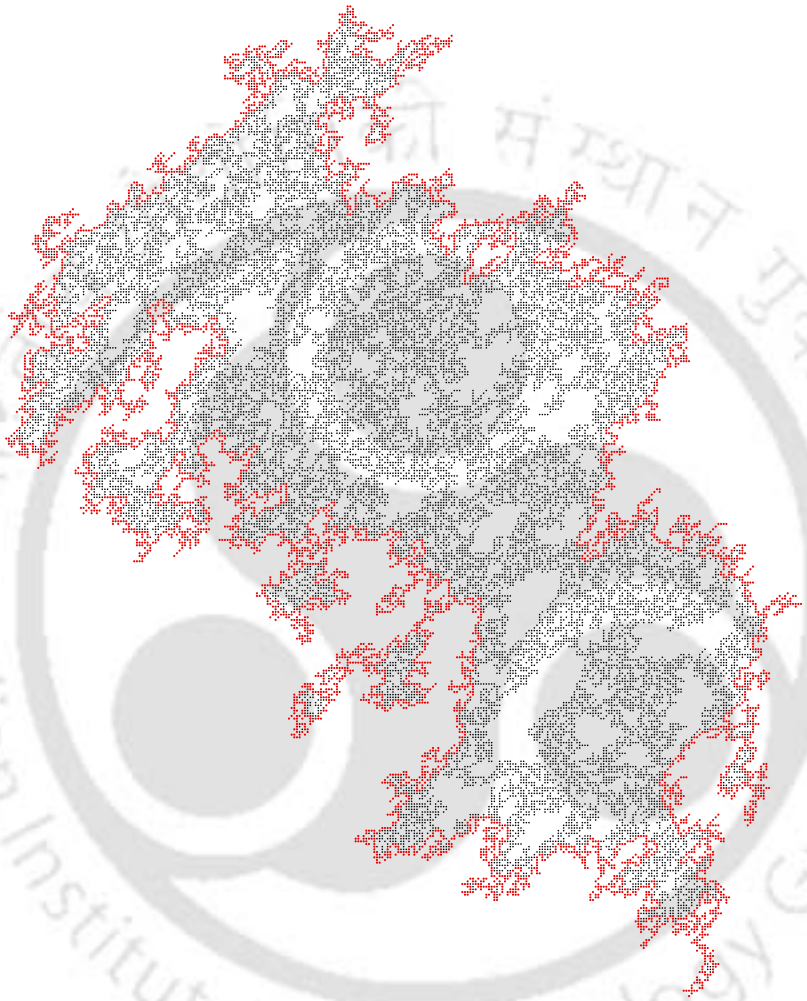

Figure 5.2: Hull of a spanning cluster of size $S = 24952$ on a $2^8 \times 2^8$ triangular lattice at the percolation threshold $p_c = 0.570$. The size of the hull is $H = 6333$. There are chiral dangling ends but the cluster is less anisotropic than the cluster on the square lattice.

5.2 Hull scaling relations

Analogous to the cluster related quantities, the hull related quantities also exhibit critical properties[21–24] at the percolation threshold p_c. The corresponding critical exponents associated to hull related quantities are expected to satisfy certain scaling relations among themselves similar to the scaling relations satisfied by the critical exponents of the cluster related quantities as described in Chapter 3. The scaling theories of the hull related quantities for the OP[22], DP[24] and SP[21] models are already available in the literature. In this section, the critical exponents of the analogous hull related quantities for the DSP model will be defined and their scaling relations will be developed. The size of a hull H is given by the number of occupied sites present on the hull as the size of a cluster is given by the number of distinct occupied sites in a cluster. At p_c, the size of the infinite cluster goes as

$$S_\infty \sim L^{d_f} \tag{5.1}$$

with the system size L, d_f is the fractal dimension of the infinite cluster. The value of d_f has already been estimated on both the square[31] and triangular[32] lattices. For hulls, a similar relation is assumed here between the size of the largest hull H_∞ with the system size L as

$$H_\infty \sim L^{d_H} \tag{5.2}$$

where d_H is the hull dimension. The value of d_H then can be determined measuring H_∞ for different system sizes L. It may be noted here that the so-called Ziff method[33] is not suitable to determine the hull dimension of the anisotropic clusters generated here. In Ziff's method, the linear distance is measured for a given number of sites along the hull. Since there are two length scales ($\xi_\parallel$ and $\xi_\perp$) involved in the DSP clusters, there will be a crossover from $\xi_\perp$ to $\xi_\parallel$ as one measures the linear distance from smaller number of sites to larger number of sites. The average length of a given number of occupied sites will be then strongly dependent on the initial point chosen.

From Eqs. 5.1 and 5.2, one can easily verify the relation between the cluster size S_∞ and the corresponding hull size H_∞ for the spanning clusters and it is given by

$$H_\infty \sim S_\infty^x, \qquad x = d_H/d_f \tag{5.3}$$

where d_H and d_f are the fractal dimensions of the hull and the corresponding percolation cluster, respectively. The value of d_H obtained from Eq. 5.2 then could be

verified measuring x and d_f independently.

The hull size distribution is defined as

$$P_H(p) = N_H/N_{tot} \tag{5.4}$$

where N_H is the number of hulls of size H and N_{tot} is the total number of hulls generated, same as the number of clusters generated. Analogous to the form of the cluster size distribution function, the scaling function form of the hull size distribution is assumed as

$$P_H(p) = H^{-\tau_H+1}\mathsf{f}[H^{\sigma_H}(p-p_c)] \tag{5.5}$$

where τ_H and σ_H are two exponents. The same scaling function form has already been verified for the spiral percolation hull[21].

Different moments of the hull size distribution $P_H(p)$, $\sum'_H H^k P_H(p)$ are expected to be singular as $p \to p_c$. The primed sum represents the sum of all finite hulls. The first, second and third moments χ_H, χ'_H and χ''_H of $P_H(p)$ are calculated. The first moment $\chi_H = \sum'_H H P_H(p)$ is the average hull size. The moments χ_H, χ'_H and χ''_H diverge with their respective critical exponents γ_H, δ_H and η_H at $p = p_c$. The critical exponents are defined as

$$\chi_H \sim |p-p_c|^{-\gamma_H},\ \ \chi'_H \sim |p-p_c|^{-\delta_H}\ \ \&\ \ \chi''_H \sim |p-p_c|^{-\eta_H}. \tag{5.6}$$

Since the hull related quantities are just different moments of the hull size distribution function $P_H(p)$, the critical exponents γ_H, δ_H and η_H then should be related to τ_H and σ_H, exponents related to $P_H(p)$. It can be shown that the kth moment of the hull size distribution becomes singular as

$$\Sigma'_H H^k P_H(p) \sim (p-p_c)^{-(k-\tau_H+2)/\sigma_H}. \tag{5.7}$$

The following scaling relations then can easily be obtained putting appropriate values of k, order of the moment of $P_H(p)$, in Eq. 5.7 and one obtains,

$$\gamma_H = (3-\tau_H)/\sigma_H,\ \ \delta_H = (4-\tau_H)/\sigma_H\ \ \&\ \ \eta_H = (5-\tau_H)/\sigma_H. \tag{5.8}$$

Eliminating τ_H and σ_H from Eq. 5.8 a scaling relation can be obtained as

$$\eta_H = 2\delta_H - \gamma_H. \tag{5.9}$$

The exponents τ_H and σ_H can also be estimated from the measured exponents γ_H, δ_H and η_H using the following relations

$$\tau_H = (3\delta_H - 4\gamma_H)/(\delta_H - \gamma_H) = (4\eta_H - 5\delta_H)/(\eta_H - \delta_H) = (3\eta_H - 5\gamma_H)/(\eta_H - \gamma_H),$$
$$\sigma_H = 1/(\delta_H - \gamma_H) = 1/(\eta_H - \delta_H) = 2/(\eta_H - \gamma_H). \tag{5.10}$$

The values of the hull fractal dimension and other critical exponents will be estimated below and the scaling theory will be verified.

5.3 Results and Discussions

In this section, estimates of the hull fractal dimension and other critical exponents of the hull related quantities will be presented for anisotropic DSP cluster hulls. A comparison will be made between the results obtained on the square and triangular lattices and also with that of the other percolation models.

To extract hulls, clusters are generated on both the square and triangular lattices at their respective percolation thresholds $p_c \approx 0.6550$ and 0.5700 respectively. Different lattice sizes starting from $L = 2^5$ to 2^{11} have been used. A total number of $N_{tot} = 5 \times 10^4$ clusters are generated for each lattice size L and every p, site occupation probability. Since each cluster has an associated hull, the number of hulls extracted are also N_{tot}. The size of the hull H is given by the number of occupied sites belonging to the hull.

5.3.1 Hull fractal dimension

The hull fractal dimension of the DSP clusters is determined following the scaling relation, $H_\infty \sim L^{d_H}$, Eq. 5.2. For different system sizes (L), average hull size H_∞ of the spanning DSP clusters are measured and given in Table 5.1. In Figure 5.3, H_∞ is plotted against the system size L. The squares represent the square lattice data and the triangles represent the triangular lattice data. The values of the hull dimension d_H are obtained as $d_H = 1.458 \pm 0.008$ for the square lattice and $d_H = 1.463 \pm 0.004$ for the triangular lattice[34]. The hull fractal dimension d_H has also been measured by box counting (BC) method generating spanning clusters on the largest lattice ($2^{11} \times 2^{11}$) considered here. The number of boxes occupied with a hull site $N_B(\epsilon) \sim \epsilon^{d_H}$, where ϵ is the box size. The results are shown in the Figure 5.4. The values of d_H obtained in the box counting method are given as 1.44 ± 0.01 for the square and 1.45 ± 0.01 for the triangular lattice. The errors

Lattice size (L)	Average hull size of spanning clusters (H_∞)	
	Square Lattice	Triangular Lattice
2^5	0.35204750×10^3	0.32066400×10^3
2^6	0.97385750×10^3	0.90653733×10^3
2^7	0.26820200×10^4	0.25031480×10^4
2^8	0.70569525×10^4	0.68916167×10^4
2^9	0.19180285×10^5	0.19372117×10^5
2^{10}	0.54187652×10^5	0.53218109×10^5
2^{11}	0.15684014×10^6	0.13969832×10^6

Table 5.1: Average hull size H_∞ of the spanning DSP clusters generated on the square and triangular lattices of various sizes L.

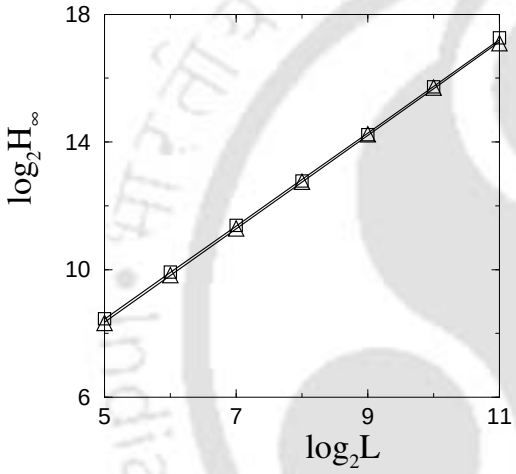

Figure 5.3: Average hull size H_∞ of the spanning clusters versus the system size L for the square ($\square$) and triangular ($\triangle$) lattices. The hull fractal dimensions are obtained as $d_H = 1.458 \pm 0.008$ for the square lattice and 1.463 ± 0.004 for the triangular lattice. The value of d_H is within error bars on the two lattices.

quoted for both the methods are the least squares fit errors taking into account the statistical error of each data point. The results obtained through box counting method and finite size scaling are within error bars. There are few things to notice. First, the hull fractal dimensions d_H measured on the square and triangular lattices in $2D$ are found the same within error bars, approximately 1.46, whereas the cluster fractal dimension d_f were found different on the same lattices[32]. It could also be seen that, the hulls shown in Figure 5.1 and 5.2 of the clusters generated on the square and triangular lattices respectively are very identical on small length scales. However, DSP clusters are more compact and less anisotropic on the triangular lattice than on the square lattice. As a consequence, the cluster fractal dimension d_f and other critical exponents of the DSP clusters were found to be different on these two lattices[32]. Thus, the extra flexibility given on the rotational constraint on the triangular lattice was only able to modify the critical behaviour of the whole cluster but unable to modify the critical properties of the external perimeter, the

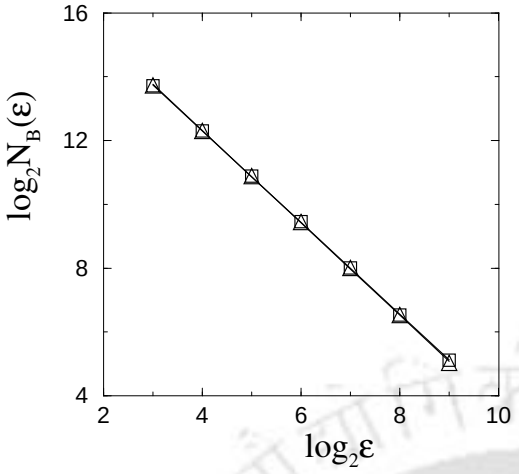

Figure 5.4: The number of boxes $N_B(\epsilon)$ is plotted against the box size ϵ for the square ($\square$) and triangular ($\triangle$) lattices. The hull fractal dimensions obtained by box counting method are $d_H = 1.44 \pm 0.01$ for the square lattice and 1.45 ± 0.01 for the triangular lattice. The values obtained here are within the error bar with the estimate by fsc method. The value of d_H is also within error bars on the two lattices.

hull.

Second, the hull fractal dimension d_H obtained here is smaller than that of OP cluster hulls (7/4). The OP cluster hulls generally contain long fjords or bays which are absent here. For OP cluster hulls, the value of $d_H = 7/4$ was conjectured by Sapoval *et al*[3–5] through a relation $d_H = 1 + 1/\nu$ connecting the hull dimension d_H and the connectivity length exponent ν studying the diffusion fronts. (In the case of OP, the value of ν is 4/3). This prediction was supported through large scale simulation by Ziff[33] and also proved analytically by Saleur and Duplantier[35]. It has already been observed that the conjecture does not hold true in the case of SP cluster hulls. The values of the connectivity exponents and hull fractal dimensions obtained for the SP clusters are: $\nu(SP) \approx 1.116$ and $d_H(SP) \approx 1.476$ $(1 + 1/\nu \approx 1.896)$ on the square lattice and $\nu(SP) \approx 1.136$ and $d_H(SP) \approx 1.466$ $(1 + 1/\nu \approx 1.880)$ on the triangular lattice[21]. Moreover, the DSP clusters are anisotropic and there are two connectivity length exponents $\nu_\parallel$ and $\nu_\perp$. The hull dimension d_H here then may not be related to the connectivity length exponents $\nu_\parallel$ and $\nu_\perp$ of the anisotropic clusters in a simple manner as it was predicted by Sapoval *et al* for the case of isotropic clusters generated in OP. Interestingly, it is found that the hull dimension d_H calculated from the following relation

$$d_H = 1 + \frac{\nu_\perp}{\nu_\parallel + \nu_\perp} \tag{5.11}$$

is very close to the numerical values obtained here. Using Eq. 5.11, the hull dimensions d_H are obtained as $d_H \approx 1.46$ on the square lattice and $d_H \approx 1.47$ on the triangular lattice. In the case of DP, the hull dimension is approximately 1.36[24] and from the conjecture in Eq. 5.11 it is approximately 1.38. It seems that for the

anisotropic clusters generated in DP and DSP, the hull dimension d_H is connected to the connectivity length exponents $\nu_{\parallel}$ and $\nu_{\perp}$ by the proposed relation in Eq. 5.11 and the relation proposed by Sapoval *et al* is valid only for the isotropic clusters generated in OP. However, an argument similar to the one given by Sapoval *et al*[3–5] would be possible only from the study of "anisotropic diffusion fronts".

Third, the values of the hull fractal dimensions obtained for both the DSP and SP clusters are close to the fractal dimension $D_e = 4/3$ of the externally accessible perimeter defined by Grossman and Aharony[36,37]. The external perimeter defined by Grossman and Aharony includes the sites available to a finite-size particle, coming from the outside, that is touching the occupied sites on the cluster. This external perimeter excludes deep fjords or bays and consequently the fractal dimension is found as 4/3. However, in the case of SP and DSP clusters, the hull is compact (or smooth) in comparison to the OP cluster hull due to the presence of rotational constraint in these models. The rotational constraint produces compact chiral dangling ends on the external boundary and makes the hull fractal dimension d_H closer to that of the Grossman-Aharony external perimeter. It should be mentioned here that a similar value of hull fractal dimension close to 4/3 was also obtained numerically by Meakin and Family[38] and Rosso[39]. The same hull fractal dimension was also found experimentally in the study of invasion percolation fronts by Birovljev *et al*[40], in the corrosion of thin Aluminum film by Balázs[41], and in spreading of mercury on silver films by Kaplan *et al*[42]. Deviation from the fractal dimension of 7/4 was also found in the study of self-stabilized etching of random systems by Sapoval *et al*[43]. In the study of diffusion driven spreading the hull dimension was also found to be 4/3[44]. Recently, Aizenman *et al*[45] proved exactly the fractal dimension of Grossman-Aharony external perimeter is 4/3. Desolneux and Sapoval showed that gradient percolation hull has fractal dimension 7/4[46].

The relation between the hull dimension d_H and the fractal dimension d_f of the percolation clusters is given by Eq. 5.3, $H_\infty \sim S_\infty^x, x = d_H/d_f$. This is verified here and the exponent x is calculated. Average hull size H_∞ corresponding to the average size S_∞ of the spanning clusters are measured on different lattices and given in Table 5.2. In Figure 5.5, H_∞ is plotted against S_∞ for both the square and triangular lattices. The slope $x = d_H/d_f$ is found as $x = 0.839 \pm 0.007$ on the square lattice and $x = 0.820 \pm 0.006$ on the triangular lattice. The errors are least squares fit error taking into account the statistical error of each data point. The values of x are found close but only slightly different on the two lattices. This small difference in the value of x is consistent with the small difference in the cluster fractal dimensions

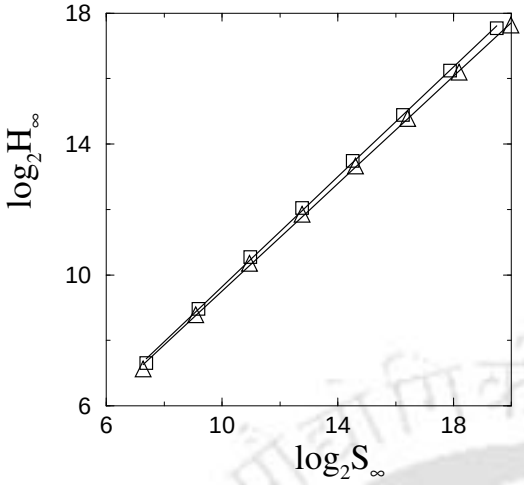

Figure 5.5: Plot of average hull size H_∞ versus corresponding average cluster size S_∞ of the spanning clusters. The squares represent the square lattice data and the triangles represent the triangular lattice data. The values of the exponent x are obtained as $x = 0.839 \pm 0.007$ for the square lattice and $x = 0.820 \pm 0.006$ for the triangular lattice.

d_f on the two lattices. The hull dimension d_H could be estimated from the relation $d_H = x \times d_f$ and compared with the measured values. As the values of d_f are already known, it is found that $d_H = 1.45 \pm 0.01$ on the square lattice and $d_H = 1.46 \pm 0.01$ on the triangular lattice which are within error bars of the measured value ≈ 1.46. The errors quoted here are the propagation errors.

5.3.2 Hull moment exponents

Now, the critical properties of different moments of the hull size distribution function are studied. The critical exponents related to the different moments of the hull size distribution $P_H(p)$ are already defined in section 5.2 and the scaling relations are also described there. In this section, the values of the critical exponents are estimated

Square lattice		Triangular lattice	
S_∞	H_∞	S_∞	H_∞
0.1658000×10^3	0.1591500×10^3	0.1537000×10^3	0.1406333×10^3
0.5789500×10^3	0.4995000×10^3	0.5436667×10^3	0.4421000×10^3
0.2017700×10^4	0.1497800×10^4	0.1975733×10^4	0.1305433×10^4
0.6925800×10^4	0.4231600×10^4	0.6940000×10^4	0.3714200×10^4
0.2333535×10^5	0.1152210×10^5	0.2500850×10^5	0.1031010×10^5
0.7774860×10^5	0.3043820×10^5	0.8678370×10^5	0.2821380×10^5
0.2413387×10^6	0.7758390×10^6	0.2986367×10^6	0.7543983×10^6
0.7390292×10^6	0.1901022×10^6	0.1034625×10^7	0.2033551×10^6

Table 5.2: Average hull size H_∞ corresponding to the average cluster size S_∞ of the spanning DSP clusters generated on the square and triangular lattices.

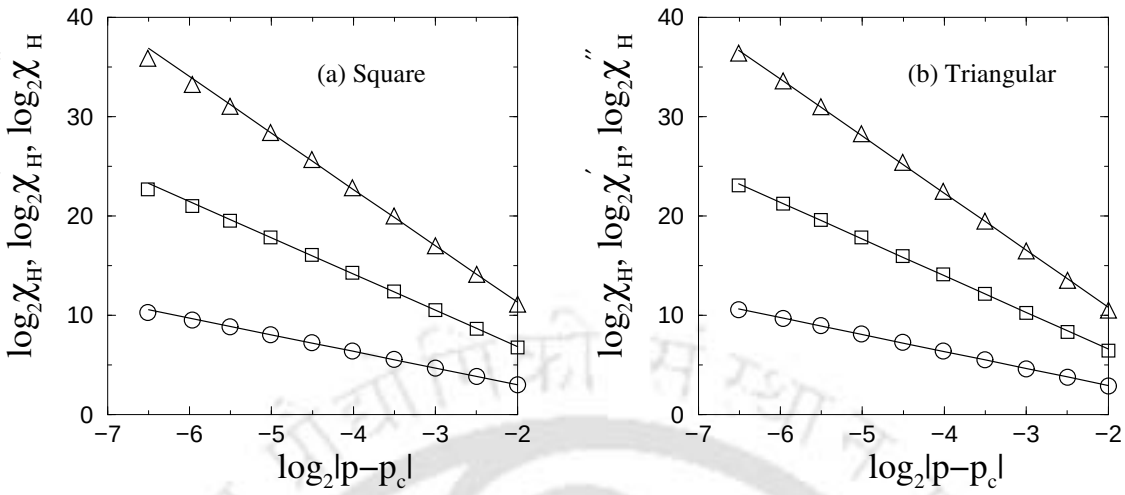

Figure 5.6: Plot of the first, second and third moments χ_H, χ'_H and χ''_H of hull size distribution versus $|p - p_c|$ for the (a) square and (b) triangular lattices of size $L = 2^{11}$. Different symbols are circles for χ_H, squares for χ'_H and triangles for χ''_H for each lattice. The solid lines represent the best fitted straight lines through the data points. The corresponding critical exponents are found as $\gamma_H = 1.68 \pm 0.02$, $\delta_H = 3.66 \pm 0.03$ and $\eta_H = 5.70 \pm 0.05$ for the square lattice and $\gamma_H = 1.71 \pm 0.02$, $\delta_H = 3.69 \pm 0.03$ and $\eta_H = 5.73 \pm 0.05$ for the triangular lattice.

and the scaling relations are verified. The first three moments χ_H, χ'_H and χ''_H are plotted against $|p - p_c|$ for the square lattice in Figure 5.6(a) and for the triangular lattice in Figure 5.6(b). The system size is taken as $L = 2^{11}$. The circles represent the average hull size χ_H, the squares represent χ'_H, the second moment and the triangles represent χ''_H, the third moment in both the plots. The values of the exponents obtained are $\gamma_H = 1.68 \pm 0.02$, $\delta_H = 3.66 \pm 0.03$ and $\eta_H = 5.70 \pm 0.05$ for the square lattice[34]. For the triangular lattice, the values of the exponents obtained are $\gamma_H = 1.71 \pm 0.02$, $\delta_H = 3.69 \pm 0.03$ and $\eta_H = 5.73 \pm 0.05$[34]. The errors quoted here are the standard least squares fit error taking into account the statistical error of each single data point. The system size L-dependence of the values of the critical exponents of different moments of the hull size distribution on the square and triangular lattices is also studied measuring the exponents' values at different L. The results are given in Table 5.3. The values of γ_H, δ_H and η_H are plotted against the inverse system size $1/L$ in the Figures 5.7(a), (b) and (c) respectively. The squares represent the square lattice data and the triangles represent the triangular lattice data in each plot. The values of the exponents obtained on these two lattices are converging to the values of the exponents obtained for $L = 2^{11}$ through MC simulation. The values of the hull moment exponents are then within error bars on

Lattice size (L)	Square lattice			Triangular lattice		
	γ_H	δ_H	η_H	γ_H	δ_H	η_H
2^7	1.71	3.70	5.79	1.76	3.79	5.91
2^8	1.70	3.68	5.74	1.74	3.74	5.81
2^9	1.69	3.67	5.71	1.73	3.71	5.75
2^{10}	1.68	3.66	5.70	1.71	3.69	5.73
2^{11}	1.68	3.66	5.70	1.71	3.69	5.73

Table 5.3: Values of the hull moment exponents γ_H, δ_H and η_H measured on the square and triangular lattices of different sizes L.

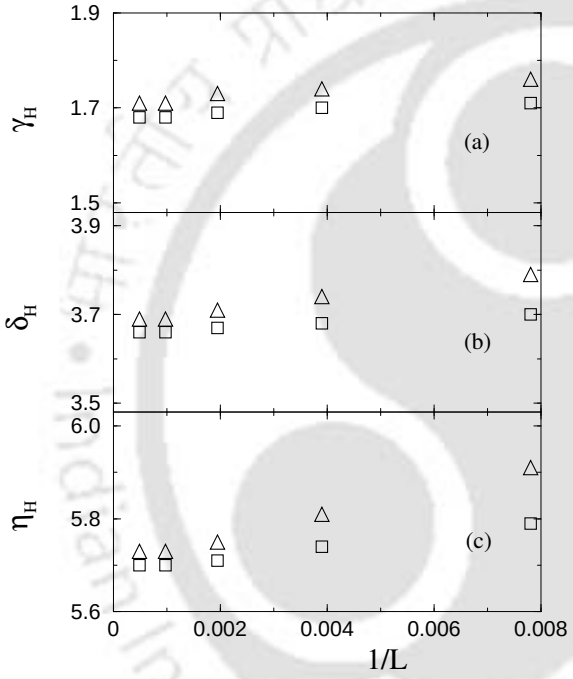

Figure 5.7: Plot of the hull moment's exponents (a) γ_H, (b) δ_H and (c) η_H against the inverse system size $1/L$. The system sizes considered are: $L = 2^7$ to 2^{11} in multiple of 2. The squares represent square lattice data and the triangles represent triangular lattice data. As $L \to \infty$, the exponents are converging to the values corresponding to $L = 2^{11}$. The values of the exponents are within the error bar on the two lattices.

the square and triangular lattices. The hull fractal dimensions d_H are already found the same on these two lattices. It should be mentioned here that the values of the critical exponents of the analogous cluster related quantities were found different on the square and triangular lattices[32]. Thus, breakdown of universality occurs in the cluster properties whereas universality holds for the associated hull properties in the DSP model in $2D$ between the square and triangular lattices. This is a new observation which appears for the first time in a percolation model. The scaling relations could be verified now. The value of $2\delta_H - \gamma_H = 5.64 \pm 0.08$ is very close to the value of the exponent $\eta_H \approx 5.70$ for the square lattice. For the triangular lattice, $2\delta_H - \gamma_H = 5.67 \pm 0.08$ and $\eta_H \approx 5.73$. The scaling relation $\eta_H = 2\delta_H - \gamma_H$ (Eq. 5.9) is then valid within the error bars on both lattices.

5.3.3 Comparison the square and triangular lattice results

In Table 5.4, the values of the hull fractal dimension and other critical exponents are summarized and a comparison of the results obtained on the square and triangular lattices as well as on the SP model has been made. The results obtained are reported in the Refs. [34,47]. It can be seen that the universality holds for the hull properties on the square and triangular lattice, as it is already mentioned, though there is a breakdown of universality for the cluster properties on the same lattices. It is interesting to note that the values of the exponents obtained here, especially the hull fractal dimension d_H, are very close to that of the SP (percolation under rotational constraint only) clusters hull[21] on both the lattices. In both the models, there exist chiral dangling ends on the perimeter. However, the SP clusters were found much more compact than the DSP clusters and are isotropic. The hull properties of both the DSP and SP clusters are then determined by the existence of chiral dangling ends on the external perimeter. These chiral dangling ends are generated due to the presence of the rotational constraint in both the models. The directional constraint then has little effect on the hull critical properties and it is mostly determined by the rotational constraint present in the model. In a physical situation like transport of classical charged particles in disordered systems in the presence of crossed electric and magnetic fields, the magnetic properties then could be extracted from the external perimeter only whereas the electrical properties could be obtained from the bulk of the cluster.

Exponents	Square lattice	Triangular lattice
d_H	1.458 ± 0.008	1.463 ± 0.004
	1.44 ± 0.01 (BC)	1.45 ± 0.01 (BC)
d_H^c	1.46 ± 0.02	1.47 ± 0.02
x	0.839 ± 0.007	0.820 ± 0.006
$d_H = xd_f$	1.45 ± 0.01	1.46 ± 0.01
γ_H	1.68 ± 0.02	1.71 ± 0.02
δ_H	3.66 ± 0.03	3.69 ± 0.03
η_H	5.70 ± 0.05	5.73 ± 0.05

Table 5.4: Comparison of the hull exponents and hull fractal dimension measured for the DSP model on the square and triangular lattices. d_H^c is the hull fractal dimension obtained through the proposed conjecture: $d_H = 1 + \nu_\perp/(\nu_\parallel + \nu_\perp)$. d_H is also measured from the relation $d_H = xd_f$ considering the values of d_f as 1.733 and 1.775 for the square and triangular lattices respectively. Measurements are found consistent in different methods adopted. The exponents are almost same within the error bars on the two lattices.

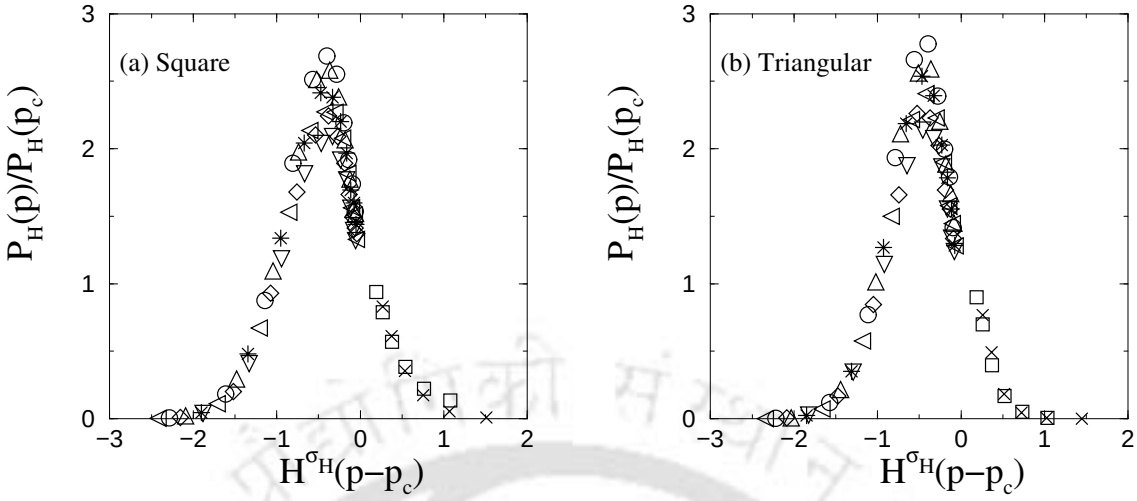

Figure 5.8: Plot of scaled hull size distribution $P_H(p)/P_H(p_c)$ versus scaled variable $H^{\sigma_H}(p-p_c)$ for different values of p on the (a) square and (b) triangular lattices. The value of σ_H is taken as $\sigma_H = 0.498$ (square) and $\sigma_H = 0.497$ (triangular). The hull size H changes from 64 to 16384. The data plotted correspond to $p - p_c = 0.007(\times)$, $0.005(\square)$, $-0.035(\nabla)$, $-0.04(\diamond)$, $-0.045(\triangleleft)$, $-0.05(*)$, $-0.055(\triangle)$, $-0.06(\bigcirc)$ for both the plots. Reasonable data collapse are observed on both the lattices. Since the value σ_H is almost the same, the scaling function form looks almost identical on the two lattices.

5.3.4 Hull scaling function form

Finally, the form of the hull size scaling function $P_H(p) = H^{-\tau_H+1}\mathsf{f}[H^{\sigma_H}(p-p_c)]$ is verified. The values of the exponents τ_H and σ_H have been estimated using the scaling relation given in Eq. 5.10. For the square lattice, the estimates of τ_H and σ_H are obtained as $\tau_H = 2.17 \pm 0.02$ and $\sigma_H = 0.498 \pm 0.003$. These values are within the error bars of the values of τ_H and σ_H obtained on the triangular lattice as $\tau_H = 2.16 \pm 0.02$ and $\sigma_H = 0.497 \pm 0.003$. The errors mentioned correspond to propagation error only. The scaling function form is verified through data collapse by plotting $P_H(p)/P_H(p_c)$ against the scaled variable $H^{\sigma_H}(p-p_c)$ for both the square and triangular lattices in Figures 5.8(a) and (b), respectively. The hull size varies from 64 to 16384 and $(p-p_c)$ is in the range 0.007 to -0.06. Not only a reasonable data collapse is observed for both the lattices but also the scaling function forms are found to be identical on the two lattices.

5.4 Conclusion

Hull of the DSP clusters are extracted generating large clusters at the percolation threshold and their properties are analyzed on both the square and triangular lattices

in $2D$. The values of the hull fractal dimension d_H and critical exponents γ_H, δ_H and η_H related to the hull size distribution function $P_H(p)$ are determined. It is found that the values obtained for the hull fractal dimension and the critical exponents related to the hull size distribution are the same within error bars on the square and triangular lattices unlike the cluster fractal dimension d_f and cluster related critical exponents of the DSP model. Thus, the universality of the hull critical exponents holds for the square and triangular lattices in $2D$ whereas there is a breakdown of universality in the corresponding cluster properties. Results are compared with that of other percolation models. The value of $d_H \approx 1.46$ obtained here is close to $4/3$, the fractal dimension of the Grossman-Aharony external perimeter and far away from $7/4$ proposed by Sapoval *et al* for the ordinary percolation hull. A new conjecture is made relating d_H and two connectivity length exponents $\nu_{\parallel}$ and $\nu_{\perp}$ for the anisotropic clusters. It is found that the values of d_H and other hull critical exponents are close to that of the SP cluster hulls. Hull critical properties are then determined more by the rotational constraint than the directional constraint present in the model. The critical exponents estimated here satisfy the scaling relations among themselves within error bars. The assumed scaling function form has been verified and found similar on both the square and triangular lattices.

Bibliography

[1] D. Avnir, *The Fractal Approach to Heterogeneous Chemistry: Surfaces, Colloids, Polymers*, Wiley, New York, 1989.

[2] H. J. Butt, K. Graf and M. Kappl, *Physics and Chemistry of Interfaces*, Wiley-VCH, 2nd edition, 2006.

[3] B. Sapoval, M. Rosso and J. F. Gouyet, J. Phys. Lett. **46**, L149 (1985).

[4] B. Sapoval, M. Rosso, J. F. Gouyet and J. F. Colonna, Solid State Ionics **18**, 21 (1986).

[5] M. Rosso, J. F. Gouyet and B. Sapoval, Phys. Rev. Lett. **57**, 3195 (1986).

[6] S. S. Manna and A. J. Guttmann, J. Phys. A: Math. Gen. **22**, 3113 (1989).

[7] A. L. Barabsi and H. Stanley, *Fractal concepts in surface growth*, Cambridge University Press, 1995.

[8] T. Vicsek, *Fractal Growth Phenomena*, World Scientific, 1989.

[9] Q. Z. Cao and P. Z. Wong, Phys. Rev. E **67**, 77 (1991).

[10] R. M. Bradley, Phys. Rev. E **49**, 1909 (1994).

[11] S. Schwarzer, S. Havlin and H. E. Stanley, Phys. Rev. E **49**, 1182 (1994).

[12] B. Sapoval and M. Rosso, Fractals **3**, 23 (1995).

[13] P. Bak and K. Sneppen, Phys. Rev. Lett. **71**, 4083 (1993).

[14] J. M. Debierre and R. M. Bradley, J. Phys. A: Math. Gen. **29**, 2337 (1996).
[15] S. Sinha, V. Kishore and S. B. Santra, Eur. Phys. Lett. **71**, 632 (2005).
[16] R. A. Ramos, P. A. Rikvold and M. A. Novotny, Phys. Rev. B **59**, 9053 (1999).
[17] J. W. Evans, Rev. Mod. Phys. **65**, 1281 (1993).
[18] S. B. Santra and B. Sapoval, Physica A **266**, 160 (1999).
[19] S. B. Santra, B. Sapoval, P. Barboux and F. Devreux, C. R. Acad. Sci. (Paris) **326**, 129 (1998).
[20] O. M. Becker, M. Bennun and A. Benshaul, J. Phys. Chem. **95**, 4803 (1991).
[21] S. B. Santra and I. Bose, J. Phys. A: Math. Gen. **26**, 3963 (1993).
[22] R. F. Voss, J. Phys. A **17**, L373 (1984).
[23] S. Schwarzer, S. Havlin and H. E. Stanley, Phys. Rev. E **49**, 1182 (1994).
[24] A. L. Owczarek, A. Rechnitzer, R. Brak and A. J. Guttmann, J. Phys. A: Math. Gen. **30**, 6679 (1997).
[25] K. Oerding and F. Wijland, J. Phys. A: Math. Gen. **31**, 7011 (1998).
[26] S. Roux and E. Guyon, J. Phys. A: Math. Gen. **24**, 1611 (1991).
[27] H. Hinrichsen, Adv. Phys. **49**, 815 (2000).
[28] R. M. Ziff, P. T. Cummings and G. Stell, J. Phys. A **17**, 3009 (1984).
[29] R. M. Ziff, X. P. Kong and E. G. D. Cohen, Phys. Rev. A **44**, 2410 (1991).
[30] P. Blaudeck et al., J. Phys. A: Math. Gen. **39**, 1609 (2006).
[31] S. B. Santra, Eur. Phys. J. B **33**, 75 (2003).
[32] S. Sinha and S. B. Santra, Eur. Phys. J. B **39**, 513 (2004).
[33] R. M. Ziff, Phys. Rev. Lett. **56**, 545 (1986).
[34] S. Sinha and S. B. Santra, Int. J. Mod. Phys. C **16**, 1251 (2005).
[35] H. Saleur and B. Duplantier, Phys. Rev. Lett. **58**, 2325 (1987).
[36] T. Grossman and A. Aharony, J. Phys. A **19**, L745 (1986).
[37] T. Grossman and A. Aharony, J. Phys. A **20**, L1193 (1987).
[38] P. Meakin and F. Family, Phys. Rev. A **34**, 2558 (1986).
[39] M. Rosso, J. Phys. A **22**, L131 (1989).
[40] A. Birovljev et al., Phys. Rev. Lett. **67**, 584 (1991).
[41] L. Balázs, Phys. Rev. E **54**, 1183 (1996).
[42] L. Kaplan, A. Shehter, Y. Lereah, H. Taitelbaum and S. Havlin, Phil. Mag. B **77**, 1427 (1998).
[43] B. Sapoval, S. B. Santra and P. Barboux, Eur. Phys. Lett. **41**, 297 (1998).
[44] E. Arapaki, P. Argyrakis and A. Bunde, Phys. Rev. E **69**, 031101 (2004).
[45] M. Aizenman, B. Duplantier and A. Aharony, Phys. Rev. Lett. **83**, 1359 (1999).
[46] A. Desolneux and B. Sapoval, Eur. Phys. Lett. **72**, 997 (2005).
[47] S. Sinha and S. B. Santra, in *Abstracts - Statphys 22, IISc. Bangalore, India, July, 2004*, page 162.

Chapter 6

Effect of Field Direction and Intensity on DSP Clusters

So far, the DSP model has been investigated under the field configurations of constant intensities applied in a given directions[1,2]. However, there are certain physical properties of a system needed to be studied in the presence of variable external biases like electric or magnetic fields. Since the electric field gives rise to a directional constraint and the magnetic field gives rise to a rotational constraint in the DSP model, the properties of disordered systems under variable crossed bias fields can be studied modifying the DSP model appropriately for variable field intensities and directions.

In this chapter, the DSP model has been modified suitably for different field orientations and variable field intensities. The modified model is then studied on the square and triangular lattices in 2-dimensions ($2D$). As the direction of a field changes, the number of components of the field on a lattice also changes. It has already been observed that the universality class of the DSP model varies from square to triangular lattice in $2D$. Microscopically, the DSP model on the triangular lattice differs from that on the square lattice only by an extra component of the rotational bias field. It is thus intriguing to verify the universality class of DSP model for different number of field components on the same lattice in the same spatial dimension. It is found that the universality class of the DSP model is independent of the direction or the number of components of the directed field on the same lattice. As the intensities of the fields change, the DSP model is expected to behave as that of OP, DP or SP models at the appropriate field intensities. By varying the external field intensities, crossover from DSP model to other percolation models has been investigated. A phase diagram is obtained for the percolation models by studying

the DSP model under variable field intensities.

Below, the modifications on the DSP model will be demonstrated for variable field directions and intensities. The effect of change of field direction will be discussed first. Intensity effect will be considered later.

6.1 DSP Model under variable field direction

Detailed description of the DSP model for a particular field direction has already been demonstrated in Chapter 2. Here the modifications of the model will be stated for different field orientations. In Chapter 2, a left to right horizontal directional constraint (or E field) and a clockwise rotational constraint (or B field) were considered. In such a field configuration, the selection of eligible sites on the square

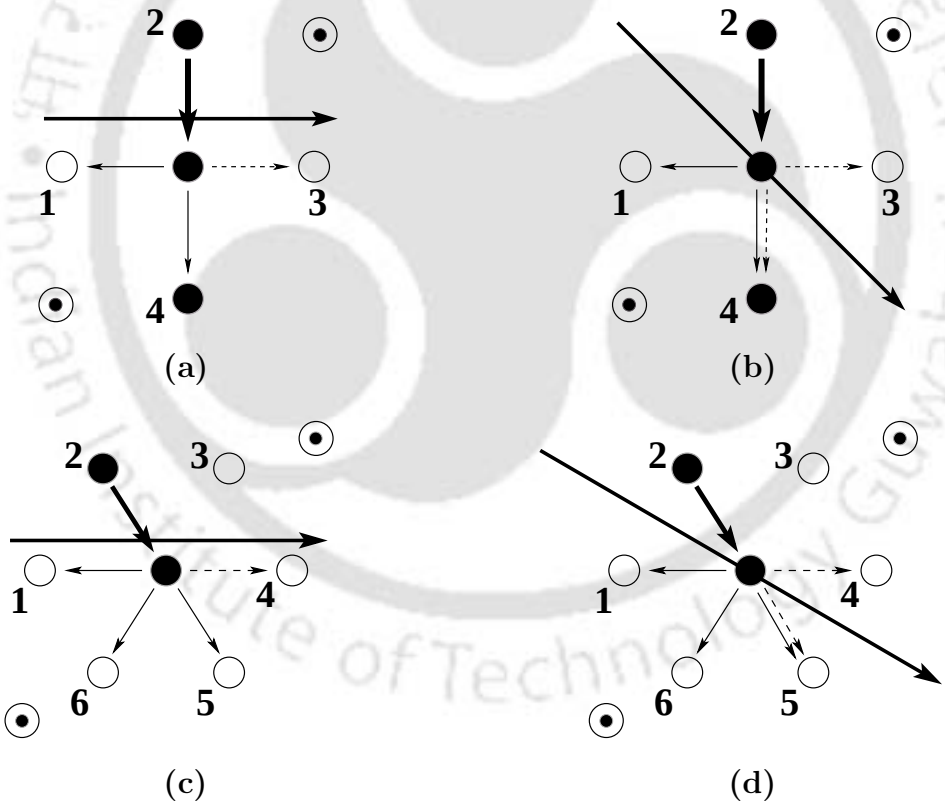

Figure 6.1: Selection of empty nearest neighbors for occupation in a MC time step on the square (a, b) and triangular (c, d) lattices. Black circles are the occupied sites and the open circles are the empty sites. Thick long arrows represent directional constraint (E). The clockwise rotational constraint (B) is shown by encircled dots. The central site is occupied from site 2 and shown by short thick arrows. The eligible sites for occupation due to E field are shown by dotted arrows and thin solid arrows indicate the same due to B field on both the lattices.

and triangular lattices are illustrated in Figures 6.1(a) and (c) respectively. The presence of E field is shown by the long arrows and the B field is shown by the dotted circles. Now the direction of the E field is rotated and correspondingly the model is modified. On the square lattice, the E field is rotated along the upper left to the lower right diagonal of the lattice as shown in Figure 6.1(b). On the triangular lattice, it is from upper left to the lower right corner of the lattice making an angle 30° with the horizontal, a semi-diagonal field, as illustrated in Figure 6.1(d). (E field along 60° with the horizontal on the triangular lattice is not considered because it will lead to anisotropic current distribution). As the direction of the E field changes, the number of eligible sites due to the presence of the E field also changes. There is one such site for the horizontal E field on both the lattices whereas there are two such sites for the diagonal E field on the square lattice and for the semi-diagonal E field on the triangular lattice as indicated by the dotted arrows in Figure 6.1. Correspondingly the algorithm is modified. While making the list of eligible sites (step 6 in the algorithm, Chapter 2), sites on the right (IV=3) and bottom (IV=4) are considered on the square lattice for the diagonal E field. Similarly for the semi-diagonal E field on the triangular lattice, sites corresponding to IV=4 and IV=5 are considered.

The number of eligible empty sites for occupation due to B field depends on the lattice structure but not on the B field direction. If the direction of B field is changed from $+z$ to $-z$ axis, only the sense of rotational constraint will be changed but the number of eligible empty sites for occupation will remain the same.

6.2 Effect of Field Direction

The critical properties of DSP model are studied numerically under diagonal E field on the square lattice and semi-diagonal E field on the triangular lattice. For the diagonal or semi-diagonal E field orientation, there are two components of the field on both the lattices along which the lattice sites could be occupied. Results obtained here are reported in Refs. [3,4]. They are compared with that of already obtained results in the previous chapters under horizontal E field orientations, single component of E field, on the respective lattices[1,2]. Lattice size is varied from $L = 2^7$ to 2^{11} in multiple of 2. Firstly the percolation thresholds (p_cs) are determined for each field configuration on a given lattice. The cluster-related quantities are then evaluated at their respective p_cs. Each data point is averaged over $N_{tot} = 5 \times 10^4$ clusters.

6.2.1 Percolation threshold

Percolation threshold p_c is the maximum site occupation probability at which a spanning cluster appears for the first time in the system. p_cs are determined here for the diagonal E field on the square lattice and semi-diagonal E field on the triangular lattice in the presence of a crossed B field. The probability to have a spanning cluster is given by $P_{sp} = n_{sp}/N_{tot}$ where n_{sp} is the number of spanning clusters out of N_{tot} clusters generated. The value of p_c for a given system size L and a given E and B field configuration is determined from the maximum slope of the curve P_{sp} versus p. Generally, p_c depends on L for finite systems. The value of p_c is then determined as function of L for a given lattice and field configuration. Data are then extrapolated to $L \to \infty$. In Figure 6.2, $p_c(L)$ is plotted against the inverse system size $1/L$ for different field configurations on both the lattices. Circles represent p_cs for the diagonal E field on the square lattice and diamonds represent the same for the semi-diagonal E field on the triangular lattice. The p_cs of infinite systems are identified in the $1/L \to 0$ limit and marked by crosses. It is found that $p_c \approx 0.619$ for diagonal E field on the square lattice and ≈ 0.545 for semi-diagonal E field on the triangular lattice respectively[3]. For the sake of comparison, p_cs for the horizontal field configuration on both the lattices for different system size are also plotted in the same figure. The squares represent data for the horizontal E field on the square lattice and triangles represent the same for the horizontal E field on the triangular lattice. It was already obtained that $p_c \approx 0.655$[1] and ≈ 0.570[2] for the horizontal E field on the square and triangular lattices respectively as it is also shown here. As usual, the value of p_c depends on the type of lattice as well as on the field situation. If the lattice structure is changed, the number of components of rotational constraint changes. If the direction of E field changes on a lattice, the

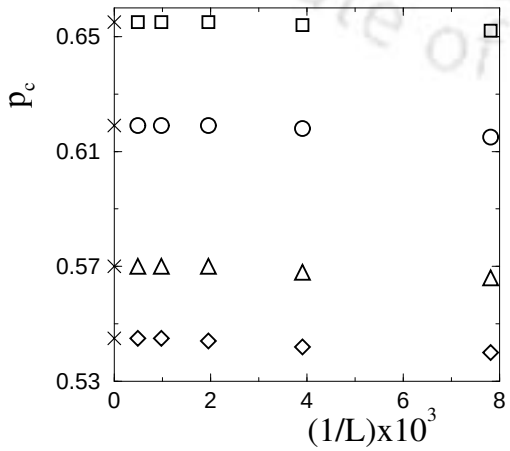

Figure 6.2: Plot of critical probability $p_c(L)$ versus $1/L$ for different E field orientations. The symbols are: (□) for the horizontal E and (◯) for the diagonal E field on the square lattice, (△) for the horizontal E and (◇) for the semi-diagonal E field on the triangular lattice. The values of $p_c(L)$ are extrapolated to $L \to \infty$ and p_cs for infinite systems are indicated by crosses.

number of components of directional constraint changes. The value of p_c is decreased if the number of field components is increased either by the rotational constraint or by the directional constraint. This is expected, because, the clusters can grow rapidly if the number of field components are higher in a given lattice.

6.2.2 Effective field and the spanning clusters

Typical spanning clusters at $p = p_c$ for the horizontal and diagonal field configurations on the square lattice of size $L = 2^8$ are represented in Figures 6.3(a) and 6.3(b) respectively. Similarly, Figures 6.3(c) and 6.3(d) represent the spanning clusters generated on the triangular lattice for the horizontal and semi-diagonal (30° with the horizontal) E field orientations respectively. The B field is always perpendicular to the E field and directed out of the plane of the lattice as shown by encircled dots. The black dots indicate the external boundary of the cluster and the gray dots represent the interior of the cluster. It can be seen that the clusters are highly rarefied, anisotropic and have chiral dangling ends. Interestingly, the elongation of the clusters are not along the applied E field. This is due to the generation of the magnetic force E_H perpendicular to the applied fields E and B. As a result, an effective field E_{eff} develops in the system and the elongation of the clusters are along the effective field. Since the direction of the effective field depends on the direction of the applied E field, the orientation of the cluster grown then depends on the direction of the applied E field. However, the clusters are not merely DP clusters along the effective field. Because, the presence of the rotational B field gives rise to chiral dangling ends at the boundary which has its own critical behaviour [5]. It is important to notice that the clusters are less anisotropic and more compact on the triangular lattice than on the square lattice. This is due to the extra flexibility given in the B field on the triangular lattice. However, the clusters look similar under different E field orientations on a given lattice except their direction of growth.

6.2.3 Fractal dimension

The fractal dimension d_f of the infinite or spanning clusters are determined by the box counting (BC) method. The number of boxes $N_B(\epsilon)$ grows with the box size ϵ as $N_B(\epsilon) \sim \epsilon^{d_f}$ where d_f is the fractal dimension. In Figure 6.4, $N_B(\epsilon)$ is plotted against the box size ϵ for the (a) square and (b) triangular lattices for all E field orientations. On the square lattice, the fractal dimensions are found as $d_f = 1.733 \pm 0.005$ for the horizontal E field and $d_f = 1.732 \pm 0.006$ for the diagonal E field [3]. Similarly

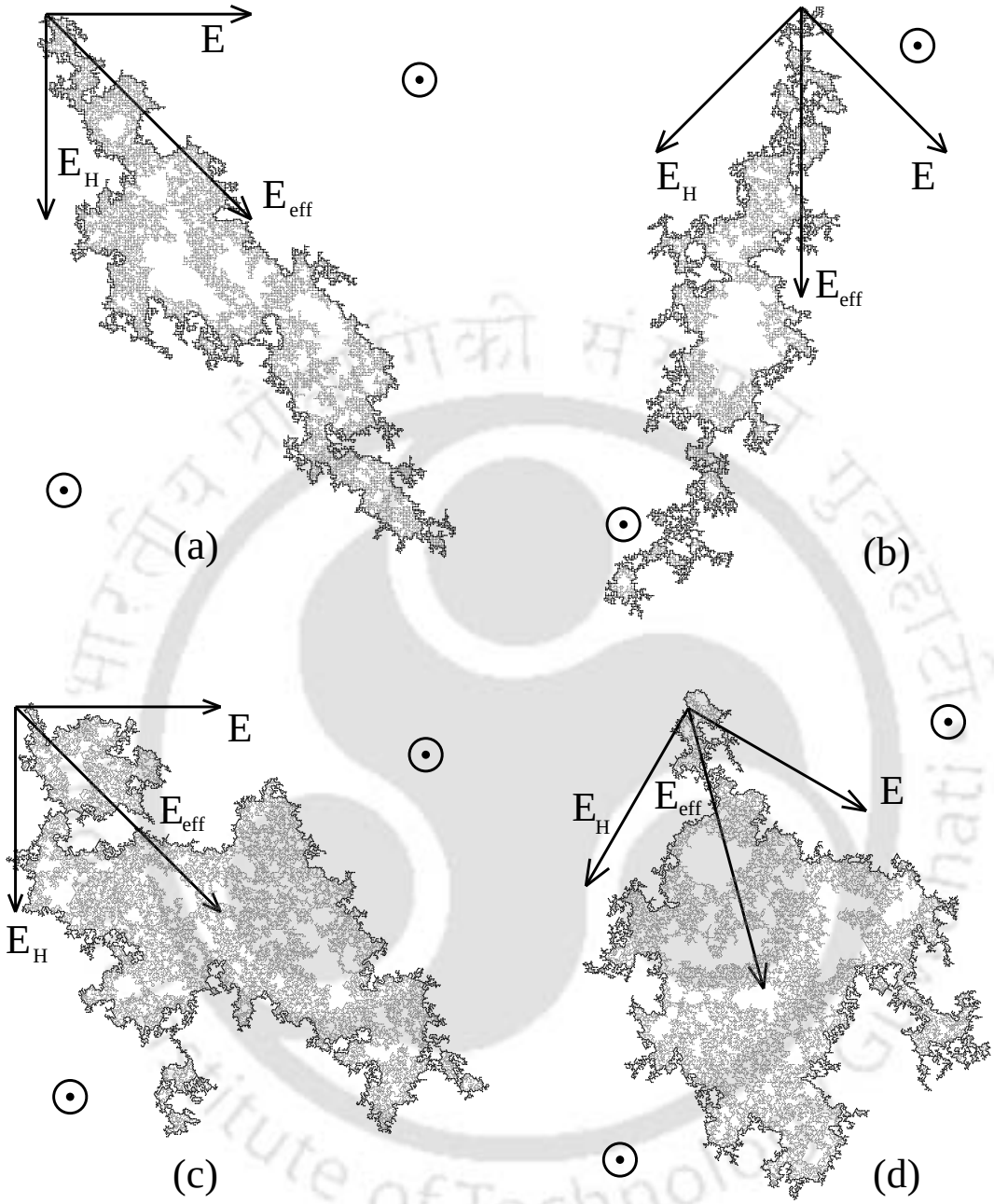

Figure 6.3: Infinite spanning clusters at $p = p_c$ on the square lattice of size $L = 2^8$ for the horizontal and diagonal E field orientations are represented in (a) and (b) respectively. On the triangular lattice, (c) and (d) represent the spanning clusters for horizontal and semi-diagonal (30° with the horizontal) E field orientations. The B field is along the z axis (directed out of the plane of the lattice). The field lines are drawn from the origin of the clusters. E_H is the magnetic force normal to both E and B. E_{eff} is the resultant field of E and E_H. The gray dots represent the interior of the clusters and the black dots represent the cluster hull. The clusters are elongated along the effective field.

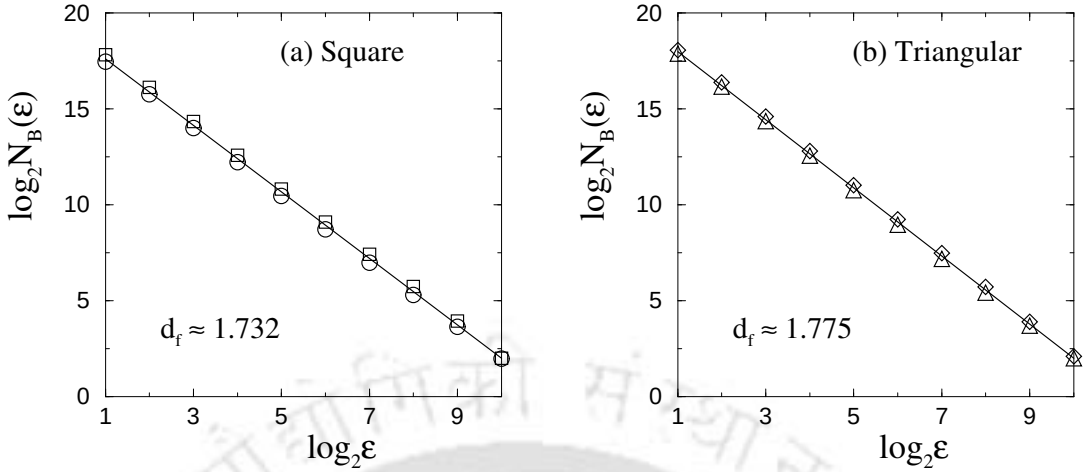

Figure 6.4: Number of boxes $N_B(\epsilon)$ is plotted against the box size ϵ for the (a) square and (b) triangular lattices to determine the fractal dimension d_f of the spanning clusters. Squares are for the horizontal E and circles are for the diagonal E field on the square lattice. Triangles are for the horizontal E and diamonds are for the semi-diagonal E field on the triangular lattice. The solid lines are guide to eye. The values of d_f are obtained as $d_f = 1.732 \pm 0.006$ for diagonal E field on the square lattice and $d_f = 1.777 \pm 0.005$ for the semi-diagonal E field on the triangular lattice. The value d_f is then independent of the E field orientation.

on the triangular lattice, it is found that $d_f = 1.775 \pm 0.004$ for the horizontal E field and $d_f = 1.777 \pm 0.005$ for the semi-diagonal E field [3]. The error is due to the least squares fit. These estimates are also confirmed by finite size (FS) analysis. In FS analysis, d_f is determined employing $S_\infty \sim L^{d_f}$, where S_∞ is the mass of the spanning cluster. The FS estimates are $d_f = 1.72 \pm 0.02$ on the square lattice and $d_f = 1.81 \pm 0.02$ on the triangular lattice for the diagonal and semi-diagonal E field respectively. It is interesting to notice that the change in the direction of the E field has no effect on the values of d_f on both the lattices. However, the values of d_f are different on the square and triangular lattices as already observed in Chapter 2 and reported in Ref. [2]. It was already found that d_f is higher on the triangular lattice than on the square lattice, consistent with the observation that the spanning clusters are more compact on the triangular lattice than on the square lattice. For a given E field direction, the DSP model on these two lattices differs only by an extra rotational direction due to B field on the triangular lattice from that on the square lattice. The change in d_f on these two lattices is then only due to the different number of branching of the rotational constraint due to the B field in the presence of a directional field. The extra flexibility of the rotational constraint allows the clusters to penetrate more and more into itself on the triangular lattice

than on the square lattice. As a result, the infinite clusters are less rarefied on the triangular lattice than on the square lattice. Since the clusters grow along the effective field direction, the orientation of the clusters is only changing with the orientation of the E field as the effective field direction is changing. Note that, the value of d_f obtained here is not only different from other percolation models but also smallest among that of OP $(91/48)$[6,7], DP (1.765)[8] and SP (1.969)[9]. The spanning clusters are then most rarefied in DSP. Since d_f obtained in DSP is different from that of DP clusters, it could be inferred that the DSP clusters are just not DP clusters along the effective field. The DSP clusters then should have its own critical behaviour at the percolation threshold as it is already observed[1]. It is now important to check the effect of E field direction on the other critical exponents.

6.2.4 Critical exponents and scaling relations

The values of some of the critical exponents are estimated and the scaling relations among them are verified in this section. The full scaling theory for DSP model is elaborated in Chapter 3. The cluster size distribution is defined as $P_s(p) = N_s/N_{tot}$ where N_s is the number of s-sited clusters in a total of N_{tot} clusters generated. Since the origin of a cluster is occupied with unit probability, the scaling function form of the cluster size distribution is assumed as

$$P_s(p) = s^{-\tau+1}\mathsf{f}[s^{\sigma}(p - p_c)] \tag{6.1}$$

where τ and σ are two exponents. The form of $P_s(p)$ has already been verified and found appropriate for DSP[1,2]. In order to verify the scaling relations among the critical exponents, the average cluster size, $\chi = \sum_s' sP_s(p) \sim |p-p_c|^{-\gamma}$, and two other higher moments, $\chi_1 = \sum_s' s^2P_s(p) \sim |p - p_c|^{-\delta}$ and $\chi_2 = \sum_s' s^3P_s(p) \sim |p - p_c|^{-\eta}$, of the cluster size distribution $P_s(p)$ are measured generating finite clusters below p_c. E field is applied diagonally on the square lattice and semi-diagonally on the triangular lattice in the presence of a crossed B field directed into the plane of the lattice. For a system size $L = 2^{11}$, χ is plotted against $|p - p_c|$ for diagonal E field on the square lattice (circles) in Figure 6.5(a) and for semi-diagonal E field on the triangular lattice (diamond) in Figure 6.5(b). Data corresponding to horizontal E field on the square (squares)[1] and triangular (triangles)[2] lattices are also plotted in the respective figures for comparison with the present data. It can be seen from Figure 6.5 that not only the absolute magnitude of the average cluster size χ but also the scaling of χ with $|p - p_c|$ remains independent of the E field orientation on

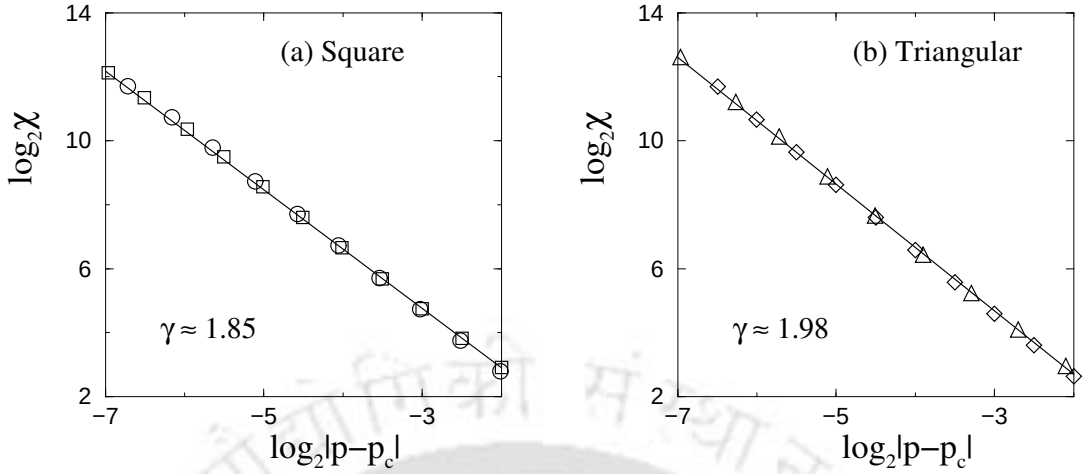

Figure 6.5: Plot of χ against $|p - p_c|$: (a) on the square and (b) on the triangular lattice for different E field configurations. The same symbol set of the previous figure is used. The solid lines are fitted to the data corresponding to the diagonal E field with slope 1.87 ± 0.01 on the square lattice in (a) and to the semi-diagonal E field with slope 2.00 ± 0.02 on the triangular lattice in (b).

both the lattices. The value of γ is found 1.87 ± 0.02 for the the diagonal E field whereas for the horizontal E field it was 1.85 ± 0.02 on the square lattice. Thus, the value of the exponent γ is within error bar for both the E field orientations on the square lattice. A similar result is also obtained on the triangular lattice. It is found that $\gamma = 2.00 \pm 0.02$ for semi-diagonal E field whereas it was 1.98 ± 0.02 for the horizontal E field on the triangular lattice. The errors quoted here include the least squares fit error and the change in γ with $p_c \pm \Delta p_c$ for $\Delta p_c = 0.0005$. Similarly, estimates of the critical exponents δ and η related to the higher moments of the cluster size distributions are also obtained. The observations are listed in Table 6.1. It can be seen that the values of all the critical exponents are very close and within error bars for different E field orientations on a given lattice. Finite size analysis of these critical exponents γ, δ and η have also been made. The values of γ, δ and η are determined on different system size L. In Figure 6.6, the exponents are plotted against the system size L. The extrapolated values of the exponents in the $L \to \infty$ limit are marked by crosses. As expected, the finite size estimates of γ, δ and η are converging to the Monte Carlo results on both the lattices as $L \to \infty$ [3]. It is interesting to notice that the exponent values are close and within error bars for different E field orientations on a given lattice although they are significantly different (out of error bars) on two different lattices in $2D$. The exponents γ, δ and η satisfy a scaling relation $\eta = 2\delta - \gamma$. The scaling relation has already been

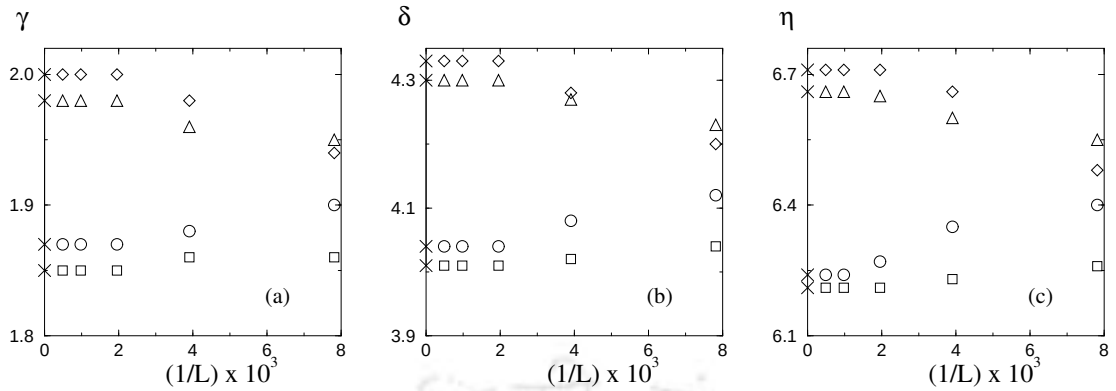

Figure 6.6: Plot of (a) γ, (b) δ and (c) η against $1/L$ on the square ($\square$, $\bigcirc$) and triangular ($\triangle$, $\diamond$) lattices for different E field configurations. The extrapolated values of the exponents are: $\gamma \approx 1.85$ and 1.87, $\delta \approx 4.01$ and 4.04 and $\eta \approx 6.21$ and 6.24 for horizontal and diagonal E field on the square lattice. On the triangular lattice, the values are: $\gamma \approx 1.98$ and 2.00, $\delta \approx 4.30$ and 4.33 and $\eta \approx 6.66$ and 6.71 for the horizontal and semi-diagonal E fields. The values of the critical exponents are within error bars for different E field orientations.

verified in Chapter 3 for horizontal E field and found holds true[1,2]. The same scaling relation has also been tested with the obtained values of the exponents for diagonal/semi-diagonal orientations of E field and it is satisfied within error bars irrespective of E field orientations on both the lattices.

Since the clusters generated here are anisotropic, there are then two connectivity lengths: $\xi_\parallel$ along the elongation of the cluster and $\xi_\perp$ along the normal to the elongation. They are defined as $\xi_\parallel^2 = 2\sum_s' R_\parallel^2(s) s P_s(p) / \sum_s' s P_s(p)$ and $\xi_\perp^2 = 2\sum_s' R_\perp^2(s) s P_s(p) / \sum_s' s P_s(p)$ where $R_\parallel(s)$ and $R_\perp(s)$ are the two radii of gyration with respect to two principal axes. The connectivity lengths, $\xi_\parallel \sim |p - p_c|^{-\nu_\parallel}$ and $\xi_\perp \sim |p - p_c|^{-\nu_\perp}$ diverge with two different critical exponents $\nu_\parallel$ and $\nu_\perp$ as $p \to p_c$. The scaling behaviour of $\xi_\parallel$ and $\xi_\perp$ are studied as function of p below p_c for diagonal E field on the square lattice and for semi-diagonal E field on the triangular lattice. For lattice size $L = 2^{11}$, $\xi_\parallel$ and $\xi_\perp$ are plotted against $|p - p_c|$ in Figure 6.7(a) for the square lattice and in Figure 6.7(b) for the triangular lattice for different E field orientations. Corresponding exponents $\nu_\parallel$ and $\nu_\perp$ are obtained from the slope of $\log \xi_\parallel$ and $\log \xi_\perp$ versus $\log |p - p_c|$ curves. The exponents $\nu_\parallel$ and $\nu_\perp$ are obtained as 1.34 ± 0.02 and 1.13 ± 0.02 respectively for diagonal E field on the square lattice[3]. On the triangular lattice, they are found as $\nu_\parallel = 1.37 \pm 0.02$ and $\nu_\perp = 1.24 \pm 0.02$ for the semi-diagonal E field[3]. Data for the horizontal E field are indicated by squares for the square lattice and by triangles for the triangular lattice. The values of $\nu_\parallel$ and $\nu_\perp$ are found within error bars for different E field orientations on both the lattices,

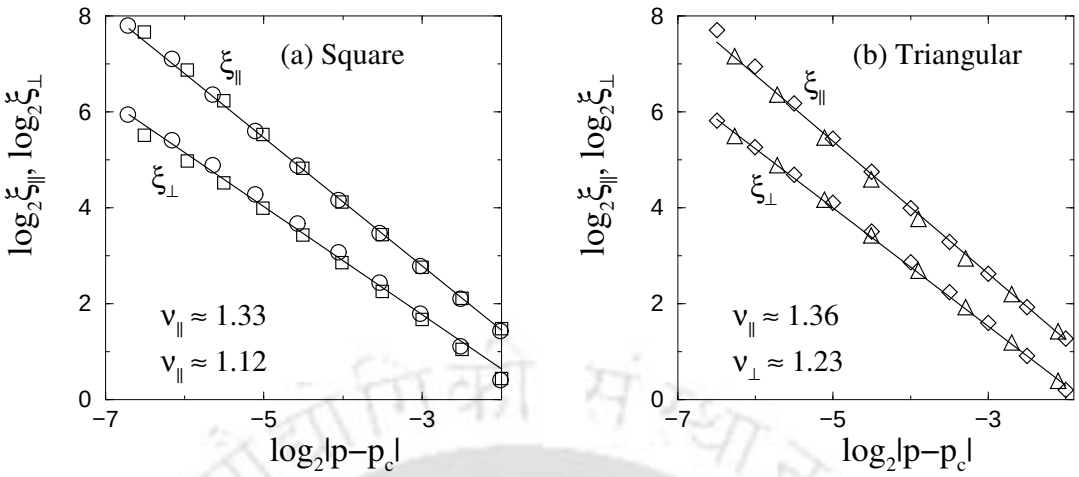

Figure 6.7: Plot of $\xi_\parallel$ and $\xi_\perp$ against $|p - p_c|$ for the (a) square and the (b) triangular lattice. The same symbol set of Figure 6.5 is used for different fields. The values of $\nu_\parallel$ and $\nu_\perp$ are found within error bars for different E field orientations.

see Table 6.1. The errors quoted here are the least squares fit errors. Finite size estimates of these exponents are also made and it is found that they are consistent with that of the MC results. The exponent $\nu_\parallel$ is almost same on the square and triangular lattices whereas $\nu_\perp$ on the triangular lattice is little higher than that of the square lattice value. $\Delta\nu = \nu_\parallel - \nu_\perp$ is ≈ 0.21 for DSP on the square lattice whereas it is ≈ 0.64 in DP [8,10,11]. The DSP clusters are then less anisotropic than that of DP clusters. This observation remains unchanged even if the direction of the effective field, along which the clusters grow, is changed. It is also noticed that the critical behaviour of the connectivity length $\xi_\parallel$ along the elongation of the cluster is similar to that of the connectivity length ξ of ordinary percolation. The value of $\nu_\parallel$ is almost equal to $\nu(\mathrm{OP}) = 4/3$ [6,7]. This is in good agreement with a recent study of magnetoresistance of a three-component composites of metallic film by Barabash *et al* [12]. It is found that the hyperscaling relations $2\delta - 3\gamma = (d-1)\nu_\perp + \nu_\parallel$ and $(d - d_f)\nu_\perp = \delta - 2\gamma$ are satisfied on the square lattice within error bars whereas they are satisfied marginally on the triangular lattice. It is already known that the hyperscaling is violated in DP [13].

The results obtained for different E field orientations on the square and triangular lattices are summarized in Table 6.1. Comparing the data given in Table 6.1 it can be concluded that the values of the critical exponents and the scaling relations among them are independent of E field orientation or the number of components of E field on both the lattices. The direction of E field is only able to change the

Exponents		Square Lattice Horizontal	Square Lattice Diagonal	Triangular Lattice Horizontal	Triangular Lattice Semi-diagonal
d_f	BC:	1.733 ± 0.005	1.732 ± 0.006	1.775 ± 0.004	1.777 ± 0.005
	FS:	1.72 ± 0.02	1.72 ± 0.02	1.80 ± 0.03	1.81 ± 0.02
γ		1.85 ± 0.01	1.87 ± 0.01	1.98 ± 0.02	2.00 ± 0.02
δ		4.01 ± 0.04	4.04 ± 0.04	4.30 ± 0.04	4.33 ± 0.04
η		6.21 ± 0.08	6.24 ± 0.08	6.66 ± 0.08	6.71 ± 0.08
$\nu_{\parallel}$		1.33 ± 0.01	1.34 ± 0.02	1.36 ± 0.02	1.37 ± 0.02
$\nu_{\perp}$		1.12 ± 0.03	1.13 ± 0.02	1.23 ± 0.02	1.24 ± 0.02

Table 6.1: Numerical estimates of the critical exponents and the fractal dimension measured for the DSP clusters on the square and triangular lattices for different E field orientations. The values of the critical exponents and the fractal dimension are found independent of the orientation of E field on both the lattices.

orientation of the clusters and not the critical properties. However, it has already been observed that the values of the critical exponents obtained in DSP model are not only different from that of the other percolation models but also are significantly different on the square and triangular lattices in $2D$. It is already reported in Ref. [2] as a breakdown of universality between the square and triangular lattices. Microscopically, the DSP model on the square and triangular lattices differs only by an extra rotational direction due to B field on the triangular lattice from that on the square lattice for a given E orientation. The values of the critical exponents then depend on the number of branching due to the rotational field B but do not depend on the number of branching due to the directional field E. By reducing the number of branching of B field from three to two on the triangular lattice and keeping E field horizontal, an artificial model has been created and the critical exponents are re-estimated. The values of the critical exponents for this particular field combination are obtained as: $d_f = 1.730 \pm 0.005$, $\gamma = 1.87 \pm 0.01$, $\delta = 4.08 \pm 0.04$ and $\eta = 6.34 \pm 0.08$. Remarkably, the values of d_f and other critical exponents are found within error bars of that of the square lattice with horizontal E field and the universality holds. It should be mentioned here that no breakdown of universality was observed in SP [9], percolation under only rotational constraint, between the square and triangular lattices. In DSP model, the presence of the directional constraint E on top of the rotational constraint B may increase the number of spiral lattice trees. Since the spiral lattice trees [14] as well as the spiral self avoiding walks [15,16] have different scaling behaviour on the square and triangular lattices, the higher number of tree like structures in the clusters generated can induced a non-trivial effect on

the critical properties of DSP at the percolation threshold and consequently the discrepancy in the exponent values on the two lattices could occur.

Though there is a breakdown of universality in the cluster property of the DSP model on the square and triangular lattices, it was already observed that the universality holds true for their hull (external perimeter) properties between the square and triangular lattices[17]. The hull properties are also verified here by changing the applied E field direction and it is found that the hull properties are independent of the E field orientations.

6.3 DSP model under variable field intensity

So far, the DSP model has been investigated under constant external field intensities. It is also useful to understand the properties of disordered system as function of the field intensity. The intensities E and B of the external fields can vary here from 0 to 1. It may be noted that for certain extreme values of the intensities E and B, the percolation model has four different varieties, DSP, DP, SP and OP. DSP corresponds to $E = 1$, $B = 1$; DP corresponds to $E = 1$, $B = 0$; SP corresponds to $E = 0$, $B = 1$ and OP corresponds to $E = 0$, $B = 0$. Thus, a complete phase diagram can also be obtained by studying the DSP model under variable field intensities between one and zero. If the field intensities are changed continuously from $(1, 1)$ to $(0, 0)$ keeping $E = B$, it is expected to have a phase change from DSP to OP. Similarly, a phase change from DSP to SP can be obtained by changing E from 1 to 0 keeping $B = 1$ and phase change from DSP to DP can be obtained by changing B from 1 to 0 keeping $E = 1$. In order to study the effect of intensities of the external applied fields, one needs to generate percolation clusters under variable field intensities and characterize their geometrical properties at the percolation threshold. The intensity dependent percolation cluster could be generated by selecting nearest neighbours of an occupied site with appropriate probabilities, function of field intensities. This is studied on a square lattice of size L. The E field is applied diagonally and the B field is applied perpendicular to the E field in the positive z direction as shown in Figure 6.1(b). However, the results of this particular field configuration should be valid for all other field configurations. Here the field intensities play role in the preparation of the list of eligible sites. If the field intensities are either $E = 1$ or $B = 1$ or both $E = B = 1$, only sites in the favourable directions, defined by the directional and rotational constraints, are eligible for occupation. Sites in other directions are not considered for occupation in all three constrained percolation models DSP, DP and

SP. The sites in the favourable directions of the fields are selected with probabilities proportional to the field intensities. If the field intensities are less than one, the sites in unfavourable directions of the fields will also be eligible for occupation due to scattering. A scattering field S is then introduced in the model. Sites in any directions (including unfavourable ones) are selected for occupation with probability S, defined as

$$S = (1 - E) \times (1 - B). \tag{6.2}$$

Notice that $S = 0$ in all three cases: $E = 1$, $B = 1$ and $E = B = 1$. That means there is no scattering and consequently no sites in unfavourable directions are eligible for occupation as in the case of DP, SP or DSP. On the other hand, when E and B both are equal to zero then $S = 1$. There will be then no favourable direction. All empty nearest neighbours of an occupied site on the square lattice are selected with unit probability for occupation. The situation corresponds to OP. Thus, a change of phase from DSP to OP, DP or SP will be possible by changing E and B continuously. As soon as the list of eligible sites is prepared they are then occupied with percolation probability p. Below, the critical properties of DSP clusters are studied varying intensity of E and B fields. For each value of E and B, the percolation threshold p_c is determined. Data are averaged over 10^5 clusters for each field intensity. The results obtained under variable field intensity are reported in Ref. [3].

6.4 Effect of field intensity

The field intensities are changed in three different ways. First, E and B are changed from $(1, 1)$ to $(0, 0)$ keeping $E = B$ and accordingly DSP is expected to change over to OP. The corresponding data will be represented by circles. Second, keeping $B = 1$, E is changed from 1 to 0, then DSP should change to SP. These data are represented by squares. Third, keeping $E = 1$, B is changed from 1 to 0, thus DP will be reached from DSP. Triangles represent the corresponding data. The percolation threshold p_c, at which a spanning cluster appears for the first time in the system, has been calculated as function of the field intensities E and B. Following the same procedure of section 3, p_cs are identified as the percolation probability p corresponding to the maximum slope of the plot of spanning probability P_{sp} against p. The values of p_cs are given in Tables 6.2 for (a) $E = B$, (b) $E = 1$ and (c) $B = 1$. In Figure 6.8, the values of p_cs are plotted against E and B for a square lattice of size $L = 2^{10}$. Each

$E = B$	p_c
1.0	0.619
0.7	0.661
0.5	0.666
0.3	0.647
0.2	0.630
0.1	0.612
0.0	0.593

(a)

$B(E = 1)$	p_c
1.0	0.619
0.5	0.669
0.3	0.686
0.2	0.692
0.1	0.699
0.0	0.705

(b)

$E(B = 1)$	p_c
1.0	0.619
0.5	0.651
0.3	0.674
0.2	0.689
0.1	0.710
0.0	0.712

(c)

Table 6.2: Percolation threshold p_c measured for (a) $E = B$, (b) $E = 1$ and (c) $B = 1$.

p_c has been determined generating 10^5 spanning clusters. It can be seen that as E and B go to zero p_c coincides with that of OP. Similarly, p_c for DP and SP are also obtained for $E = 1, B = 0$ and $E = 0, B = 1$ respectively.

The percolation clusters are isotropic for OP and SP whereas they are anisotropic in the case of DP and DSP. For anisotropic clusters, there are two connectivity lengths $\xi_\perp$ and $\xi_\parallel$ and for isotropic clusters there is only one connectivity length. Since $\xi_\perp$ and $\xi_\parallel$ diverge with two critical exponents $\nu_\perp$ and $\nu_\parallel$ respectively as $p \to p_c$, the ratio of two connectivity lengths $\xi_\parallel/\xi_\perp$ should diverge as $|p - p_c|^{-\Delta\nu}$ where $\Delta\nu = \nu_\parallel - \nu_\perp$. For isotropic clusters, $\nu_\parallel$ is equal to $\nu_\perp$ since the clusters grow equally in all directions. Thus, $\Delta\nu$ is zero for OP and SP clusters and $\Delta\nu$ is finite for anisotropic clusters of DP and DSP. In DSP, $\Delta\nu$ is approximately 0.21 [1] whereas in DP, it is approximately 0.64 [8,10,11]. The values of the connectivity exponents $\nu_\perp$ and $\nu_\parallel$ are determined for different values of E and B. In Figure 6.9, $\Delta\nu$ is plotted against E and B. As the field intensities are taken to $E = 0$ and $B = 0$ or $E = 0$ and $B = 1$ corresponding to OP and SP models the value of $\Delta\nu$ continuously goes to zero. As the field intensities are taken to $E = 1$ and $B = 0$ corresponding to the DP model, the value of $\Delta\nu$ approaches 0.64 as it is expected for DP. Not only the difference but also the absolute value of the connectivity exponent matches with the respective percolation models. Thus, there is a smooth crossover from DSP to OP, DP and SP at the appropriate values of E and B as they are changed continuously.

In order to determine other critical properties, fractal dimension d_f of the spanning clusters and average cluster size exponent γ are also determined varying the field intensities and they are tabulated in Tables 6.3 and 6.4 respectively. In Figures 6.10(a) and (b), d_f and γ are plotted against E and B respectively. The value of d_f in different percolation model are: $d_f(\text{OP}) = 91/48 \approx 1.896$ [6,7], $d_f(\text{DP}) \approx 1.765$ [8,11],

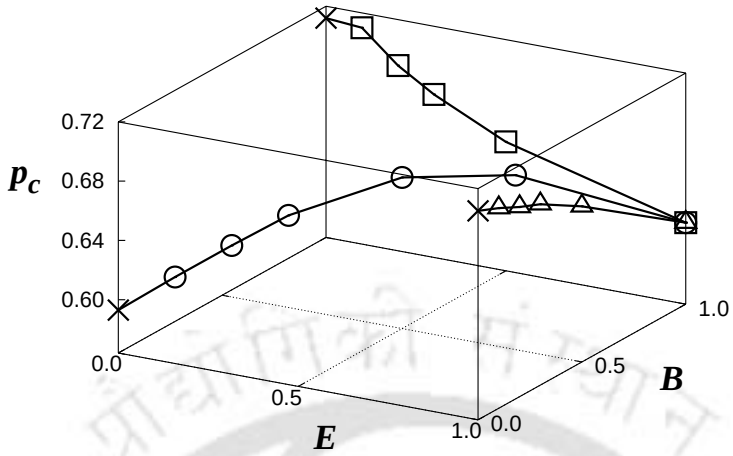

Figure 6.8: Plot of percolation threshold p_c against field intensities E and B for a square lattice of size $L = 2^{10}$. For appropriate values of E and B, p_cs correspond to that of respective percolation models.

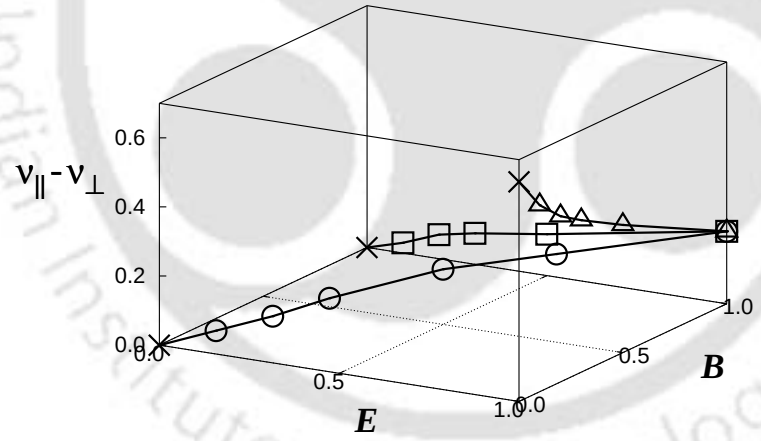

Figure 6.9: Plot of $\Delta\nu = \nu_{\parallel} - \nu_{\perp}$ against field intensities E and B. $\Delta\nu$ continuously goes to zero as the field intensities goes to $E = B = 0$ for OP and $B = 1$, $E = 0$ for SP respectively. $\Delta\nu$ is also approaching 0.64 corresponding to DP for $E = 1$ and $B = 0$.

$d_f(\text{SP}) \approx 1.957$[9] and $d_f(\text{DSP}) \approx 1.733$[1]. The values of d_f for OP, DP and SP are marked by crosses in Figure 6.10. It can be seen that the value of d_f changes continuously and approaches to the expected values of d_f of the respective percolation models as the intensities of E and B are changed appropriately. In

$E = B$	d_f
1.0	1.732
0.7	1.743
0.5	1.751
0.3	1.773
0.2	1.786
0.1	1.823
0.0	1.896

(a)

$B(E = 1)$	d_f
1.0	1.732
0.5	1.734
0.3	1.735
0.2	1.736
0.1	1.745
0.0	1.765

(b)

$E(B = 1)$	d_f
1.0	1.732
0.5	1.755
0.3	1.770
0.2	1.790
0.1	1.818
0.0	1.957

(c)

Table 6.3: Fractal dimension d_f measured for (a) $E = B$, (b) $E = 1$ and (c) $B = 1$.

$E = B$	γ
1.0	1.87
0.7	1.89
0.5	1.90
0.3	1.95
0.2	1.97
0.1	2.08
0.0	2.39

(a)

$B(E = 1)$	γ
1.0	1.87
0.5	1.95
0.3	2.02
0.2	2.07
0.1	2.14
0.0	2.2772

(b)

$E(B = 1)$	γ
1.0	1.85
0.5	1.86
0.3	1.87
0.2	1.90
0.1	1.96
0.0	2.19

(c)

Table 6.4: Average cluster size exponents γ measured for (a) $E = B$, (b) $E = 1$ and (c) $B = 1$.

Figure 6.10(b), the values of γ of different percolation models are also indicated by crosses, $\gamma(\text{OP}) = 43/18 \approx 2.389$[6,7], $\gamma(\text{DP}) \approx 2.2772$[8], $\gamma(\text{SP}) \approx 2.19$[9] and $\gamma(\text{DSP}) = 1.85$[1]. Similar to the fractal dimension, the value of the critical exponent γ is also changing continuously to that of the other percolation models as the intensities of E and B are changed appropriately. However, for most of the E and B values, the values of d_f and other critical exponents are found close to that of DSP. It could also be noticed that in the presence of small field intensities of E or B, the universality class of OP is changed. Similarly for DP and SP, a small intensity of the other field is able to change the universality class of the models to that of DSP. This is a new and important observation.

A phase diagram for percolation models under external bias fields now can be plotted in the space of directional (E) and rotational (B) bias fields. Different percolation models are identified on the $E - B$ space by black circles in Figure 6.11. Each point in this space corresponds to a second order phase transition point. The thick lines from left lower to right upper diagonal and parallel to the E and B axes

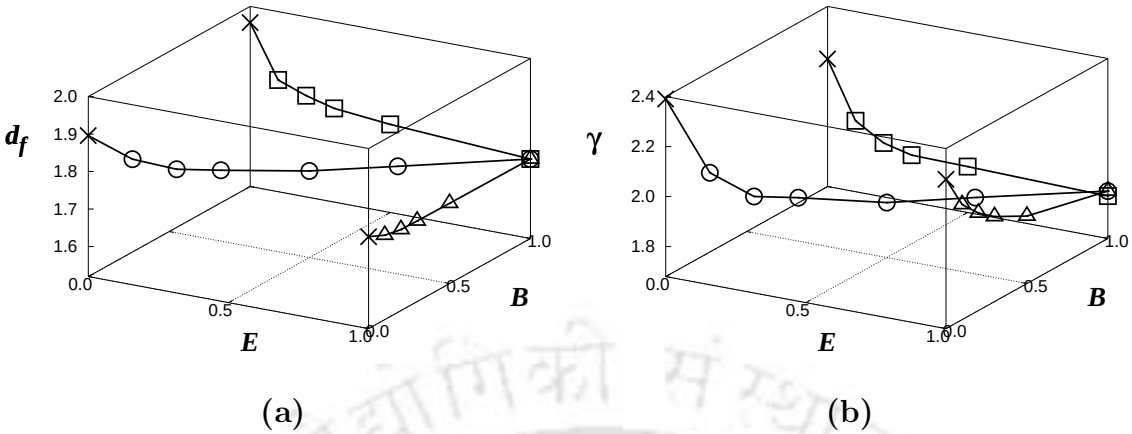

Figure 6.10: Plot of (a) fractal dimension d_f of the spanning clusters and (b) average cluster size exponent γ against field intensities E and B. As E and B change continuously, the values of d_f and γ approach to that of the respective percolation models at the appropriate values of E and B.

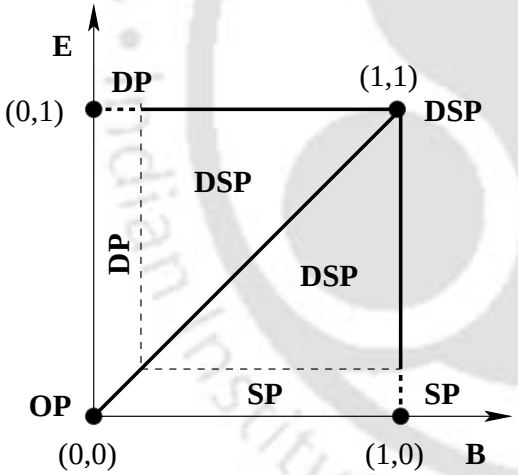

Figure 6.11: Phase diagram of the percolation models under crossed external bias fields. Different percolation models are represented by black circles. DSP changes continuously to OP, DP or SP for the field intensities of E and B are changed to the appropriate values.

of the phase diagram represent lines of second order phase transition points. The two ends of the diagonal line correspond to OP and DSP. The line parallel to E connects SP and DSP whereas the line parallel to B connects DP and DSP. The dotted lines define the regions of DP and SP as indicated. DSP model then can be considered as the most generalized model of percolation under external bias fields whose different limiting situations correspond to other percolation models like OP, DP or SP.

6.5 Summary

The DSP model has been studied varying the applied field directions and their intensities on the square and triangular lattices in $2D$. The critical properties of the cluster related quantities in this model were already shown to be very different from the other percolation models like OP, DP and SP and accordingly DSP belongs to a new universality class. It is found here that the critical properties as well as the universality class of the DSP clusters remain invariant on the directions of the applied E and B fields. Change of E field direction corresponds to the change in the number of components of the E field on both the lattices. However, this is not the case for the B field. Change in the number of components in the E field corresponds to the change in orientations of the clusters only whereas change in the number of components in the B field corresponds to the change in the universality class of DSP. Changing the intensity of the applied fields, a smooth crossover from DSP to OP, DP and SP is observed. A phase diagram is obtained for the percolation models under external bias fields. OP, DP or SP could be obtained as a limiting situation of DSP by changing the field intensities. The DSP model then can be considered as a most general model of percolation under external bias fields. The model will be applicable to the physical situations where crossed directional and rotational force fields are present in disordered systems.

Bibliography

[1] S. B. Santra, Eur. Phys. J. B **33**, 75 (2003).
[2] S. Sinha and S. B. Santra, Eur. Phys. J. B **39**, 513 (2004).
[3] S. Sinha and S. B. Santra, Int. J. Mod. Phys. C **17**, 1285 (2006).
[4] S. Sinha and S. B. Santra, in *Proceedings - 9th World Multi-Conference on Systemics, Cybernetics and Informatics, Orlando, USA, July, 2005.*
[5] S. B. Santra and I. Bose, J. Phys. A: Math. Gen. **26**, 3963 (1993).
[6] M. P. M. den Nijs, J. Phys. A **12**, 1857 (1997).
[7] B. Nienhuis, J. Phys. A **15**, 199 (1982).
[8] B. Hede, J. Kertész and T. Vicsek, J. Stat. Phys. **64**, 829 (1991).
[9] S. B. Santra and I. Bose, J. Phys. A **25**, 1105 (1992).
[10] J. W. Essam, K. DéBell, J. Adler and F. M. Bhatti, Phys. Rev. B **33**, 1982 (1986).
[11] J. W. Essam, A. J. Guttmann and K. DéBell, J. Phys. A: Math. Gen. **21**, 3815 (1988).
[12] S. V. Barabash, D. J. Bergman and D. Stroud, Phys. Rev. B **64**, 174419 (2001).
[13] M. Henkel and V. Privman, Phys. Rev. Lett. **65**, 1777 (1990).
[14] S. B. Santra, J. Phys. I France **5**, 1573 (1995).

[15] H. J. W. Blöte and H. J. Hilhorst, J. Phys. A **17**, L111 (1984).
[16] K. Y. Lin, J. Phys. A **18**, L145 (1985).
[17] S. Sinha and S. B. Santra, Int. J. Mod. Phys. C **16**, 1251 (2005).

Chapter 7

Multifractility of DSP Spanning Clusters

Fractals are characterized geometrically by a single fractal dimension. While multifractals are characterized by a set of fractal dimensions. Multifractals appear in a wide range of situations like energy dissipation in turbulent flows[1], electronic eigenstates at metal insulator transition[2–4], diffusion in porous structures[5], diffusion limited aggregation[6], fluctuations in finance[7,8], dynamics of human heartbeat[9,10] and many others. Multifractal properties associated with the infinite DSP clusters at the percolation threshold p_c is considered in this chapter. In ordinary percolation (OP)[11], each site of a percolation cluster has two states, occupied or empty. The infinite percolation cluster of ordinary site percolation is found to be a monofractal. In order to study the multifractal aspects of percolation clusters, a current distribution[12–15] or a random walker[16,17] is generally introduced. However, due to the presence of rotational constraint on the directed spiral percolation model, an occupied site has always a direction associated with it and a site can be re-occupied from different directions. A site can be occupied at most Z times from Z different directions on a given lattice with coordination number Z. Other than DSP, in the case of spiral percolation (SP)[18,19] also a lattice site could be re-occupied from different directions. In these models, a state variable s_i then can be assigned to each lattice site and whose value will correspond to the number of times a site is visited during the growth of the cluster. The value of s_i can change from 0 to 4 on a square lattice and 0 to 6 on a triangular lattice for SP and DSP models whereas it has only two states 1 and 0 in case of OP. In this chapter, a new methodology is proposed to study the percolation transition in terms of the state variable s_i for the DSP model. The same method can also be applied for the SP model. Studying the

physical properties associated with the state variable s_i, the percolation transition is possible to establish at the same percolation threshold p_c defined geometrically. The spanning clusters at $p = p_c$ are monofractal. Distribution of s_i on the fractal substrate is very similar to mass distribution on a geometrical support usually taken for multifractal study [20–22]. In order to explore the multifractal aspects of the spanning percolation clusters in these rotationally constrained percolation models at $p = p_c$, it is now possible to define a suitable multifractal measure in terms of s_i. In this way, one does not need to introduce any other external agency like electric current or random walker in the model as it is usually done in the case of OP clusters. The variable s_i is inbuilt in the rotational models and represents an inherent property of DSP and SP. It is found that the exponents associated with the q moments of the measure defined in terms of s_i are not limited by any linear dependence on the moment q for the rotational percolation models. It then indicates that the measure has multifractal character.

Percolation clusters are generated here in the presence of rotational constraint on the square and triangular lattices of linear size $L = 2^{10}$ for both DSP and SP models. The percolation transition will be established first at the original p_c by calculating "spontaneous magnetization" in terms of s_i. The multifractal aspects of the measure distribution on the spanning clusters, defined in terms of s_i, are then investigated for both anisotropic DSP and isotropic SP clusters at $p = p_c$. The cluster properties are averaged over 5×10^4 spanning clusters. The model and the results obtained in the multifractal analysis are reported in Ref. [23–25].

7.1 Percolation threshold of the $s_i = Z$ model

Geometrically, the critical percolation probability p_c is the maximum probability below which no spanning cluster appears. At $p = p_c$, a spanning cluster appears for the first time in the system. In single cluster growth approach, the threshold p_c is generally identified by measuring the probability to have a spanning cluster (P_∞) as a function of p, the occupation probability. P_∞ goes to zero continuously as p tends to p_c from above. In the state variable formalism, the value of p_c can be identified in terms of "spontaneous magnetization" $M(p)$ defined in terms of the state variable s_i. $M(p)$ is defined as

$$M(p) = \frac{1}{N_{tot}} \sum_{j=1}^{N_{tot}} m_j(p), \qquad m_j(p) = \frac{1}{L^2} \sum_{i=1}^{L^2} s_i(p) \tag{7.1}$$

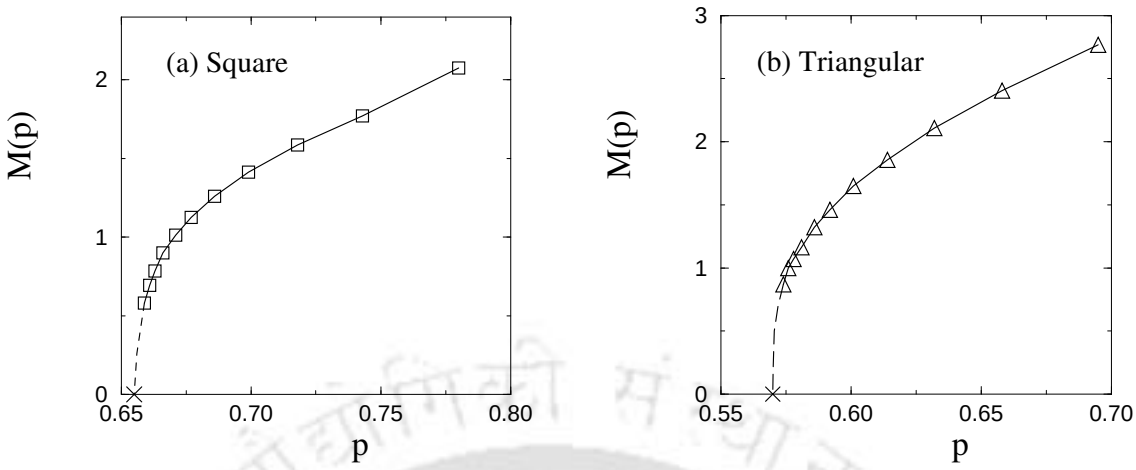

Figure 7.1: Plot of spontaneous magnetization $M(p)$ against p for DSP model defined on the (a) square and (b) triangular lattices of linear size $L = 2^{10}$. Percolation thresholds p_c on the individual lattices are marked by crosses on the p axis in both the plots.

where L is the lattice size and N_{tot} is the total number of spanning clusters generated. $m_j(p)$ represents the magnetization per site for the jth spanning cluster generated using single cluster growth method. At $p = 1$, all the sites of an infinite cluster are expected to be occupied Z times where Z is the coordination number of the lattice and the size of the infinite cluster will be of the order of L^2, square of the system size. Thus, $M(1)$ is equal to Z. As p tends to the percolation threshold p_c from above, $M(p)$ is expected to go to zero continuously from its maximum value Z at $p = 1$ not only because the sites will be occupied less number of times but also the spanning cluster will disappear. $M(p)$ is measured for DSP model and it is plotted against p in Figure 7.1(a) for the square lattice ($Z = 4$) and in Figure 7.1(b) for the triangular lattice ($Z = 6$). It can be seen that for both the lattices, it is approaching to zero at $p = p_c$ as expected and the values of p_cs are the same as those determined by geometrical approach: $p_c = 0.6550 \pm 0.0005$ for the square lattice and 0.5700 ± 0.0005 for the triangular lattice[26–28]. Thus, $M(p)$ is a new order parameter for the percolation transition in the state variable formalism[23]. It is also expected that $M(p)$ becomes singular at $p = p_c$ with an exponent β as $M(p) \sim (p - p_c)^\beta$, similar to P_∞. In Figure 7.2, the power law has been verified and the exponent β is determined as 0.32 ± 0.02 and 0.35 ± 0.02 for the square and triangular lattices respectively. The values obtained here are close to the already obtained values 0.31 ± 0.06 for the square lattice and 0.34 ± 0.08 for the triangular lattice (Chapter 3). The state variable formalism of the rotationally constrained percolation models is then consistent with that of the usual geometrical approach.

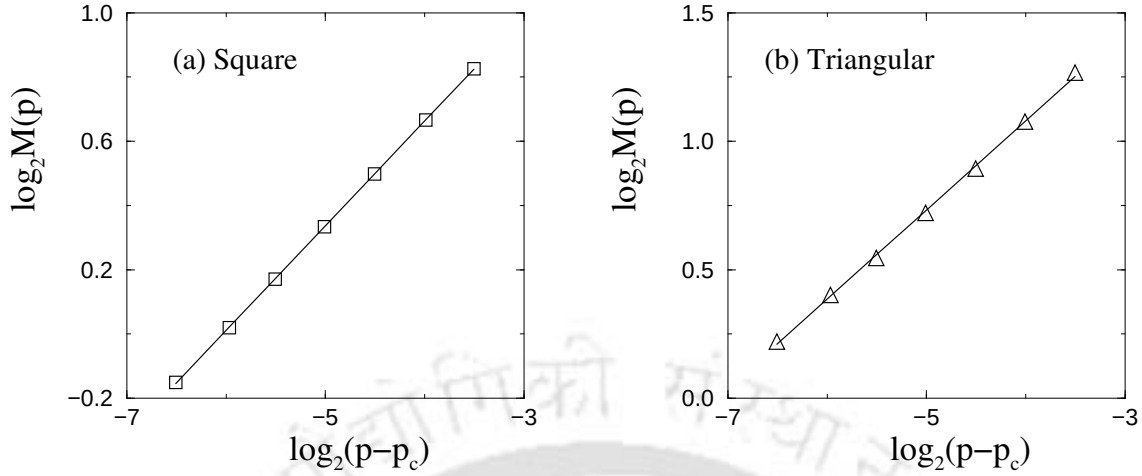

Figure 7.2: Plot of spontaneous magnetization $M(p)$ with $(p-p_c)$ for DSP model defined on the (a) square and (b) triangular lattices of linear size $L = 2^{10}$. From the slope, the exponent β is obtained as 0.32 ± 0.02 for the square lattice and 0.35 ± 0.02 for the triangular lattice.

The value of p_c has also been recovered within error bar in the case of SP. Other critical properties of the models can also be identified in terms of the state variable s_i and a scaling theory is possible to develop.

7.2 Spanning cluster of the spin model

Distribution of spin on the DSP spanning clusters generated at $p = p_c$ on the $L = 2^7$ square and triangular lattices are shown in Figures 7.3 and 7.4 respectively. Different values of the state variable s_i are represented by the dots of different colours as $s_i = 0$ by white space, $s_i = 1$ by yellow, $s_i = 2$ by green, $s_i = 3$ by blue, $s_i = 4$ by red, $s_i = 5$ by brown and $s_i = 6$ by black. It can be seen that not only the state variables s_i are randomly distribution of over the spanning cluster but also the higher states form small islands all over the spanning cluster. This is similar to the situation of mass distribution on a geometrical support generally taken for multifractal study[20]. However, the state distribution over the spanning cluster is not a simple iterative process of mass distribution over a geometrical support. The spanning clusters consist of subsets of sites occupied once, twice up to a subset of sites occupied Z times where Z is the coordination number of the lattice considered. A particular subset may appear several times in a spanning cluster at different stages of growth of the cluster during a large number of MC steps. A multiplicative cascade of these subsets is then formed in a complicated manner during the growth of the

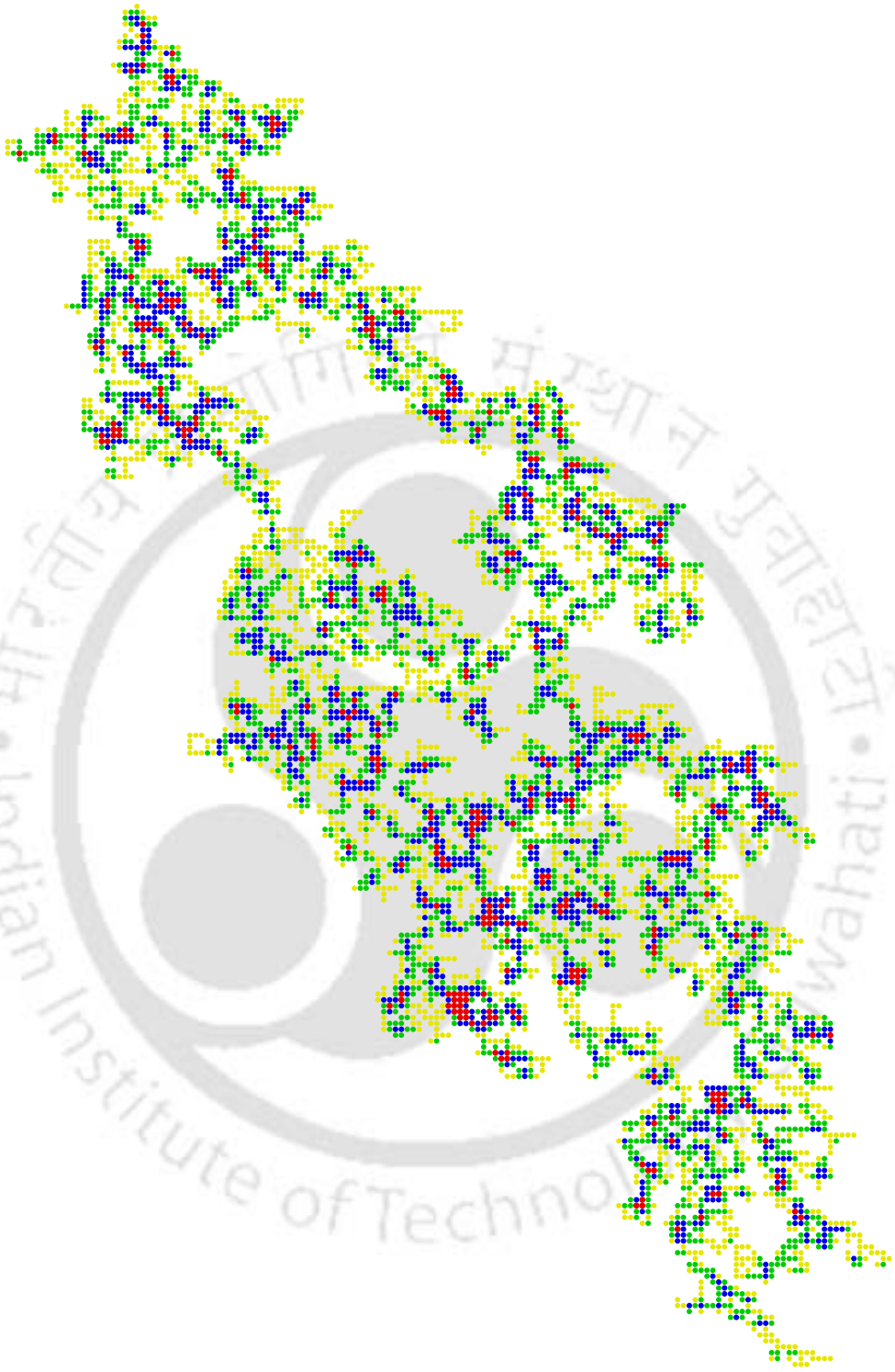

Figure 7.3: DSP spanning cluster at $p = p_c$ on the square lattice of size $L = 2^7$. Different colours in the cluster represent different values of s_i as yellow (●) for $s_i = 1$, green (●) for $s_i = 2$, blue (●) for $s_i = 3$ and red (●) for $s_i = 4$. The empty white space represents $s_i = 0$. It can be seen that the state variable is randomly distributed over the fractal spanning cluster.

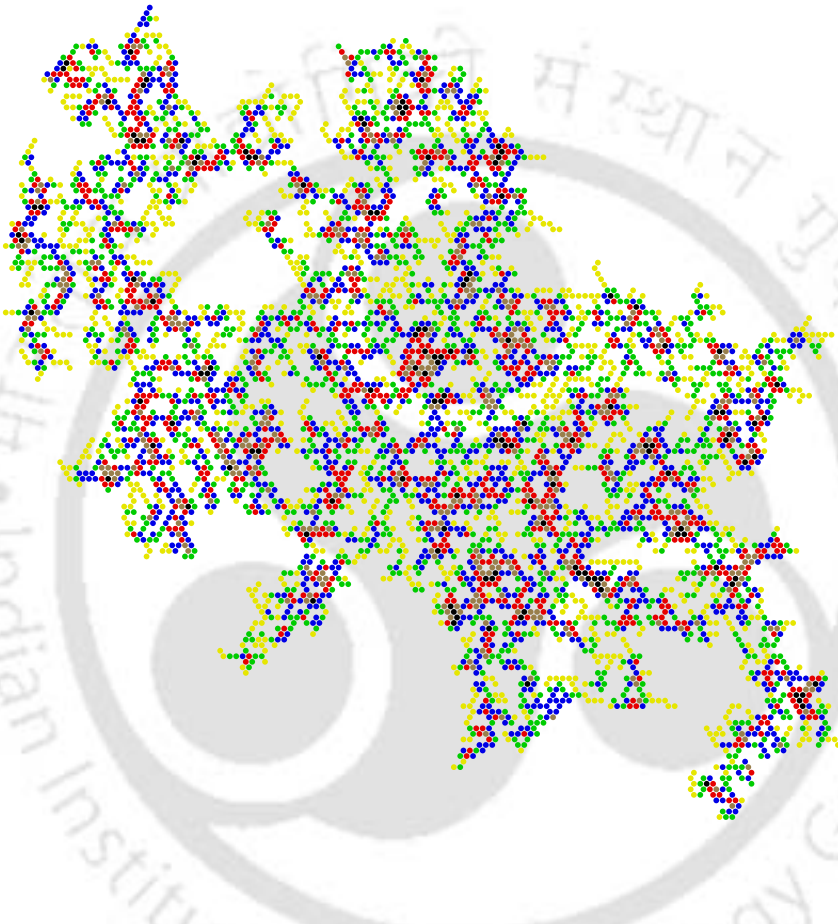

Figure 7.4: DSP spanning cluster at $p = p_c$ on the triangular lattice of size $L = 2^7$. Different colours in the cluster represent different values of s_i as yellow (•) for $s_i = 1$, green (•) for $s_i = 2$, blue (•) for $s_i = 3$, red (•) for $s_i = 4$, brown (•) for $s_i = 5$ and black (•) for $s_i = 6$. The empty white space represents $s_i = 0$. It can be seen that the state variable is randomly distributed over the fractal spanning cluster.

cluster. The s_i distribution on the spanning cluster is then expected to have many folds in both the rotational percolation models, DSP and SP. It is then interesting to investigate the moments of the s_i distribution over fractal objects, the spanning clusters here. The SP cluster is compact and isotropic but the DSP cluster is highly rarefied and anisotropic. The elongation of the DSP cluster is along the effective field E_{eff} appeared in the system. However, the clusters are not merely DP clusters along E_{eff}. It has already been found that both SP[18,19] and DSP[26,27] belong to new universality classes than that of DP or OP. The fractal dimension d_f of the spanning clusters were found as $d_f \approx 1.733$[26,27] (square lattice) and $d_f \approx 1.775$[28,29] (triangular lattice) for DSP and ≈ 1.957[18,19] for SP. Geometrical properties of the percolation clusters are governed by this single exponent d_f. However, in the following section it will be demonstrated that a measure defined in terms of the state variable s_i is not restricted by a single exponent but rather needs a sequence of fractal dimensions to characterize the measure.

7.3 Multifractal analysis of the spanning cluster

In order to study multifractality a suitable measure has to be defined. In general, a multifractal measure is related to the distribution of a physical quantity on a geometrical support[20–22]. The geometrical support here is the spanning percolation cluster at $p = p_c$ for the rotationally constrained percolation models. The distribution of the relative probability of a state over fractal substrates is a possible multifractal measure here. It is similar to the mass distribution on a geometrical support. The multifractal measure μ_i is then defined as

$$\mu_i = s_i / \sum_{i=1}^{L^2} s_i \tag{7.2}$$

where s_i is the state variable associated with each lattice site. μ_i can be called as relative state variable. Note that the measure μ_i is normalized to unity when summed over the whole lattice. The maximum value of the measure is $\mu_{max} = Z/\sum s_i$ and the minimum non-zero measure is $\mu_{min} = 1/\sum s_i$ where Z is the coordination number of the lattice. To obtain the multifractal nature of the distribution μ_i, it is necessary to study the scaling of the q-moments of the measure over different length scales on the geometrical support. If the measure μ_i is multifractal and the support is divided into n_ϵ boxes of size ϵ, then the weighted number of boxes $N(q,\epsilon)$ is given

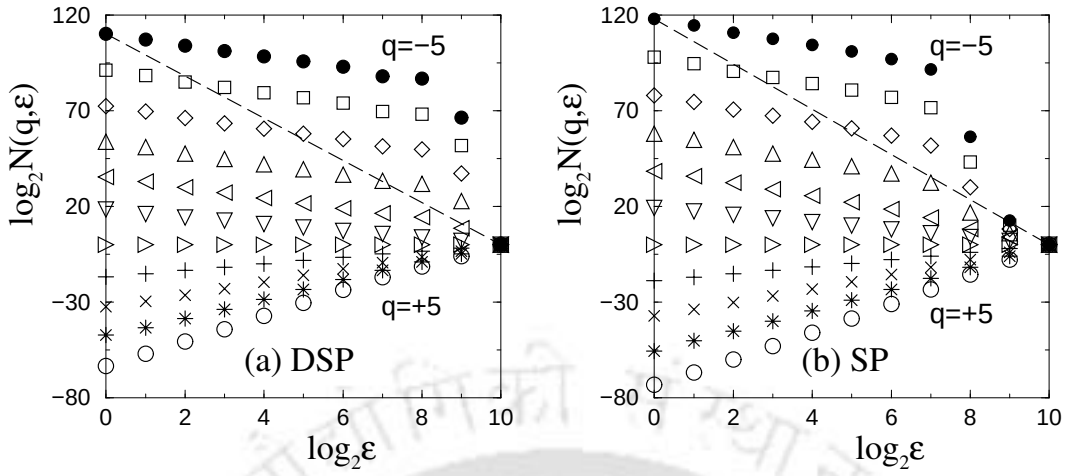

Figure 7.5: Plot of weighted number of box $N(q,\epsilon)$ versus the box size ϵ for $q=-5$ to $q=5$ in step of 1 for DSP in (a) and for SP in (b) for the spanning clusters generated on the square lattice of linear size $L=2^{10}$. The symbols are: ($\bullet$) for $q=-5$, ($\square$) for $q=-4$, ($\diamond$) for $q=-3$, ($\triangle$) for $q=-2$, ($\triangleleft$) for $q=-1$, ($\triangledown$) for $q=0$, ($\triangleright$) for $q=1$, ($+$) for $q=2$, ($\times$) for $q=3$, ($*$) for $q=4$, and ($\circ$) for $q=5$. It can be seen that box counting method is not working for $q<0$. The expected behaviour is shown by dashed lines for $q=-5$ in both (a) and (b).

by

$$N(q,\epsilon)=\sum_{j=1}^{n_\epsilon}\mu_j^q\approx\epsilon^{-\tau(q)} \tag{7.3}$$

where μ_j is the sum of the relative state variable in the jth box. Here $\tau(q)$ can be called as "state exponent". The weighted number of box $N(q,\epsilon)$ is determined as a function of the box size ϵ using box counting method for a given q. The boxes with at least one occupied site are only considered. The weighted number of boxes $N(q,\epsilon)$ are plotted against the box size ϵ for $q=-5$ to $q=+5$ for DSP in Figure 7.5(a) and for SP in Figure 7.5(b) generating spanning clusters on the square lattice of linear size $L=2^{10}$. It can be seen that the slopes of the plots change continuously for positive q up to $q=0$. For $q<0$, it seems that the usual box counting method adopted here is not working. The values of $N(q,\epsilon)$ remain unchanged over several box sizes ϵ starting from the smallest box size for a given q in both the models. It is expected that the plot should follow a straight line passing through the points at $\epsilon=1$ and $\epsilon=2^{10}$, the system size, in log-log scale since these two extreme points are not effected by the box size. It is shown by dashed lines for $q=-5$ in both the plots. It is observed that the value of $N(q,\epsilon)$ jumps suddenly when the box size is reduced less than one quarter of the system size. This is due to the fact that at this box

size there is at least one box appearing with a small measure and consequently the sum in Eq. 7.3 diverges due to negative moment. The appearance of large box sizes with small measures is because of the fact that the spanning percolation clusters contain holes of all possible sizes. Difficulties in determining weighted number of boxes for $q < 0$ for the measure distribution on random structures are already reported in the literature[30–32].The slopes of the plots in Figure 7.5 also remain almost unchanged with the moment q for $q < 0$. The weighted number of boxes has increased proportionally with higher negative moments. It has been verified that the estimation of $\tau(q)$ by fitting only through the smaller box sizes leads to a discontinuity in the plot of $\tau(q)$ versus q which is expected to be a smooth function of q. Discontinuity in the plot of $\tau(q)$ versus q was also observed in the cases of resistance fluctuations in randomly diluted networks[12] and in diffusion limited aggregation[33,34]. In these cases, there are breakdown of multifractal characters for negative moments due to exponential decay of the smallest measures.

Multifractal characteristics of the spanning clusters of rotationally constrained percolation models are then analyzed here taking large positive moments, changing q from 0 to 32. Analysis has been made on the square and triangular lattices of linear size $L = 2^{10}$ for both DSP and SP models and the results are compared with that of the OP model. In Figure 7.6, $\tau(q)$ is plotted against q, (a) for DSP model and (b) for SP model. In both the plots the squares represent the square lattice data and the triangles represent the triangular lattice data. Circles represent the data obtained for OP model. It is found that $\tau(0)$ is $\approx d_f$, the fractal dimension of the corresponding spanning clusters and $\tau(1)$ is ≈ 0 here for all three models, OP, SP and DSP. $\tau(0)$ corresponds to the dimension of the support which are the spanning percolation clusters of different models considered here and $\tau(1)$ is zero because $\sum_i \mu_i = 1$. It is interesting to notice that the values of $\tau(q)$ for DSP and SP models depend on the moment q in a nonlinear way for positive moments[23]. If the measure μ_i is characterized by a single fractal dimension d_f, the state exponent $\tau(q)$ should have a constant gap between two consecutive exponents[35] and consequently should have a linear dependence on q. In that case, a relationship between $\tau(q)$ and q in terms of d_f can be obtained as

$$\tau(q) = -(q-1)d_f. \tag{7.4}$$

This relation is shown in Figure 7.6 by a solid line for OP taking $d_f = 91/48 \approx 1.896$. The values of $\tau(q)$ obtained numerically for OP (circles) considering a two state

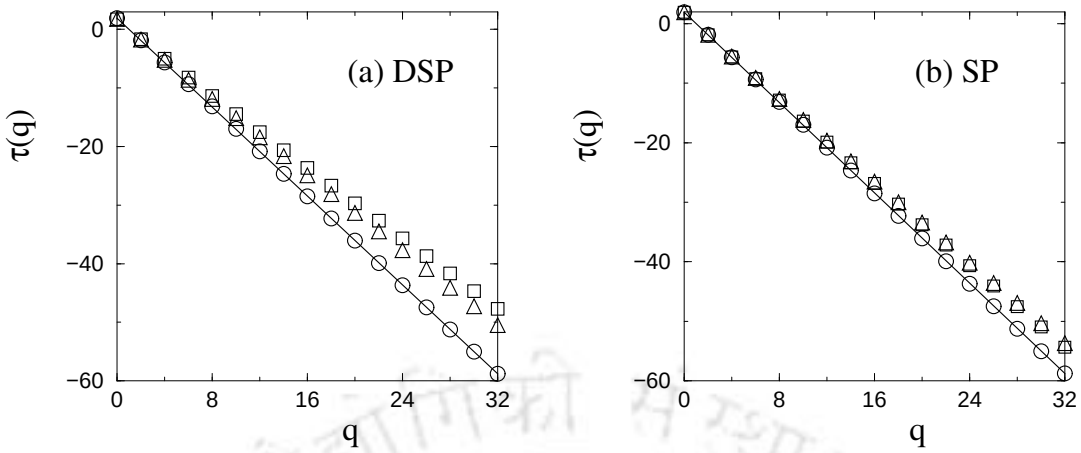

Figure 7.6: Plot of the state exponent $\tau(q)$ versus the moment q for DSP in (a) and for SP in (b) for $q \geq 0$. Squares represent the square lattice data and triangles represent triangular lattice data respectively. Circles represent data of OP spanning clusters on a square lattice. The solid straight line represents the linear dependence of $\tau(q)$ on q expressed in Eq. 7.4 for OP. The measured values of $\tau(q)$ for OP follows the straight line behaviour. For DSP and SP, $\tau(q)$ has a non-linear dependence on the moment q.

model for which $s_i = 0$ and 1 are in good agreement with with Eq. 7.4. There are few more things to notice. First, the state exponents of OP obey the constant gap equation given in Eq. 7.4 as expected. The constant gap scaling was also observed for the mean number of distinct sites visited by a random walker on spanning percolation cluster by Murthy *et al*[36]. As a consequence, the measure distribution is mono-fractal. Second, the values of $\tau(q)$ for DSP and SP are deviated from straight line behaviour and have non-linear dependence on the moment q. Thus, each moment of the measure μ_i needs a new exponent to characterize in these models. Third, the functional dependence of $\tau(q)$ on q is found different for all three models. This is expected because the models, OP, SP and DSP, belong to different universality classes. Fourth, the $\tau(q)$ values on the square and triangular lattices are almost the same for the SP model whereas they are considerably different for the DSP model. This is also in agreement with the fact that the critical properties hold universality in the SP model whereas there is a breakdown of universality in DSP model between the square and triangular lattices in two dimensions[28,29,37]. Finally, the fact that a sequence of exponents is required to characterize the moments of the measure confirms the multifractal nature of μ_i distribution in DSP and SP models. It should be noted here that in DSP and SP the spanning clusters consist of four or six subsets depending on the number of nearest neighbours on a given lattice. The values of $\tau(q)$ then may be possible to obtain in terms of the fractal dimensions of the subsets

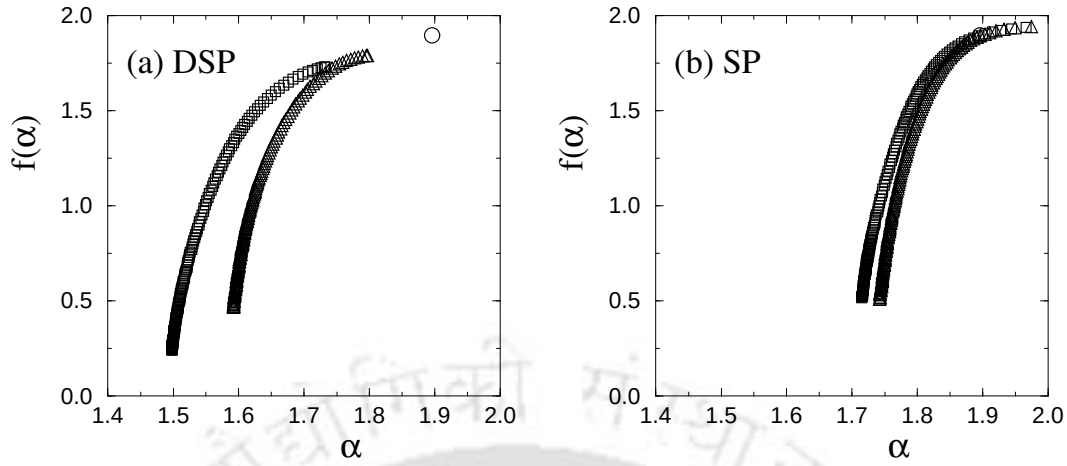

Figure 7.7: Plot of fractal dimension $f(\alpha)$ against the Lipschitz-Hölder exponent α for (a) DSP and (b) SP. Squares represent the square lattice data and triangle represent triangular lattice data respectively. For OP, it is a single point at $f(\alpha) = \alpha = d_f$ and represented by a circle. For DSP and SP, different spectra of $f(\alpha)$s are obtained. The spectra on the square and triangle lattice differ considerably for DSP whereas for SP they are almost identical.

consisting the spanning cluster coupled with a nonlinear dependence on q. However, it is difficult to determine the fractal dimensions of the individual subsets as they are generally small isolated islands in a spanning cluster as well as the nonlinear nature of $\tau(q)$.

The associated fractal dimensions $f(\alpha)$ with the measure and the corresponding Lipschitz-Hölder exponent α can be obtained through a Legendre transformation [21] of the sequence $\tau(q)$. The Legendre transformation is given below

$$\alpha(q) = -\frac{d\tau(q)}{dq}, \qquad f(\alpha) = q\alpha(q) + \tau(q). \tag{7.5}$$

The fractal dimensions $f(\alpha)$ are plotted against α in Figure 7.7. The values of $f(\alpha)$ obtained for DSP clusters are shown in Figure 7.7(a) and that of the SP clusters are shown in Figure 7.7(b). Since in the case of OP, the state exponent follows a constant gap equation (Eq. 7.4) it is expected that $f(\alpha)$ versus α will be represented by a point $f(\alpha) = \alpha = d_f$. It is shown by an open circle in Figure 7.7. It has been verified measuring slopes at different regions of $\tau(q)$ versus q for OP that the slopes remain within the error bar of the point shown. In the cases of DSP and SP, spectra of $f(\alpha)$ against α are obtained because $\tau(q)$ has a non linear dependence on q [23]. The symbols square and triangle correspond to the square lattice and the triangular lattice data respectively. There are a few things to observe. First,

$f_{max}(\alpha)$ corresponds to d_f of the respective models. Second, the $f(\alpha)$ curves are always $\leq d_f$ since the supports are spanning percolation clusters of fractal dimension d_f. Third, the spectrum of fractal dimensions $f(\alpha)$ for SP and DSP are found to be different. It means that not only the mass fractal dimension d_f is different but also the whole set fractal dimensions $f(\alpha)$s are different. It is expected because SP and DSP belong to different universality classes. Fourth, in case of SP, the spectrum of $f(\alpha)$ for the square lattice is identical with that of the triangular lattice for lower moments (starting from the same mass fractal dimension) and slightly different at large positive moments. In case of DSP, the spectra of $f(\alpha)$ on the two lattices are considerably different over the full range of positive moments considered here, starting from two different mass fractal dimensions. This again confirms the universality of critical exponents in SP and breakdown of universality of critical exponents in DSP between square and triangular lattices in two dimensions[28,29,37]. Fifth, the values of $f(\alpha_{min})$ for both SP and DSP clusters are not equal to zero. This means that in these cases, the rarest regions of measure μ_{max} distribution are still fractal in the limit $q \to \infty$. It is evident from the spanning clusters configurations given in Figures 7.3 and 7.4 that the μ_{max} distribution appears in small islands all over the spanning clusters and not as a point distribution. The fractal dimension of μ_{max} distribution of SP clusters is found to be little higher than that of DSP clusters. This is due to the presence of an extra directional constraint in the DSP model which takes the growth of the cluster away from a μ_{max} point whereas due to pure rotational constraint in the SP model the probability of growth around a μ_{max} point is little higher in comparison to DSP. It can also be noticed that, in case of DSP, the whole $f(\alpha)$ spectrum is shifted upward in order to match with the mass fractal dimension of the spanning DSP clusters on the triangular lattice. However this is not so in the case in SP model. Finally, the values of $f(\alpha)$ converges at a minimum of Lipschitz-Hölder exponent α_{min}. The Lipschitz-Hölder exponent $\alpha(\xi)$ is defined as $\mu_\xi = \delta^{\alpha(\xi)}$ where $\mu_\xi = \mu(\xi+\delta) - \mu(\xi)$ is the increment in the measure over a length ξ to $\xi + \delta$[20]. The α_{min} value corresponds to the minimum of ξ, the length scale associated with μ_{max} clusters in this case. It could also be noticed that in both SP and DSP, the values of α_{min} on the triangular lattice is found little higher than that of the square lattice. This is due to the fact that the number of μ_{max} points are generally higher on the triangular lattice than that on the square lattice.

7.4 Conclusion

Using the concept of state variable, the percolation transition in rotationally constrained models is established at the same percolation threshold p_c defined geometrically. A relative state variable is defined to study the multifractal aspects of the spanning clusters at $p = p_c$. It is found that the q-moments of the measure is characterized by a sequence of "state exponents" $\tau(q)$ for both the SP and DSP models. The existence of a sequence of state exponents confirms the multifractal character of the distribution of relative state variable on the infinite clusters of SP and DSP. The OP spanning clusters are not found multifractal in this measure. Taking Legendre transformation of $\tau(q)$, different spectra of associated fractal dimensions $f(\alpha)$ as a function of Lipschitz-Hölder exponents α are obtained. The formalism of state variable is thus found suitable for studying percolation transition and multifractal aspects of certain percolation models. It is found that two different spectra of fractal dimensions are needed to characterize the spanning percolation clusters on the square and triangular lattices for the DSP model while that is not the case of SP model. The universality of critical exponents in the SP model and breakdown of universality in the DSP model are then confirmed again by the multifractal spectrum of fractal dimensions. DSP model thus belongs to a new universality class with a peculiar property of breakdown of universality in $2D$. It would be now interesting to see the effect of the topological bias developed in the DSP cluster on the dynamical properties of a system.

Bibliography

[1] B. B. Mandelbrot, *Statistical Model of Turbulence*, volume 12, Springer, New York, 1972.

[2] F. Milde, R. A. Römer and M. Schreiber, Phys. Rev. B **55**, 9463 (1997).

[3] B. Huckestein and R. Klesse, Phil. Mag. B **77**, 1181 (1998).

[4] S. M. Nishigaki, Phys. Rev. E **59**, 2853 (1999).

[5] S. B. Santra and B. Sapoval, Fractals **13**, 9 (2005).

[6] M. H. Jensen, A. Levermann, J. Mathiesen and I. Procaccia, Phys. Rev. E **65**, 046109 (2002).

[7] J. P. Bouchaud, M. Potters and M. Meyer, Eur. Phys. J. B **13**, 595 (2000).

[8] J.-F. Muzy, D. Sornette, J. Delour and A. Arneodo, Quantitative Finance **1**, 131 (2001).

[9] P. C. Ivanov et al., Nature **399**, 461 (1999).

[10] P. C. Ivanov et al., Chaos **11**, 641 (2001).

[11] A. Bunde and S. Havlin, *Fractals and Disordered Systems*, Springer-Verlag, Berlin, 1991.
[12] R. Blumenfeld, A. A. Y. Meir and A. B. Harris, Phys. Rev. B **35**, 3524 (1987).
[13] O. Stenull and H. K. Janssen, Eur. Phys. Lett. **55**, 691 (2001).
[14] O. Stenull and H. K. Janssen, Phys. Rev. E **65**, 036124 (2002).
[15] H. Hinrichsen, O. Stenull and H. K. Janssen, Phys. Rev. E **65**, 045104 (2002).
[16] A. Bunde, S. Havlin and H. E. Roman, Phys. Rev. A **42**, 6274 (1990).
[17] E. Eisenberg, A. Bunde, S. Havlin and H. E. Roman, Phys. Rev. E **47**, 2333 (1993).
[18] P. Ray and I. Bose, J. Phys. A **21**, 555 (1988).
[19] S. B. Santra and I. Bose, J. Phys. A **24**, 2367 (1991).
[20] J. Feder, *Fractals*, Plenum Press and New York and London, 1998.
[21] C. J. G. Evertsz and B. B. Mandelbrot, *in the appendix of* Chaos and Fractals *by H. O. Peitgen, H. Jürgens and D. Saupe*, Springer, New York, 1992.
[22] F. C. Moon, *Chaotic and Fractal Dynamics*, John Wiley & Sons Inc., New York, 1992.
[23] S. Sinha and S. B. Santra, Physica A **376**, 351 (2007).
[24] S. Sinha and S. B. Santra, in *Proceedings - 50th DAE Solid State Phys. Symp., BARC Mumbai, India, Dec., 2005*, page 165.
[25] S. Sinha and S. B. Santra, in *ICTP International Conference on Recent Advances in the Interdisciplinary Applications of Statistical Physics, ICTS Beijing, China, Sept., 2006*.
[26] S. B. Santra, Eur. Phys. J. B **33**, 75 (2003).
[27] S. B. Santra, Int. J. Mod. Phys. B **17**, 5555 (2003).
[28] S. Sinha and S. B. Santra, Eur. Phys. J. B **39**, 513 (2004).
[29] S. Sinha and S. B. Santra, Int. J. Mod. Phys. C **17**, 1285 (2006).
[30] A. Block, W. von Bloh and H. J. Schellnhuber, Phys. Rev. A **42**, 1869 (1990).
[31] P. Grassberger, Int. J. Mod. Phys. C **4**, 515 (1993).
[32] M. Yamaguti and C. P. C. Prado, Phys. Rev. E **55**, 7726 (1997).
[33] J. Lee and H. E. Stanley, Phys. Rev. Lett. **61**, 2945 (1988).
[34] R. Blumenfeld and A. Aharony, Phys. Rev. Lett. **62**, 2977 (1989).
[35] D. Stauffer and A. Aharony, *Introduction to Percolation Theory*, Taylor and Francis, London, 2nd edition, 1994.
[36] K. P. N. Murthy, L. K. Gallos, P. Argyrakis and K. W. Kehr, Phys. Rev. E **54**, 6922 (1996).
[37] S. Sinha and S. B. Santra, Int. J. Mod. Phys. C **16**, 1251 (2005).

Chapter 8

Dynamical Scaling in DSP

Critical properties of the static geometrical quantities of the DSP model has been elaborated so far in the previous chapters. In this chapter, the dynamical properties of the DSP model will be described and the values of the corresponding dynamical exponents will be reported. Connection will then be made with the static properties.

There is a great deal of interest in the transport properties of disordered[1–8] systems due to their applications. Transport properties like diffusivity, electrical conductivity and magnetoresistance are the main subjects of interest and they show anomalous behaviour[9–12] in disordered systems. The electrical conductivity of disordered systems are determined studying different percolating systems[13–24], random resistor[25–33] and random diode networks[34,35], diluted random systems[36–38], deterministic fractals[39–42] at suitable conditions. Since diffusivity is connected to the electrical conductivity by Einstein relation[9,10,18], in most of the cases diffusion process has been primarily studied in these random systems and the connection has been made to the electrical conductivity. The diffusion process in disordered systems can be efficiently modeled by performing random walks on the percolation clusters as introduced by de Gennes in 1976[43].

An external bias E having a fixed direction in space produces a global bias. Under such a bias, the diffusing particle has higher probability to move in the favoured direction and the diffusion process is called biased diffusion. On the disordered structure, the scaling behaviour of the root mean square (rms) distance is determined by the competition of three different processes namely, diffusion due to random motion of the particles, drift due to the applied bias and trapping in the disordered structure. Bötger and Bryksin in 1982[44] suggested that the mean velocity of a diffusing particle will be a non-monotonic function of the bias field because of trapping in the dangling ends in disordered media. Their work triggered several analytical and

numerical studies in this subject[45–50]. Analytically it has been found that the drift velocity vanishes above a critical bias E_c on disordered systems above p_c[13,47,51] which was not observed in earlier numerical simulations[46,52]. The controversy between the theoretical predictions and the numerical results has been resolved in favour of a transition by Dhar and Stauffer[50] through extensive simulation in $3D$.

Local bias B imposes a rotational constraint on the motion of the diffusing particle. Under such a rotational constraint, the diffusing particle at time t has the same probability to move in the same direction as in the earlier time step $t-1$ and to turn in a specific rotational direction, say clockwise. The probability of moving in any other direction is smaller than the probability of moving in the forward direction or in the clockwise rotational direction. Under the rotational bias field, it has been found that the behaviour of the random walker is always diffusive except at infinite field strength[53]. The same behaviour of the random walkers has also been observed by Seifert and Suessenbach[52] in a slightly different model.

Imposing both the directional and rotational bias fields simultaneously on the random walker, an extensive study of diffusion property in disordered system has been made by Santra and Seitz[54]. In their model, biased random walks were performed on the ordinary percolation clusters. Depending on the strength of the bias fields, transition from diffusion to drift to trapping has been demonstrated. A complete phase diagram has also been obtained for all three phases depending on the strength of the bias fields as well as disorder.

In this thesis, the transport properties of $2D$ disordered systems are studied under crossed electric and magnetic fields when the magnetic field is applied perpendicular to the plane of the lattice. Instead of performing biased random walk on the ordinary percolation cluster, unbiased random walk is performed on the DSP clusters grown under the presence of the crossed bias fields. In effect it is the topological bias (the anisotropic DSP spanning clusters) which affects the behaviour of the random walkers. The diffusion is expected to be anisotropic due to the cluster anisotropy though there is no external bias applied on the walker. It has already been verified by performing random walks on directed percolation clusters[55–57]. Studying direction dependent anomalous diffusion properties on the DSP cluster, the electro-magnetic transport properties of $2D$ disordered systems will be extracted here. Their critical properties will be studied varying the site occupation probability p, the measure of disorder of the system and the dynamical scaling behaviour will be established.

8.1 The model

Directed spiral percolation clusters at different values of $p \geq p_c$ are generated on the square and triangular lattices of size $2^{11} \times 2^{11}$ by the single cluster growth algorithm described in Chapter 2. Only the infinite clusters are considered for the study of dynamical properties. Close to p_c, many small finite clusters appear in the system. All the finite clusters are rejected until a spanning cluster is generated. In order to study the transport properties, random walks are performed on the spanning clusters only. The walk starts from a randomly chosen occupied site of a spanning DSP cluster at $t = 0$. In order to implement the random walk on a $2D$ square lattice, a random number r uniformly distributed between 0 and 1 is called. The interval $0-1$ is then divided into four equal sub-intervals, say, $1, 2, 3$ and 4. The sub-intervals $1, 2, 3, 4$ correspond to the four directions west, north, east and south respectively from the present site. If the random number r corresponds to the first interval, the random walker is eligible to make a move to the west. The random walker jumps to a nearest neighbour corresponding to the right interval in which r falls if the site is occupied. Otherwise it stays at the same place. Time t is incremented to $t + 1$ at each attempt of motion. This is demonstrated in Figure 8.1. The black dots represent occupied sites of a spanning DSP cluster generated on a 9×9 square lattice. The randomly chosen starting point of the random walker is marked by a cross. As the random walk is unbiased, the jump probabilities w_1, w_2, w_3 and w_4 along the four directions are equal. A random number is then called to select an interval as described above. From the present position, the particle can move on the occupied sites only in the directions 2 and 3 here. It can not move in the directions

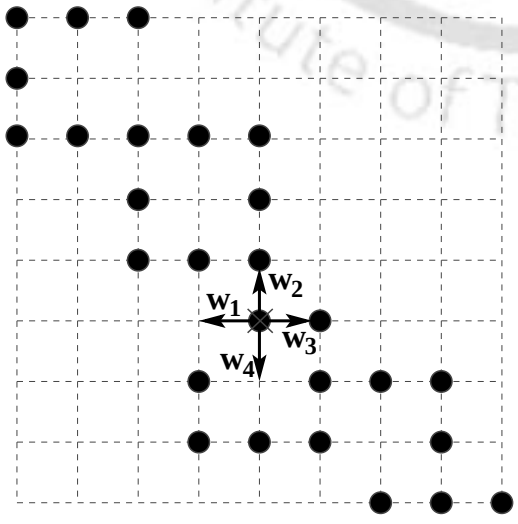

Figure 8.1: Demonstration of unbiased random walk on a DSP cluster. The walk is started from a randomly chosen site marked by a cross. Equal jump probabilities in the four directions are denoted by w_1, w_2, w_3 and w_4. However, the particle can only move towards the directions 2 and 3 here as the other nearest neighbours are empty.

1 and 4 since there is no occupied site. However any attempt to move to 1 or 4, time t will be incremented by 1. It can be seen that the walk will be highly affected by the topological bias of the DSP clusters though there is no external bias on the walk. If the particle hits one of the dangling ends it has to wait until it follows the same path to come out from the trap. Since the DSP clusters are anisotropic in nature, the diffusion process is then expected to be anisotropic on the DSP clusters.

8.2 Dynamical critical exponents and scaling

Diffusion and conductivity:

In the DSP model the directional constraint from left to right can be considered as an in-plane electric field $\mathbf{E} = \hat{i}E$ on a positively charged particle in the positive x direction. The clockwise rotational constraint may arise from a magnetic field $\mathbf{B} = \hat{k}B$ along z direction considering the lattice on the xy plane. As a result, a magnetic force $\mathbf{E_H} = -\hat{j}E_H$ is developed in the system perpendicular to both $\mathbf{E}$ and $\mathbf{B}$. Due to the presence of crossed bias fields in the system a Hall field is generated in the opposite direction of $\mathbf{E_H}$. The in-plane electric field $\mathbf{E}$ and the magnetic force $\mathbf{E_H}$ generates an effective field E_{eff} along the top left to the right lower diagonal of the lattice and the cluster grows in the effective direction. The DSP clusters generated are anisotropic in nature. The electrical conductivity σ in an isotropic system is related to the diffusivity D of the particle via Nernst-Einstein relation[9,10,18] given by, $\sigma = ne^2D/(k_bT)$ where e is the electric charge, n is density of the mobile particles, k_b is the Boltzmann constant and T is the temperature of the system. However in an anisotropic system, the conductivity is no longer a scalar quantity and becomes a tensor quantity, a 2×2 matrix here. The eigenvalues of the conductivity tensor correspond to the components of electrical conductivity, $\sigma_\parallel$ along the direction of E_{eff} (longitudinal or easy direction) and $\sigma_\perp$ in the direction perpendicular to E_{eff} (transverse direction), are expected to have different critical behaviour. The conductivities in the two perpendicular directions can be expressed in terms of the diffusivities along those directions[55,58,59]. $\sigma_\parallel$ and $\sigma_\perp$ are therefore obtained as

$$\sigma_\parallel = \frac{ne^2}{k_BT}D_\parallel \quad \text{and} \quad \sigma_\perp = \frac{ne^2}{k_BT}D_\perp. \tag{8.1}$$

Below p_c, no current flows in the system due to finite clusters and $\sigma_{\parallel,\perp} = 0$. On the other hand, at $p = 1$ the current will be maximum. In the critical regime above p_c, $\sigma_\parallel$ and $\sigma_\perp$ are expected to show power law behaviour characterized by the conductivity

exponents $\mu_{\parallel}$ and $\mu_{\perp}$ defined as

$$\sigma_{\parallel} \sim (p - p_c)^{\mu_{\parallel}} \quad \text{and} \quad \sigma_{\perp} \sim (p - p_c)^{\mu_{\perp}}. \tag{8.2}$$

It is then possible to determine the electrical conductivity of the system by measuring the diffusion coefficients $D_{\parallel}$ and $D_{\perp}$ along the growth of the cluster (longitudinal direction) and perpendicular (transverse direction) to that. The longitudinal diffusion coefficient $D_{\parallel}$ relates to the rate of diffusion along the effective field E_{eff} and the transverse diffusion coefficient $D_{\perp}$ describes the rate of diffusion in the direction perpendicular to E_{eff}. In the long lime limit ($t \to \infty$), $D_{\parallel}$ and $D_{\perp}$ are defined as

$$D_{\parallel} = \frac{1}{2}\frac{d\langle r_{\parallel}^2(t)\rangle}{dt} \quad \text{and} \quad D_{\perp} = \frac{1}{2}\frac{d\langle r_{\perp}^2(t)\rangle}{dt} \tag{8.3}$$

where $\langle r_{\parallel}^2(t)\rangle$ and $\langle r_{\perp}^2(t)\rangle$ are mean square displacements in the two perpendicular directions respectively.

On a regular euclidean lattice, the mean square displacement $\langle r^2(t)\rangle$ of a random walker goes linearly with time, *i.e.* $\langle r^2(t)\rangle \sim t$ which leads to the regular diffusion. However, the situation on a percolation cluster is complicated. At the percolation threshold, the spanning cluster is self similar and fractal containing holes, dangling ends, bottlenecks and loops appearing in all length-scales. Correspondingly, the motion of the random walker slows down in all length scales. The mean square displacement traveled in time t by the walker then can be written as $\langle r^2(t)\rangle \sim t^{2/d_w}$ with $d_w > 2$ for fractals and the diffusion is called anomalous. Here d_w is called the walk dimension which is equal to 2 in the regular diffusion. In the case of DSP clusters, as the diffusion is anisotropic, the walk dimensions in the two perpendicular directions are expected to be different. They can therefore be defined as,

$$\langle r_{\parallel}^2(t)\rangle \sim t^{2/d_{w\parallel}} \quad \text{and} \quad \langle r_{\perp}^2(t)\rangle \sim t^{2/d_{w\perp}} \tag{8.4}$$

where $d_{w\parallel}$ and $d_{w\perp}$ are the walk dimensions in the longitudinal and transverse directions, respectively.

Dynamical scaling relations:

If the diffusion is performed on the large spanning clusters, the occupied sites in the infinite cluster only contribute to the dc conductivity. In that case, density of the

mobile particles in Eq. 8.1, $n \sim P_\infty \sim (p - p_c)^\beta$. This yields,

$$D_\parallel \sim (p - p_c)^{\mu_\parallel - \beta} \quad \text{and} \quad D_\perp \sim (p - p_c)^{\mu_\perp - \beta}. \tag{8.5}$$

Similarly, for the x component, $D_x \sim (p - p_c)^{\mu_B - \beta}$. Above the percolation threshold p_c, the clusters are infinite and the fractal structure appears only within the correlation length $\xi(p)$. The anomalous diffusion law, Eq. 8.4, generally occurs only below the corresponding crossover time $t_\xi \sim \langle r^2(t_\xi)\rangle^{d_w/2} \sim \xi^{d_w}$. Therefore, above t_ξ, $D_{\parallel,\perp} = \frac{1}{2} d\langle r^2_{\parallel,\perp}\rangle/dt \equiv \langle r^2_{\parallel,\perp}\rangle/t$ and the mean square displacement $\langle r^2_{\parallel,\perp}(t)\rangle$ behaves as

$$\langle r^2_{\parallel,\perp}(t)\rangle \sim t(p - p_c)^{\mu_{\parallel,\perp} - \beta} \quad , \quad t > t_{\xi\parallel,\perp}. \tag{8.6}$$

On the other hand, for time t below t_ξ or distances $r < t_\xi^{1/d_w}$,

$$\langle r^2_{\parallel,\perp}(t)\rangle \sim t^{2/d_{w\parallel,w\perp}}, \quad t < t_{\xi\parallel,\perp}. \tag{8.7}$$

Now, by definition, at $t = t_\xi$ the span of the walk is equal to the connectivity length and therefore, $\langle r^2_{\parallel,\perp}(t)\rangle \sim \xi^2_{\parallel,\perp} \sim (p - p_c)^{-2\nu_{\parallel,\perp}}$. Substituting this in Eqs. 8.6 and 8.7 and expressing them in terms of $(p - p_c)$, the following scaling relations between the static and dynamic exponents are obtained as,

$$d_{w\parallel} = 2 + (\mu_\parallel - \beta)/\nu_\parallel \quad \text{and} \quad d_{w\perp} = 2 + (\mu_\perp - \beta)/\nu_\perp. \tag{8.8}$$

Note that, the scaling relations connect the static exponents $\nu_\parallel, \nu_\perp$ and β with the dynamic exponent $\mu_\parallel, \mu_\perp$ through the walk dimensions $d_{w\parallel}, d_{w\perp}$. Measuring the mean square displacements $\langle r^2_\parallel(t)\rangle$ and $\langle r^2_\perp(t)\rangle$ with time, it is then possible to determine the diffusivities as a function of $(p - p_c)$. Estimating the diffusivity exponents $(\mu_\parallel - \beta)$ and $(\mu_\perp - \beta)$ and knowing the order parameter exponent β, the conductivity exponents $\mu_\parallel$ and $\mu_\perp$ can be determined. The dynamic scaling relations can then be verified for the DSP model.

Magnetoresistance:

Magnetotransport in disordered systems are being studied by several approaches available in the literature[60–66]. Since in the DSP model the effect of the electric and the magnetic fields on the motion of a classical charged particle are taken care by the directional and rotational constraints simultaneously, the model could be useful to study the Hall effect and magnetoresistance in disordered systems. If a

conducting material is placed in crossed electric and magnetic fields according to the field configurations considered in the present problem and a positively charged particle moves along the electric field, the transverse magnetoresistance is defined as

$$\rho_B = \sigma_B^{-1} = \frac{E_x}{j_x} \tag{8.9}$$

where j_x and E_x are the current density and electric field along x direction and here $E_x = E$. Here σ_B is the magnetoconductivity. This is similar to the dc conductivity along the direction of applied external electric field in presence of transverse magnetic field. However, σ_B depends on the intensity of the magnetic field B since j_x is function of B. A relation between the magnetoconductivity σ_B and the diffusivity along x direction can therefore be defined by Nernst-Einstein relation in DSP model as

$$\sigma_B = \rho_B^{-1} = \frac{ne^2}{k_B T} D_x \tag{8.10}$$

where D_x is the diffusion coefficient along x direction. Thus, it is possible to calculate the magnetoconductivity by measuring the mean square displacement $\langle r_x^2(t)\rangle$ along x direction and calculating $D_x = \frac{1}{2} d\langle r_x^2(t)\rangle/dt$. As p approaches to p_c from above, it is expected that σ_B will go to zero with a power law,

$$\sigma_B \sim (p - p_c)^{\mu_B} \tag{8.11}$$

where μ_B is a critical exponent.

8.3 Results and discussions

Simulations are performed on the large spanning DSP clusters generated on the square and triangular lattices of size $2^{11} \times 2^{11}$. For each value of p, 1000 different spanning clusters are generated. On each cluster, 1000 different starting points are chosen randomly. A total number of $N = 10^6$ walks are thus performed for a given p. Each walk is performed up to $N_t = 2^{20}$ time steps. If any particle hits the boundary of the lattice, the periodic boundary conditions are applied and the motion continues. The displacement $\mathbf{r}(t)$ is also adjusted accordingly. The mean square displacement of the diffusing particle in the longitudinal and transverse directions are then estimated

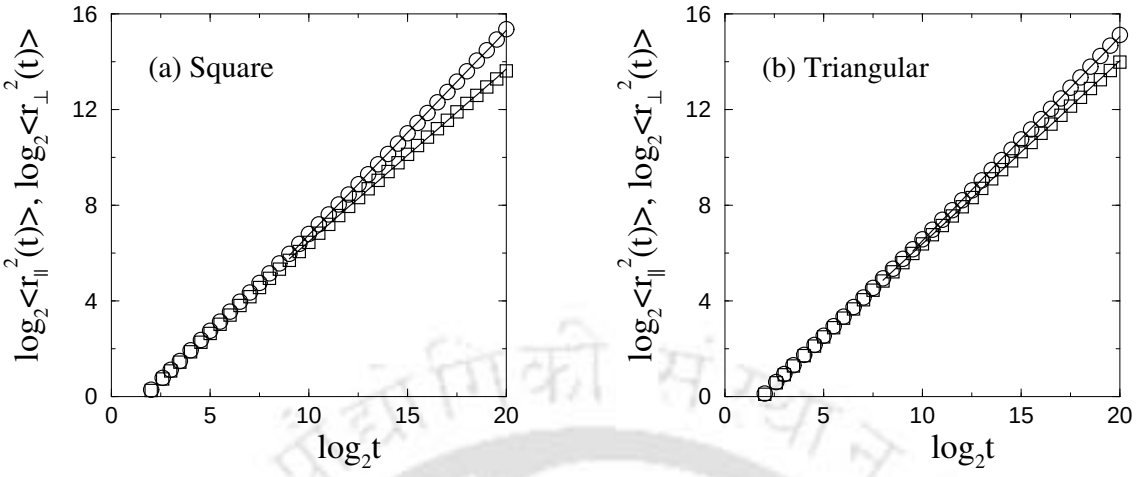

Figure 8.2: Plot of mean square displacements $\langle r_{\parallel}^2(t)\rangle$ (○) and $\langle r_{\perp}^2(t)\rangle$ (□) with time. From the slopes, the walk dimensions are obtained as, $2/d_{w\parallel} = 0.854 \pm 0.002$ and $2/d_{w\perp} = 0.720 \pm 0.003$, *i.e.* $d_{w\parallel} = 2.342 \pm 0.002$ and $d_{w\perp} = 2.778 \pm 0.003$ for the square lattice. For the triangular lattice, they are obtained as $2/d_{w\parallel} = 0.853 \pm 0.003$ and $2/d_{w\perp} = 0.765 \pm 0.002$, *i.e.* $d_{w\parallel} = 2.345 \pm 0.003$ and $d_{w\perp} = 2.614 \pm 0.002$.

as

$$\begin{aligned} \langle r_{\parallel}^2(t)\rangle &= \frac{1}{N}\sum_{i=1}^{N}\{\big|\mathbf{r}_i(t) - \mathbf{r}_i(0)\big|\cos\theta_i(t)\}^2 \quad \text{and} \\ \langle r_{\perp}^2(t)\rangle &= \frac{1}{N}\sum_{i=1}^{N}\{\big|\mathbf{r}_i(t) - \mathbf{r}_i(0)\big|\sin\theta_i(t)\}^2 \end{aligned} \tag{8.12}$$

where $\theta_i(t)$ is the angle between the position vector $\mathbf{r}_i(t)$ at time t and the direction of the effective field E_{eff}. To estimate the walk dimensions $d_{w\parallel,w\perp}$, displacements $\langle r_{\parallel}^2(t)\rangle$ and $\langle r_{\perp}^2(t)\rangle$ are measured as a function of time on the square and triangular lattices at the respective percolation thresholds. In Figure 8.2, they are plotted with time t. The values of $2/d_{w\parallel,w\perp}$ are obtained from the slopes in the long time limit. For the square lattice, the walk dimensions are obtained as, $2/d_{w\parallel} = 0.854 \pm 0.002$ and $2/d_{w\perp} = 0.720 \pm 0.003$, *i.e.* $d_{w\parallel} = 2.342 \pm 0.002$ and $d_{w\perp} = 2.778 \pm 0.003$. For the triangular lattice, they are obtained as $2/d_{w\parallel} = 0.853 \pm 0.003$ and $2/d_{w\perp} = 0.765 \pm 0.002$, *i.e.* $d_{w\parallel} = 2.345 \pm 0.003$ and $d_{w\perp} = 2.614 \pm 0.002$.

A few things are to be noticed here. First, the walk dimensions in the two perpendicular directions are different beyond the error bars for both the lattices. This implies that walk in the parallel and perpendicular directions have different scaling behaviour with time, leading to anisotropic diffusion. This is due to the

topological anisotropy in the interior of the DSP clusters. Second, both of exponents are higher than 2 and therefore the diffusion is anomalous in both the directions. It is due to the presence of holes, chiral dangling ends appearing in all possible length scales. Third, the value $d_{w\parallel}$ is smaller than $d_{w\perp}$ on a given lattice which implies that the particles diffuse much faster in the direction of E_{eff}. Fourth, values of $d_{w\parallel}$ for the square and triangular lattices are identical within error bar whereas $d_{w\perp}$ is little less on the triangular lattice. Therefore, it is not only the static cluster properties but also the dynamical properties of the DSP clusters generated on the square and triangular lattices are different. The topological bias provided by the two lattices then have a strong effect on the diffusion process. Since the value of $d_{w\perp}$ is little less on the triangular lattice, the diffusion is faster in the transverse direction on the triangular than that on the square lattice. Note that, the transverse connectivity length exponent $\nu_\perp$ is also higher on the triangular lattice than on the square lattice. Finally, it can be noticed that both the values of $d_{w\parallel}$ and $d_{w\perp}$ are less than the walk dimension on the OP clusters ($d_w \approx 2.878$)[17–20]. The walk dimensions obtained on the DSP cluster are then new.

Next, in order to measure the diffusivities as a function of p, spanning DSP clusters are generated at different values of $p > p_c$. Random walks are performed on them and the displacements $\langle r^2_{\parallel,\perp}(t)\rangle$ are measured with time t. In the long time limit ($t \to \infty$), the diffusion coefficients $D_\parallel$ and $D_\perp$ are obtained from the derivatives $d\langle r^2_{\parallel,\perp}(t)\rangle/dt$ as defined in Eq. 8.3. For the parallel component, the results are described in Figures 8.3 and 8.4 for the square and triangular lattices respectively. Figures 8.3(a) and 8.4(a) show the mean square displacement $\langle r^2_\parallel(t)\rangle$ in the parallel direction as a function of time at different values of p for the two lattices. For the square lattice the values of p considered are, 0.655($\bigcirc$), 0.659($\triangle$), 0.661($\diamond$), 0.663($\triangleleft$), 0.666($+$), 0.671(∇), 0.677($*$), 0.686($\triangleright$) and 0.699($\square$). For the triangular lattice the values are, 0.570($\bigcirc$), 0.574($\triangle$), 0.576($\diamond$), 0.578($\triangleleft$), 0.581($+$), 0.586(∇), 0.592($*$), 0.601($\triangleright$) and 0.614($\square$). The derivatives are then calculated using central difference technique given by

$$\frac{d\langle r^2_\parallel(t)\rangle}{dt} = \frac{\langle r^2_\parallel(t+\Delta t)\rangle - \langle r^2_\parallel(t-\Delta t)\rangle}{2\Delta t} + O\{(\Delta t)^2\} \tag{8.13}$$

where $\Delta t = 2^{16}$ and $O\{(\Delta t)^2\}$ is order of error. It should be noted that, using the above derivative, the diffusion coefficient can be calculated from Eq. 8.3 in the $t \to \infty$ limit. In Figures 8.3(b) and 8.4(b), $d\langle r^2_\parallel(t)\rangle/dt$ are plotted against the inverse time $1/t$ for the two lattices. It can be seen that, $d\langle r^2_\parallel(t)\rangle/dt$ shows a non-linear

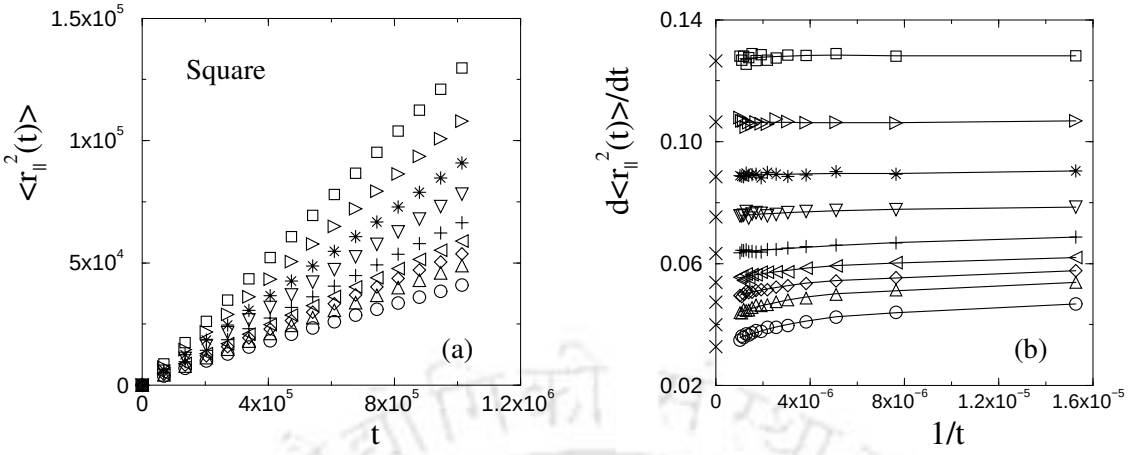

Figure 8.3: Plot of (a) $\langle r_{\parallel}^2(t)\rangle$ and (b) $d\langle r_{\parallel}^2(t)\rangle/dt$ with time for the square lattice. Different symbols correspond to different values of $p = 0.655(\bigcirc)$, $0.659(\triangle)$, $0.661(\diamond)$, $0.663(\triangleleft)$, $0.666(+)$, $0.671(\nabla)$, $0.677(*)$, $0.686(\triangleright)$ and $0.699(\square)$. In (b), to obtain the values of $D_{\parallel}$, the derivatives are extrapolated to $t \to \infty$ by a polynomial fitting and marked by crosses.

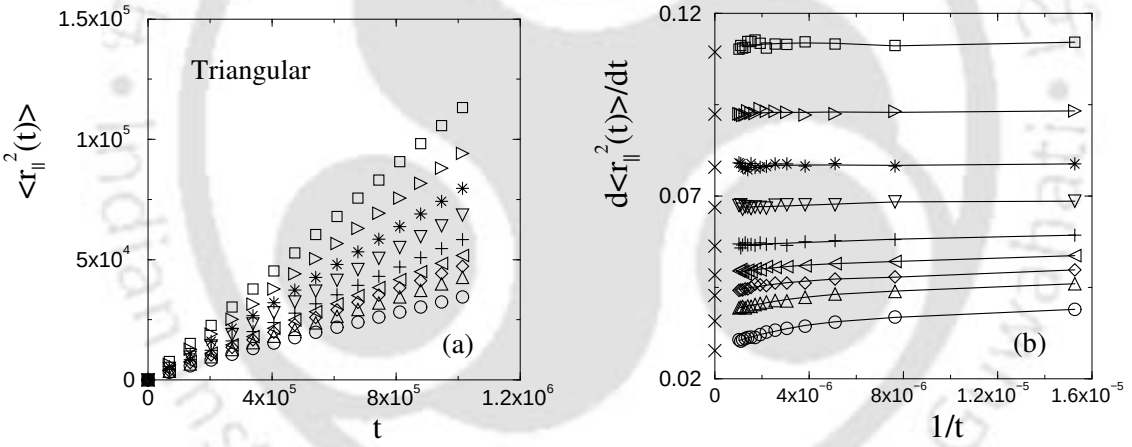

Figure 8.4: Plot of (a) $\langle r_{\parallel}^2(t)\rangle$ and (b) $d\langle r_{\parallel}^2(t)\rangle/dt$ with time for the triangular lattice. Different symbols correspond to different values of $p = 0.570(\bigcirc)$, $0.574(\triangle)$, $0.576(\diamond)$, $0.578(\triangleleft)$, $0.581(+)$, $0.586(\nabla)$, $0.592(*)$, $0.601(\triangleright)$ and $0.614(\square)$. The derivatives are then extrapolated to $t \to \infty$ in (b) and marked by crosses to obtain the values of $D_{\parallel}$.

behaviour with time[16,21] as the percolation threshold is approached. A polynomial line $y = A_0 + A_1x + A_2x^2 + ... + A_nx^n$ then can be fitted through the data points where $x = 1/t$ and $y = d\langle r_{\parallel}^2(t)\rangle/dt$ here. A reasonable fitting is obtained for the present data up to $n = 3$. The values of the derivatives in the $t \to \infty$ limit are then obtained from the intercepts on the vertical y axis which correspond to the values of A_0. The extrapolated values are marked by crosses. The longitudinal diffusion

Square Lattice			Triangular Lattice		
p	$D_{\parallel}$	$D_{\perp}$	p	$D_{\parallel}$	$D_{\perp}$
0.655	0.0164	0.0036	0.570	0.0139	0.0044
0.659	0.0200	0.0074	0.574	0.0179	0.0102
0.661	0.0238	0.0103	0.576	0.0214	0.0135
0.663	0.0269	0.0134	0.578	0.0242	0.0167
0.666	0.0317	0.0178	0.581	0.0282	0.0208
0.671	0.0377	0.0251	0.586	0.0335	0.0269
0.677	0.0443	0.0329	0.592	0.0390	0.0337
0.686	0.0533	0.0432	0.601	0.0462	0.0416
0.699	0.0633	0.0563	0.614	0.0547	0.0521

Table 8.1: Values of $D_{\parallel}$ and $D_{\perp}$ measured on spanning DSP clusters generated on the square and triangular lattices of size $2^{11} \times 2^{11}$ at different values of p.

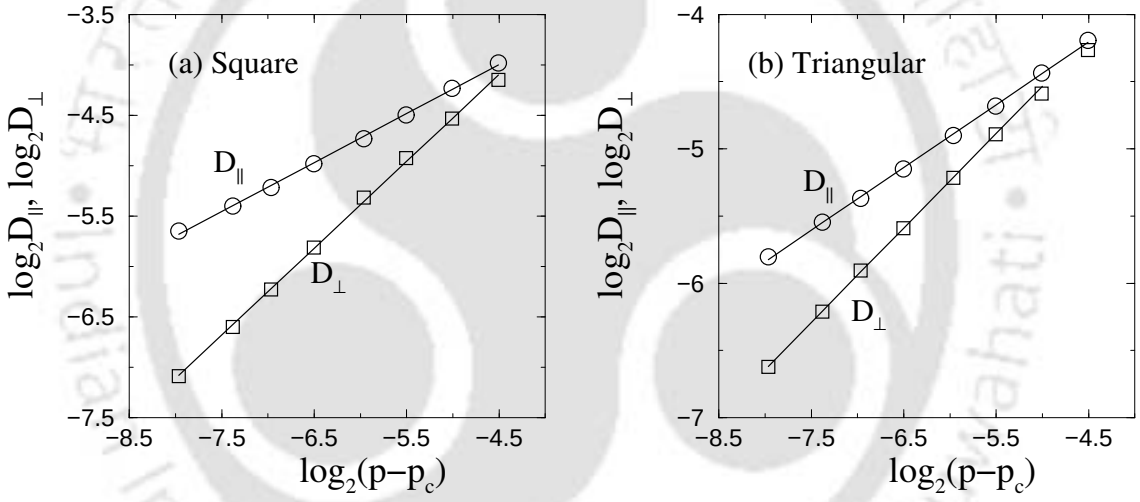

Figure 8.5: Plot of $D_{\parallel}$ (○) and $D_{\perp}$ (□) with $(p-p_c)$ for the (a) square and (b) triangular lattices. From the slopes, the exponents are obtained as $\mu_{\parallel} - \beta = 0.48 \pm 0.01$ and $\mu_{\perp} - \beta = 0.86 \pm 0.01$ for the square lattice. For the triangular lattice, they are obtained as, $\mu_{\parallel} - \beta = 0.47 \pm 0.01$ and $\mu_{\perp} - \beta = 0.70 \pm 0.01$.

coefficient $D_{\parallel}$ is then calculated as a function of p. Similar treatment has been performed for the transverse component and values of $D_{\perp}$ has been estimated for both the square and triangular lattices.

Values of the diffusion coefficients obtained at different values of p are tabulated in Table 8.1. In Figure 8.5, $D_{\parallel}$ and $D_{\perp}$ are plotted against $(p - p_c)$ for the square and triangular lattices. It can be seen that, values of $D_{\parallel}$ are higher than those of $D_{\perp}$ for different values of p for the individual lattices. Also notice that, close to p_c, the difference is much more higher. As p is increasing, the difference decreases

continuously and both $D_{\parallel}$ and $D_{\perp}$ approach to the same value. It is due to the decrease of disorder of the cluster at high p. At p_c, the percolation cluster is a self similar and fractal object and correspondingly the disorder is maximum. Here, due to the anisotropy of the DSP cluster, diffusivities in the two directions are different. As p is increased, more and more sites are occupied and one can have a completely ordered and isotropic system at $p = 1$ with all the sites of the lattice occupied. Obviously, the diffusivities in all directions will be same at this point. From the slopes of the Figure 8.5(a), $(\mu_{\parallel} - \beta)$ is obtained as 0.48 ± 0.01 and $(\mu_{\perp} - \beta)$ is obtained as 0.86 ± 0.01 for the square lattice. For the triangular lattice, from the slopes of Figure 8.5(b) $(\mu_{\parallel} - \beta)$ and $(\mu_{\perp} - \beta)$ are obtained as 0.47 ± 0.01 and 0.70 ± 0.01 respectively. The values of the critical exponents along the elongation and transverse directions are very different on both the lattices. It should be noticed here again that the topological bias produced by the DSP cluster on the diffusivity then has a very strong effect with respect to the randomness of the medium. Secondly, the values of $(\mu_{\parallel} - \beta)$ on the two lattices are almost the same whereas that of $(\mu_{\perp} - \beta)$ are found little different on the two lattices as it is observed for many other exponents.

The dynamical scaling relations, given in Eq. 8.8, connecting the static and dynamic exponents of the DSP model can be verified now. For the square lattice, connectivity length in the longitudinal direction $\nu_{\parallel} = 1.33 \pm 0.01$ and therefore $2 + (\mu_{\parallel} - \beta)/\nu_{\parallel} = 2.36 \pm 0.01$ whereas $d_{w\parallel} \approx 2.342$. Similarly in the transverse direction, $\nu_{\perp} = 1.12 \pm 0.03$ and $2 + (\mu_{\perp} - \beta)/\nu_{\perp} = 2.77 \pm 0.03$ whereas $d_{w\perp} \approx 2.778$. Thus the dynamical scaling relations are satisfied within error bar for both the components for the square lattice. For the triangular lattice, in the longitudinal direction, $\nu_{\parallel} = 1.36 \pm 0.02$ and therefore $2 + (\mu_{\parallel} - \beta)/\nu_{\parallel} = 2.35 \pm 0.02$ whereas $d_{w\parallel} \approx 2.345$. In the transverse direction, $2 + (\mu_{\perp} - \beta)/\nu_{\perp} = 2.57 \pm 0.02$ whereas $d_{w\perp} \approx 2.614$. Therefore, the dynamical scaling relation in the parallel direction is satisfied within error bar for the triangular lattice. However in the transverse direction, it is satisfied marginally. The little mismatch in the scaling relation in the transverse direction may be related to the little disagreement of the hyperscaling relation on the triangular lattice.

Since the values of the order parameter exponent β on the square and triangular lattices are already known (Chapter 3 and 7) it is then possible to extract the conductivity exponents $\mu_{\parallel,\perp}$. The value of β obtained using the spin representation of DSP model in Chapter 7 are considered due to high accuracy than the other measurement. For the square lattice, the value of β was obtained as 0.32 ± 0.02. Therefore, the conductivity exponents come out to be, $\mu_{\parallel} = 0.80 \pm 0.03$

Dynamical exponents	Ordinary percolation	Directed percolation	Directed spiral percolation	
			Square	Triangular
d_w	2.878 [17–20]	–	$d_{w\parallel} = 2.342 \pm 0.002$ $d_{w\perp} = 2.778 \pm 0.003$	2.345 ± 0.003 2.614 ± 0.002
μ	1.3101 [17]	$\mu_\parallel \approx 0.8$ [67]	$\mu_\parallel = 0.80 \pm 0.03$ $\mu_\perp = 1.18 \pm 0.03$	0.82 ± 0.03 1.05 ± 0.03

Table 8.2: Comparison of the dynamical critical exponents obtained for the DSP model with those of other models OP and DP.

and $\mu_\perp = 1.18 \pm 0.03$ on the square lattice. On the triangular lattice, the value of β was obtained as 0.35 ± 0.02. Accordingly, the conductivity exponents are then obtained as $\mu_\parallel = 0.82 \pm 0.03$ and $\mu_\perp = 1.05 \pm 0.03$. Thus the conductivity exponents $\mu_\parallel$ and $\mu_\perp$ in the two directions are found different on both the lattices. This means that the conductivity is anisotropic. The value of $\mu_\parallel$ is found to be identical within error bar on the square and triangular lattices whereas the value of $\mu_\perp$ is found slightly different. Estimates of the conductivity exponents for OP and DP models are available in literature. For OP, μ is estimated using numerical finite size scaling[17,27,30,31,68,69], random walks[16,20,21,70] and series expansion[28,71] methods. The value of μ was found around 1.31. For DP, measurement of $\mu_\parallel$ has been done by numerical finite size scaling[72], node elimination technique[38], renormalization group calculations[67,73] and by the determination of backbone[22] and the estimate of $\mu_\parallel$ was reported around 0.8. The values of the conductivity exponents obtained for the DSP model are listed in Table 8.2 and compared with that of the OP and DP model results. It can be seen that the exponent $\mu_\parallel$ is found close to that on the directed percolation cluster whereas $\mu_\perp$ is found close to the conductivity exponent μ on the ordinary percolation cluster. It seems that, the development of the resultant effective field E_{eff} in the longitudinal direction, similar to the directed percolation problem, makes the critical behaviour of the conductivity $\sigma_\parallel$ close to that on the DP cluster. The value of $\mu_\perp$ is not available in the literature to our knowledge and a comparison to that of the DP model is not possible. It is therefore not only the static cluster property but also the dynamical critical properties of the DSP model are found not trivial and different from that of the OP model. This observation again confirms different universality class of the DSP model than that of the other percolation models. Experimental measurement of dc conductivity for carbon-wax mixture near the percolation threshold was performed by Chakrabarty *et al*[74–76]. The conductivity exponent was measured as 2.1 ± 0.2 in $3D$.

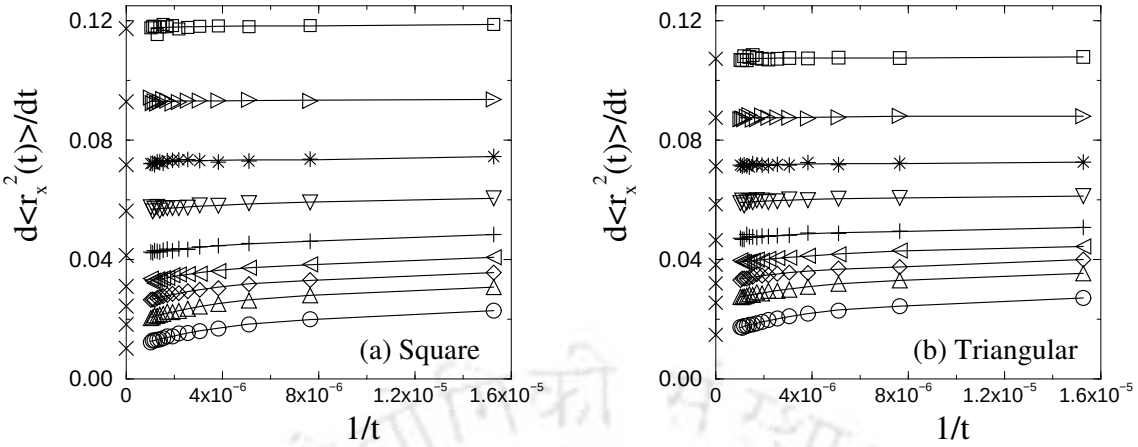

Figure 8.6: Plot of $d\langle r_x^2(t)\rangle/dt$ with the inverse time $1/t$ for the (a) square and (b) triangular lattice. Same symbol sets of the previous figures are used for different values of p for the individual lattices. The plots are extrapolated to $t \to \infty$ by nonlinear fitting and marked by crosses.

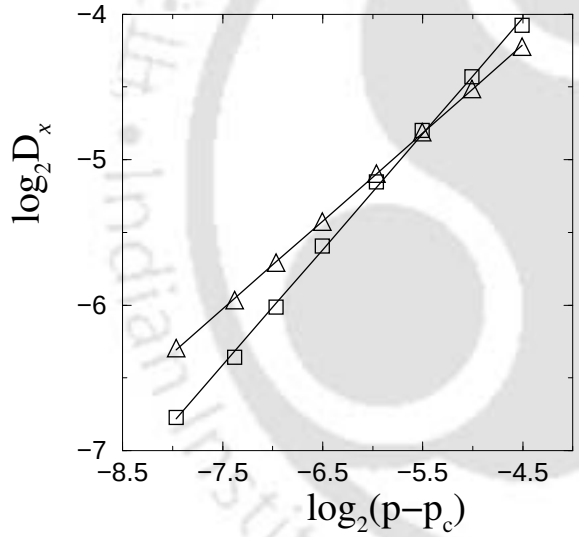

Figure 8.7: Plot of the diffusion coefficient D_x in the x direction with $(p - p_c)$ for the square (□) and triangular (△) lattices. From the slope, the exponent $\mu_B - \beta$ is obtained as 0.81 ± 0.01 for the square lattice and 0.61 ± 0.01 for the triangular lattice.

The magnetoconductivity σ_B is studied at different values of p by measuring the diffusivity D_x along x direction. In Figure 8.6, $d\langle r_x^2(t)\rangle/dt$ is plotted against inverse time $1/t$ and extrapolated to $t \to \infty$ for the (a) square and (b) triangular lattices. The extrapolated values are marked by crosses. D_x is then calculated and plotted with p in Figure 8.7 for the two lattices. In the figure, squares represent square lattice data and triangles represent triangular lattice data. From the slopes, $(\mu_B - \beta)$ is obtained as 0.80 ± 0.01 for the square lattice and 0.61 ± 0.01 for the triangular lattice. The magnetoconductivity exponent can then be obtained as $\mu_B = 1.11 \pm 0.07$ and 0.95 ± 0.09 for the two lattices, respectively. It can be seen that values of μ_B are

very close to the transverse conductivity exponents $\mu_\perp$ for both the lattices.

The results obtained in the study of magnetoresistance of a model of a three-component composites consisting of cylindrical insulator and perfect conductors in a metallic host film by Barabash *et al*[1] can be compared with the results of the present DSP model in 2 dimensions as it is already mentioned in Chapter 3. It is found by Barabash *et al* that the magnetoconductivity exponent is approximately 1.30, as in conventional $2D$ percolation problem. The value of the magnetoconductivity exponent obtained here is approximately 1.11 which is close to 1 obtained in the "effective medium approximation" of their model[6,7].

8.4 Conclusion

In this chapter, dynamical properties like diffusivity and conductivity of the DSP percolating clusters are studied on the square and triangular lattices. The diffusion process is modeled by the simple random walk on spanning DSP clusters and found that it is anomalous due to the presence of self holes, dangling ends, bottlenecks and loops at all length scales in the spanning cluster. Due to the topological anisotropy of the clusters, the diffusion process is also found anisotropic and therefore the components of the diffusivity are measured in the longitudinal and transverse directions. Using Nernst-Einstein relation, components of dc conductivities are estimated and corresponding dynamical exponents are determined. It is found that the walk dimensions as well as the critical exponents related to diffusivity are different from that of the other percolation models. It is then important to notice that not only the static structural properties at the critical point but also the dynamical properties of the model at the criticality are different from that of the percolation models. It is then a new universality class at all respect. Some of the critical exponents are also found to be different on the square and triangular lattices. The breakdown of universal characteristics of this model seem propagating through its topological bias. Dynamical scaling relations are verified within error bar in most of the cases. The results are then consistent with that of static scaling exponents measured in the previous chapters. Attempt has also been made to study the magnetotransport in a percolating system using DSP model. Results are compared with that of other model calculations of magnetoconductivity in composite systems and some agreements are found. Thus the DSP model can be considered as the simplest model to study the electric and magnetic properties of a disordered system in the presence of crossed external bias fields.

Bibliography

[1] S. V. Barabash, D. J. Bergman and D. Stroud, Phys. Rev. B **64**, 174419 (2001).
[2] R. Zallen, *The Physics of Amorphous Solids*, Wiley, New York, 1983.
[3] D. J. Bergman and Y. M. Strelniker, Phys. Rev. B **49**, 16256 (1994).
[4] D. J. Bergman and Y. M. Strelniker, Phys. Rev. B **51**, 13845 (1994).
[5] D. J. Bergman and Y. M. Strelniker, Phys. Rev. B **59**, 2180 (1999).
[6] D. J. Bergman, Phys. Rev. B **62**, 13820 (2000).
[7] D. J. Bergman, Phys. Rev. B **64**, 024412 (2001).
[8] E. López, S. V. Buldyrev, S. Havlin and H. E. Stanley, Phys. Rev. Lett. **94**, 248701 (2005).
[9] Y. Gefen, A. Aharony and S. Alexander, Phys. Rev. Lett. **50**, 77 (1983).
[10] J. F. Gouyet, *Physics and Fractal Structures*, Springer-Verlag, Berlin, New York, 1996.
[11] A. Bunde and S. Havlin, *Fractals in Science*, Springer-Verlag, Berlin, 2nd edition edition, 1995.
[12] J. Feder, *Fractals*, Plenum Press and New York and London, 1998.
[13] M. Barma and D. Dhar, J. Phys. C: Solid State Phys. **16**, 1451 (1983).
[14] R. Biller, J. Phys. A: Math. Gen. **17**, 3583 (1984).
[15] R. Biller, J. Phys. A: Math. Gen. **18**, 989 (1985).
[16] R. B. Pandey, D. Stauffer, A. Margolina and J. G. Zabolitzky, J. Stat. Phys. **34**, 427 (1984).
[17] P. Grassberger, Physica A **262**, 251 (1999).
[18] D. Ben-Avraham and S. Havlin, *Diffusion and Reactions in Fractals and Disordered Systems*, Cambridge University Press, UK, 2000.
[19] D. Ben-Avraham and S. Havlin, J. Phys. A: Math. Gen. **15**, L691 (1982).
[20] S. Havlin, D. Ben-Avraham and H. Sompolinsky, Phys. Rev. A **27**, 1730 (1983).
[21] O. J. Poole and D. W. Salt, J. Phys. A: Math. Gen. **29**, 7959 (1996).
[22] I. Balberg and N. Binenbaum, Phys. Rev. B **33**, 2017 (1986).
[23] B. C. Harms and J. P. Straley, J. Phys. A: Math. Gen. **15**, 1865 (1982).
[24] X. H. Wang, E. Perlsman and S. Havlin, Phys. Rev. E **67**, 050101 (2003).
[25] B. J. Last and D. J. Thouless, Phys. Rev. Lett. **27**, 1719 (27).
[26] D. Adler, L. P. Flora and S. D. Senturia, Solid State Commun. **12**, 9 (1973).
[27] J. P. Straley, Phys. Rev. B **15**, 5733 (1977).
[28] R. Fisch and A. B. Harris, Phys. Rev. B **18**, 416 (1978).
[29] C. J. Lobb and D. J. Frank, J. Phys. C: Solid State Phys. **12**, L827 (1979).
[30] R. Fogelholm, J. Phys. C: Solid State Phys. **13**, L571 (1980).
[31] B. Derrida and J. Vannimenus, J. Phys. A: Math. Gen. **15**, L557 (1982).
[32] D. J. Frank and C. J. Lobb, Phys. Rev. B **37**, 302 (1988).
[33] Y. M. Strelniker, S. Havlin, R. Berkovits and A. Frydman, J. Appl. Phys. **99**, 905 (2006).
[34] O. Stenull and H. K. Janssen, Phys. Rev. E **64**, 016135 (2001).
[35] H. K. Janssen and O. Stenull, Phys. Rev. E **67**, 046115 (2003).

[36] J. M. Luck, J. Phys. A: Math. Gen. **17**, 2069 (1984).
[37] J. W. Kim, E. Perfect and H. Choi, Water Resources Research **43**, W01405 (2007).
[38] B. M. Arora, M. Barma, D. Dhar and M. K. Phani, J. Phys. C: Solid State Phys. **16**, 2913 (1983).
[39] R. Dasgupta, T. K. Ballabh and S. Tarafder, Phys. Stat. Sol. **181**, 313 (1994).
[40] R. Dasgupta, T. K. Ballabh and S. Tarafder, J. Phys. A: Math. Gen. **32**, 6503 (1999).
[41] M. Maitra, D. Mal, R. Dasgupta and S. Tarafder, Physica A **346**, 191 (2005).
[42] D. H. N. Anh, K. H. Hoffmann, S. Seeger and S. Tarafder, Eur. Phys. Lett. **70**, 109 (2005).
[43] P. G. de Gennes, La Recherche **7**, 919 (1976).
[44] H. Böttger and V. V. Bryksin, Phys. Status. Solidi (b) **113**, 9 (1982).
[45] S. Bustingorry, E. R. Reyes and M. O. Cáceres, Phys. Rev. E **62**, 7664 (2000).
[46] R. B. Pandey, Phys. Rev. B **30**, 489 (1984).
[47] S. R. White and M. Barma, J. Phys. A: Math. Gen. **17**, 2995 (1984).
[48] D. Stauffer, J. Phys. A: Math. Gen. **18**, 1827 (1985).
[49] D. Stauffer and D. Sornette, Physica A **252**, 271 (1998).
[50] D. Dhar and D. Stauffer, Int. J. Mod. Phys. C **9**, 349 (1998).
[51] D. Dhar, J. Phys. A: Math. Gen. **17**, L257 (1984).
[52] E. Seifert and M. Suessenbach, J. Phys. A: Math. Gen. **17**, L703 (1994).
[53] S. B. Santra, PhD thesis, University of Calcutta, Calcutta, 1994.
[54] S. B. Santra and W. A. Seitz, Int. J. Mod. Phys. C **11**, 1357 (2000).
[55] P. E. Parris, Phys. Rev. B **36**, 5437 (1987).
[56] A. K. Sarychev and A. P. Vinogradoff, J. Phys. C: Solid State Phys. **16**, L1073 (1983).
[57] R. Muralidhar, D. J. Jacobs, D. Ramkrishna and H. Nakanishi, Phys. Rev. A **43**, 6503 (1991).
[58] R. Y. Pai, H. W. Ellis, G. R. Akridge and E. W. McDaniel, Phys. Rev. A **12**, 1781 (1975).
[59] G. Vahala, Phys. Rev. Lett. **29**, 93 (1972).
[60] B. Movaghar and L. Schweitzer, J. Phys. C: Solid State Phys. **11**, 125 (1978).
[61] J. T. Chalker and S. L. Sondhi, Phys. Rev. B **59**, 4999 (1999).
[62] A. Carl, G. Dumpich and S. Friedrichowski, Physica A **191**, 454 (1992).
[63] A. Carl, G. Dumpich, C. Buchal and B. Stritzker, Z. Fur Phys. B: Cond. Mat. **90**, 261 (1993).
[64] S. Friedrichowski, A. Carl and G. Dumpich, Eur. Phys. Lett. **32**, 247 (1995).
[65] F. Evers, A. D. Mirlin, D. G. Polyakov and P. Wolfle, Physica E **12**, 260 (2002).
[66] C. Oleksy, Phys. Rev. E **59**, 3864 (1999).
[67] H. K. Janseen and O. Stenull, Phys. Rev. E **63**, 025103 (2001).
[68] J. M. Normand, H. J. Herrman and M. Hajjar, J. Stat. Phys. **52**, 551 (1988).
[69] J. G. Zabolitzky, Phys. Rev. B **30**, 4077 (1984).
[70] D. C. Hong, S. Havlin, H. J. Herrmann and H. E. Stanley, Phys. Rev. B **30**, 4083 (1984).
[71] J. Adler, Y. Meir, A. Aharony and A. B. Harris, J. Stat. Phys. **58**, 511 (1990).

[72] S. Redner and P. R. Mueller, Phys. Rev. B **26**, 5293 (1982).
[73] S. Rednerin *Percolation Structure and Processes*, edited by G. Deutscher, R. Zallen and J. Adler, Adam Hilger, Bristol, 1983.
[74] R. K. Chakrabarty, K. K. Bardhan and A. Basu, Phys. Rev. B **44**, 6773 (1991).
[75] R. K. Chakrabarty, K. K. Bardhan and A. Basu, J. Phys.: Condens. Matter **5**, 2377 (1993).
[76] K. K. Bardhan and R. K. Chakrabarty, Phys. Rev. Lett. **72**, 1068 (1994).

Chapter 9

Summary and Conclusion

In order to study the electro-magnetic properties of disordered systems in the presence of both the electric and magnetic fields, a new site percolation model called directed spiral percolation (DSP) is proposed in this thesis. The motivation is due to a lot of recent interest on the electric an magnetic properties of disordered systems due to their applications. The electric field produces a directional constraint and the magnetic field produces a rotational constraint when the motion of a charged particle is considered. The DSP model is constructed by imposing both the directional and rotational constraints simultaneously on the ordinary percolation (OP)[1–4] model. If both the fields are present perpendicular to each other in a material system, the electrons get deflected due to Lorentz force and a Hall field will appear in the system perpendicular to both the fields. The DSP model then can also be applied to study the Hall effect in such systems[5].

A single cluster growth Monte Carlo (MC) algorithm is developed in Chapter 2 to generate the DSP clusters on the square and triangular lattices in $2D$ under the effect of directional and rotational constraints present simultaneously. The percolation threshold is then determined for both the lattices. Morphologically, a new type of percolation cluster is found in this model having distinct features. Clusters are found anisotropic but the growth is not along the applied directional constraint. This is very different from directed percolation (DP)[6–8] clusters. The presence of two different constraints, directional and rotational, leads to the development of a fictitious Hall field in the system and the clusters grow in an effective field direction. They are found highly rarefied containing holes of all possible sizes. The clusters also contain chiral dangling ends similar to the spiral percolation (SP)[9–11] clusters. Thus the DSP clusters contain some of the features of both the DP and SP clusters besides certain new features of its own. Moreover, the spanning clusters seem more

compact and less anisotropic on the triangular lattice than on the square lattice. The universality class of the DSP model has been characterized by studying the critical properties of the DSP clusters at and below percolation threshold by several different methods and techniques. Different methods used in this thesis are MC simulation, finite size scaling, characterization of hull, effect of field direction and intensities, multifractality and the dynamical scaling behaviour.

In order to characterize the singularities associated with the cluster related geometrical quantities a full scaling theory is developed for the DSP model in Chapter 3. Corresponding critical exponents are then estimated numerically on the square and triangular lattices. Apart from the new geometrical features in the cluster morphology, two new and important observations are made. First, the critical exponents are found different from that of the other percolation models like OP, DP and SP. Consequently, the model belongs to a new universality class. Second, most of the critical exponents are found significantly different on the two lattices in the same space dimension. Though this is unusual in critical phenomena except for the spiral self-avoiding walks[12,13] and spiral lattice animals[14]. Several features like cluster morphology, scaling relations and the data collapse support the values of the critical exponents obtained on the individual lattices[15,16]. The MC results are then verified and the model studied further using different approaches.

One of the potential source of error in the estimation of critical exponents numerically is the finite size of the system. In a finite system, there is rounding off and shifting of critical singularities depending on the ratio of correlation length ξ to the linear size L of the system. Effect of finite system size (L) on the MC results are studied extensively by finite-size scaling in the Chapter 4. Results are then verified using two different approaches. First, by measuring the L-dependent critical exponents on different finite systems and extrapolating the exponents to the $L \to \infty$ limit. In another approach, an L-dependent scaling function is developed for the cluster properties of the anisotropic DSP model. The proposed scaling function form is verified[17,18] via numerical simulation. The results obtained here in finite-size scaling are found in good agreement with the previous results. This confirms the new universality class as well as the breakdown of universality between the square and triangular lattices in $2D$. The appearance of more and more tree like structures at and below the percolation threshold on the triangular lattice than on the square lattice is believed to be the cause of the breakdown of universality.

Apart from the bulk structural properties of the DSP clusters, the hull or the external perimeter of the clusters are also characterized. It is known that the hull of

percolation clusters exhibit scaling behaviour different from that of the clusters. The hulls are extracted from the DSP clusters by the well known Ziff method and the critical properties of these anisotropic chiral hulls are then studied in the Chapter 5. Interestingly, it is observed that the hull fractal dimension and the critical exponents related to the hull size distribution are the same within error bars on the square and triangular lattices unlike the cluster properties. Thus, the universality of the hull critical exponents holds for the square and triangular lattices in $2D$ [19,20]. DSP hulls are found to be compact and the hull fractal dimension is found close to 4/3, the Grossmann Aharony dimension [21]. A new conjecture has been made here for the hull fractal dimension relating it with the the two connectivity length exponents for the anisotropic clusters. DSP hulls contain chiral dangling ends similar to SP hulls and it is found that the values of hull dimension and other hull critical exponents are also close to that of the SP cluster hulls. Thus the effect of the rotational constraint is more dominant in the hull properties than the directional constraint.

The DSP model is then modified in order to study the model under variable field orientations and field intensities. The study of the DSP model under such field conditions are made on the square and triangular lattices and the results are reported in the Chapter 6. The critical properties as well as the universality class are found invariant on the directions of the applied directional and rotational fields. While changing the intensity of the applied fields, a smooth crossover from the DSP to other percolation models OP, DP and SP is observed [22,23]. A phase diagram is then developed for the percolation models under the external bias fields. Depending on the field intensity the DSP model corresponds to different percolation models on the phase diagram. Thus the DSP model with variable field intensities can be treated as a general model for all the four said percolation models.

In the Chapter 7, a new methodology is proposed to study the rotationally constrained percolation models as a spin model defined in terms of the occupation states. The same percolation transition is then established at the same percolation threshold by the introduction of the state variable for the DSP and also for the SP models. The multifractal aspects of the spanning clusters of these models without introducing any other external agency have been studied. A measure is defined in terms of a relative state variable and a sequence of state exponents are obtained. The existence of a spectrum of state exponents then confirms the multifractal characteristics of the DSP and SP spanning clusters. Spectra of fractal dimensions are obtained via a Legendre transformation. The spectra not only show the distinct multifractal characteristics of the DSP model from that of the other models but

also confirm the breakdown of universality in this model [24–26]. The state variable formalism is found consistent to study percolation transition as well the multifractal properties of rotational percolation models.

After the detailed study of static properties of the DSP model, the critical behaviour of the dynamical properties are studied in the Chapter 8. Modeling the diffusion process by simple random walk on the DSP clusters, it is found that diffusion is anomalous and anisotropic. Other transport properties, the dc conductivity, magnetoconductivity are then studied as a function of disorder. The corresponding dynamical exponents are estimated. Dynamical scaling relations connecting the static and dynamic exponents are found satisfied within error bars. The random walks on the DSP clusters are characterized by new walk dimensions. The critical exponents related to the diffusivity and conductivity are also found different from that of the other percolation models. Some of the dynamical critical exponents are also found different on the square and triangular lattices. The new universality class of the DSP model again confirmed by its dynamical aspects. The results obtained here are compared with that of the other model calculation of magnetoconductivity in composite materials [27].

In brief, a generalized percolation model, directed spiral percolation (DSP), is proposed to study the geometrical properties of disordered systems at the percolation threshold in the presence of external bias fields. DSP model is constructed imposing directional and rotational constraints simultaneously on the percolation model. The DSP clusters incorporate many new features along with the characteristics of DP and SP clusters. It is the first percolation model in which the appearance of a Hall like field is observed. The model exhibits a new critical behaviour at the percolation threshold and belongs to a new universality class. A full scaling theory has been developed and found consistent with the numerical results obtained. A peculiarity of the model is the breakdown of universality of critical exponents between the square and triangular lattices. The critical behaviour of the model is verified by different methods and techniques such as finite size scaling, determination of hull, variation of field direction and intensity, multifractality and the dynamical critical behaviour. An anisotropic finite size scaling (FSS) theory has been developed to verify the effect of finite system size on the MC results and the results are found in good agreement. Though there is breakdown of universality in the cluster properties, the critical behaviour of hull exhibits universal character in $2D$. A phase diagram has been obtained in the parameter space of field intensities. The DSP model corresponds to different percolation models depending on the field intensities. The DSP spanning

clusters are found multifractal. The multifractal spectrum confirms the universality class of the model. The dynamical critical exponents characterized by the topological bias are in accordance with that of the static scaling exponents and reconfirm the universality class of the DSP model.

The DSP model can be used to study the critical properties of disordered systems under crossed external bias fields. The bias fields could be of electric and magnetic in nature when the motion of charged particles are considered. The model can be extended to $3D$ in order to study the bulk properties of disordered materials in the presence of external fields. Apart from the extension of the model to $3D$, several open questions are still left for further study. Examples are, persistence in the DSP cluster, the spin fluctuation in the spanning clusters, the alternating current conductivity of the DSP cluster, and many more.

Bibliography

[1] D. Stauffer and A. Aharony, *Introduction to Percolation Theory*, Taylor and Francis, London, 2nd edition, 1994.

[2] A. Bunde and S. Havlin, *Fractals and Disordered Systems*, Springer-Verlag, Berlin, 1991.

[3] N. R. Moloney and K. Christensen, *Complexity And Criticality*, Imperial College Press, 2005.

[4] B. Bollobás and O. Riordan, *Percolation*, Cambridge University Press, 2006.

[5] S. B. Santra, Eur. Phys. J. B **33**, 75 (2003).

[6] S. P. Obukhov, Physica A **101**, 145 (1980).

[7] M. Barma and D. Dhar, J. Phys. C: Solid State Phys. **16**, 1451 (1983).

[8] H. Hinrichsen, Adv. Phys. **49**, 815 (2000).

[9] P. Ray and I. Bose, J. Phys. A **21**, 555 (1988).

[10] S. B. Santra and I. Bose, J. Phys. A **24**, 2367 (1991).

[11] S. B. Santra and I. Bose, J. Phys. A **25**, 1105 (1992).

[12] H. J. W. Blöte and H. J. Hilhorst, J. Phys. A **17**, L111 (1984).

[13] K. Y. Lin, J. Phys. A **18**, L145 (1985).

[14] S. B. Santra, J. Phys. I France **5**, 1573 (1995).

[15] S. Sinha and S. B. Santra, Eur. Phys. J. B **39**, 513 (2004).

[16] S. Sinha and S. B. Santra, in *Proceedings - 46th DAE Solid State Phys. Symp., Jiwaji Univ, Gwalior, India, Dec., 2003*, page 33.

[17] S. Sinha and S. B. Santra, Indian J. Phys. **(communicated)** (2007).

[18] S. Sinha and S. B. Santra, in *Abstracts - Condensed Matter Days 2006, Tezpur Univ., Assam, India, Aug., 2006.*

[19] S. Sinha and S. B. Santra, Int. J. Mod. Phys. C **16**, 1251 (2005).

[20] S. Sinha and S. B. Santra, in *Abstracts - Statphys 22, IISc. Bangalore, India, July, 2004*, page 162.
[21] T. Grossman and A. Aharony, J. Phys. A **19**, L745 (1986).
[22] S. Sinha and S. B. Santra, Int. J. Mod. Phys. C **17**, 1285 (2006).
[23] S. Sinha and S. B. Santra, in *Proceedings - 9th World Multi-Conference on Systemics, Cybernetics and Informatics, Orlando, USA, July, 2005.*
[24] S. Sinha and S. B. Santra, Physica A **376**, 351 (2007).
[25] S. Sinha and S. B. Santra, in *Proceedings - 50th DAE Solid State Phys. Symp., BARC Mumbai, India, Dec., 2005*, page 165.
[26] S. Sinha and S. B. Santra, in *ICTP International Conference on Recent Advances in the Interdisciplinary Applications of Statistical Physics, ICTS Beijing, China, Sept., 2006.*
[27] S. V. Barabash, D. J. Bergman and D. Stroud, Phys. Rev. B **64**, 174419 (2001).

List of publications

1. *"Directed Spiral Percolation on the Triangular Lattice"*, S. Sinha and S. B. Santra, Proceedings - 46th DAE Solid State Phys. Symp., Jiwaji Univ, Gwalior, Madhya Pradesh, India, Dec. 26-30, 2003, page 33.

2. *"Breakdown of Universality in Directed Spiral Percolation"*, S. Sinha and S. B. Santra, Eur. Phys. J. B **39**, 513 (2004).

3. *"Hull properties of Directed Spiral Percolation Clusters"*, S. Sinha and S. B. Santra, Statphys 22, IISc. Bangalore, India, July 4-9, 2004, page 162.

4. *"Directed Spiral Percolation: A Model to Study Disordered Systems under Crossed External Fields"*, S. Sinha and S. B. Santra, Proceedings - 9th World Multi-Conference on Systemics, Cybernetics and Informatics, Orlando, Florida, USA, July 10-13, 2005, page 155.

5. *"Self-organized dynamical equilibrium in the corrosion of random solids"*, S. Sinha, V. Kishore and S. B. Santra, Eur. Phys. Lett. **71**, 632 (2005).

6. *"Directed Spiral Percolation Hull on the Square and Triangular Lattices"*, S. Sinha and S. B. Santra, Int. J. Mod. Phys. C **16**, 1251 (2005).

7. *"Multifractility in Directed Spiral Percolation"*, S. Sinha and S. B. Santra, Proceedings - 50th DAE Solid State Phys. Symp., BARC Mumbai, India, Dec. 4-9, 2005, page 165.

8. *"Finite-Size Scaling Theory for Anisotropic Percolation Clusters"*, S. Sinha and S. B. Santra, Condensed Matter Days 2006, Tezpur Univ., Assam, India, Aug. 29-31, 2006, page 51.

9. *"Effect of Field Direction and Field Intensity on Directed Spiral Percolation"*, S. Sinha and S. B. Santra, Int. J. Mod. Phys. C **17**, 1285 (2006).

10. *"Finite-Size Scaling and Multifractality in Directed Spiral Percolation"*, S. Sinha and S. B. Santra, ICTP Asian Pacific School of Statistical Physics and Interdisciplinary Applications and International Conference on Recent Advances in the Interdisciplinary Applications of Statistical Physics, ICTS Beijing, China, Sept. 11-22, 2006.

11. *"Multifractality in Rotational Percolation Models"*, S. Sinha and S. B. Santra, Physica A **376**, 351 (2007).

12. *"Finite-Size Scaling for Directed Percolation Models"*, Santanu Sinha and S. B. Santra, communicated, Indian J. Phys. (2007).